CENTREPORT SHIPPING CHANNEL DEEPENING PROJECT

Numerical model studies of the wave, current and sediment dynamics

Prepared for CentrePort Ltd

PO Box 441, New Plymouth, New Zealand
T: 64-6-7585035 E: enquiries@metocean.co.nz

Draft for public consultation

MetOcean Solutions Ltd: Report P0283-01

April 2016

Report status

Version	Date	Status	Approved by
Rev0	01/04/2016	Draft for consultation	McComb

It is the responsibility of the reader to verify the currency of the version number of this report.

PO Box 441, New Plymouth, New Zealand
T: 64-6-7585035 E: enquiries@metocean.co.nz

Draft for public consultation

EXECUTIVE SUMMARY

CentrePort Limited is investigating the deepening of the Wellington Harbour entrance shipping channel and the Thorndon Container Wharf area, and has commissioned MetOcean Solutions Ltd to undertake a detailed study program of the oceanographic and sediment dynamics to support and inform this proposed activity. This includes an evaluation of the effects of the capital dredging on the wave, current and sediment dynamics throughout the harbour, the effects of dredging and disposal on water quality, and the effects of sediment disposal on the receiving environment.

This report is a technical reference document that details the methodologies used, the validation undertaken, and the results from the numerical modelling of waves, currents and sediment dynamics associated with the channel deepening and offshore disposal. Interpretation of the results in terms of the physical effect is provided in the companion report (MSL P0214-03). Consideration of the effects of the Thorndon Container Wharf deepening and disposal are provided in a separate report (MSL Report P0214-02).

Industry-standard numerical models have been established and validated using historical and contemporary measurements. It has been demonstrated that the models can replicate the dominant physical processes in the area, and may be reliably used to examine the potential physical effects arising from the CentrePort Channel Deepening Project.

- A 35-year wind hindcast at 4 km resolution was used to prescribe the spatially-varying wind conditions in the harbour and in the Cook Strait region. These data have been used as the boundary conditions to hydrodynamic and wave simulations.

- The 2- and 3-dimensional hydrodynamics have been modelled at various spatial scales with regular, curvilinear and finite-element numerical domains. A 10-year regional hindcast of the tidal and non-tidal flows was utilised, along with a nested tidal domain for the Wellington Harbour. These data were used to describe the existing flow regime in the entrance channel as well as in the vicinity of the proposed offshore disposal ground.

- Wave conditions were considered with a high-resolution model that includes the tidal hydrodynamics as well as local wind-wave generation inside the harbour. A 10-year hindcast was produced for the Wellington Harbour, which was nested inside a 35-year national wave hindcast.

- The sediment dynamics were simulated with a fully-coupled wave, current and sediment transport model. Climatic conditions were modelled to consider potential transport and morphology evolution over decadal time scales, as well as the discrete outcomes from a series of energetic historical events.

This suite of models was used to make an assessment of the likely effects of deepening the entrance channel, and disposing of capital volumes in an offshore ground in Fitzroy Bay. This was achieved by undertaking identical simulations with, and without, the dredging / disposal activity. Two potential channel designs were tested in this manner, along with the respective disposal volumes. An evaluation of the impact of plumes associated with dredging and disposing has also been made.

Draft for public consultation

TABLE OF CONTENTS

Draft for public consultation

LIST OF FIGURES

LIST OF TABLES

Draft for public consultation

1. INTRODUCTION

CentrePort Limited (CentrePort) is investigating the deepening of the Wellington Harbour entrance shipping channel and the Thorndon Container Wharf area. Globally, the future container shipping fleet will have larger vessels, which require greater depths for safe transit in and out of the harbour. Accordingly, to maintain an existing container service and to provide for the future growth of the port, deepening of the navigation channel and berth area is an essential requirement. Similar deepening projects are being undertaken at other ports around New Zealand, including Lyttleton, Tauranga and Dunedin.

CentrePort has commissioned MetOcean Solutions Ltd (MSL) to undertake a detailed study program of the oceanographic and sediment dynamics, which is required to support and inform this proposed activity. This includes an evaluation of the effects of the capital dredging on the wave, current and sediment dynamics throughout the harbour, the effects of dredging and disposal on water quality, and the effects of sediment disposal on the receiving environment. Specifically, the scope of the study program is to:

- Assess the expected sediment transport at the dredge sites, during and after dredging.
- Assess the expected sediment transport at the disposal sites, during and after dredging, and estimate the required extent of the disposal area.
- Assess changes in wave climate within the harbour and the disposal area as a result of the deepening.
- Identify appropriate measures to avoid, remedy, or mitigate effects, with specific consideration of the sites of interest identified during consultation.

This report presents the technical details and results from the numerical modelling of waves, currents and sediment dynamics associated with the channel deepening and offshore disposal. The purpose is to provide technical reference material to support and inform other aspects of the project. A summary of the physical effects is provided in the companion report MSL P0214-03, along with the discussion and interpretation of the results. Consideration of the effects of the Thorndon Container Wharf deepening and disposal are provided in a separate report (MSL Report P0214-02).

1.1. Report structure

The report is structured as follows. Section 2 details the modelling methods used to assess changes in waves and currents. Numerical methods for assessing the sediment dynamics are detailed in Section 3 and the sediment plume dispersal methodology is outlined in Section 4. Results from the modelling are presented in Section 5, including the characterisation of the existing climate, effects of channel deepening, the changes to the morphodynamics and plumes from the dredging and disposal. A summary is provided in Section 6 and references cited are listed in Section 7.

Draft for public consultation

1.2. Harbour Channel Deepening Project description

The deepening project design is based on future vessel dimensions with up to 14.5 m draught, 300 m LOA, 48 m beam dimension and transit speeds of 10 knots.

An extensive optimisation exercise was undertaken to define the most appropriate design for the future entrance channel (see MSL Report P0222-01). The finalised design ensures the maximum safe navigability for transit under all tides and weather, excepting the extreme storm conditions. The locations of the proposed dredging and disposal areas are shown on Figure 1.1.

Along the entrance channel, the design dredging depth (below Chart Datum) ranges from 16.5 m in the northern section, sloping to 17.2 m in the south. This profile has a 178 Ha area of seabed that may be disturbed by dredging, and the estimated maximum dredge volume is 6.0 M m^3. The proposed disposal location for the sediment is Fitzroy Bay, very close to the previously-consented disposal area. The dimensions of this area have been adjusted to ensure effects on the receiving environment are minimised, while allowing the capacity for the maximum expected dredging volume to be adequately contained. The area of the ground is 140 Ha.

At the Thorndon Container Wharf, an area up to 14 Ha may be disturbed by dredging to the maximum design depths. This will give rise to a disposal volume 270,000 m^3, and a nearby disposal ground has been identified as a suitable site to retain these sediments. This ground has an area of 13.27 Ha.

The dredging operations may not necessarily be undertaken in a single campaign to achieve the design depths. The three indicative scenarios have been suggested:

Scenario 1 – staged dredging

- 12.0 m vessel design (14.0-14.7 m depth and <1.6 M m^3)
- 12.5 m vessel design (14.5-15.2 m depth and <2.4 M m^3)
- 13.5 m vessel design (15.5-16.2 m depth and <4.0 M m^3)
- 14.5 m vessel design (16.5-17.2 m depth and <6.0 M m^3)

Scenario 2 – multi-year program

- Dredging over several years using a low volume vessel. This assumes dredging up to 6 days week for 50 weeks/year, daylight hours only and subject to operational limitations such as weather, sea state and mechanical downtime.

Scenario 3 – single event

- Dredging and disposal to consented maximum depths and volumes. Estimated duration 10-20 weeks.

Draft for public consultation

2. WAVE AND CURRENT MODELLING METHODS

2.1. Bathymetry data sources

The bathymetric dataset used for the development of the regional and local model domain bathymetries combined data from several sources, including harbour soundings (single and multi-beam surveys) and digitised nautical charts (ENCs).

2.2. Winds

The surface wind fields used for the wave and hydrodynamic modelling were sourced from a 35-year regional atmospheric hindcast. The WRF (Weather Research and Forecasting) model was established over all New Zealand at 12 km resolution, with a nested ~4 km resolution domain over the central NZ region, including Wellington Harbour. The WRF model boundaries were prescribed from the CFSR (Climate Forecast System Reanalysis) dataset distributed by NOAA (Saha et al., 2010).

The hindcast has been successfully validated at many locations throughout New Zealand, and a local comparison of measured and modelled winds for Wellington Airport shows good agreement (Figure 2.1 and Figure 2.2).

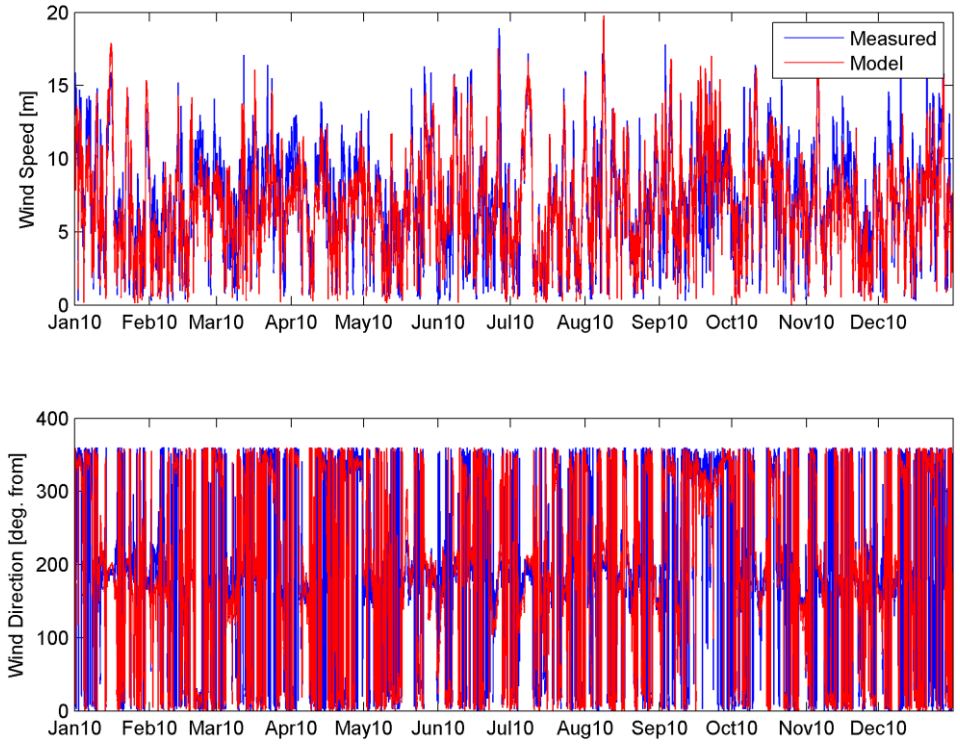

Figure 2.1 Comparison of measured and modelled wind speed / direction at Wellington Airport (174.804,-41.322).

Draft for public consultation

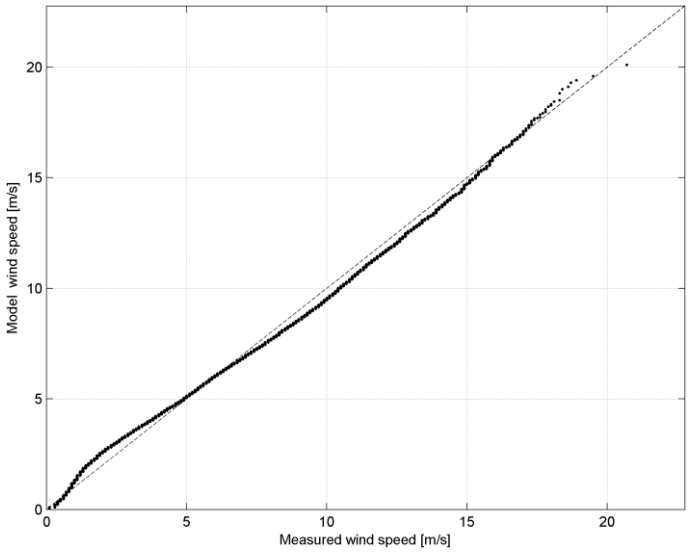

Figure 2.2 Quantile-quantile plot of the measured and modelled wind speed at Wellington Airport (174.804,-41.322).

2.3. Waves

2.3.1. Numerical model

SWAN (Simulating WAves Nearshore) was used to prepare a high resolution 10-year duration hindcast (2004-2013) of the wave climate in the Wellington Harbour region. SWAN is a third generation ocean wave propagation model, which solves the spectral action density balance equation for wavenumber-direction spectra. This means that the growth, refraction and decay of each component of the complete sea state, each with a specific frequency and direction, is solved, giving a complete and realistic description of the wave field as it changes in time and space. A detailed description of the model equations, parameterisations, and numerical schemes can be found in Holthuijsen, (2007) or the SWAN online documentation[1].

Physical processes that are simulated include the generation of waves by surface wind, dissipation by white-capping, resonant nonlinear interaction between the wave components, bottom friction and depth limited breaking. All 3rd generation physics are included. The Collins (1972) friction scheme is used for wave dissipation by bottom friction with a friction factor of 0.015.

The solution of the wave field is found for the non-stationary (time-stepping) mode. Boundary conditions, wind forcing and resulting solutions are all time dependent, allowing the model to capture the growth, development and decay of the wave field.

2.3.2. Model domain and boundary conditions

The wave hindcast involved a three-level SWAN downscaling, with full spectral boundaries for each domain. The boundaries for the lowest resolution domain (i.e. New Zealand scale) were prescribed from the MetOcean Solutions implementation of the global wave model WW3 (Tolman, 1991). This outermost domain covers all of New Zealand at a

[1] http://swanmodel.sourceforge.net/online_doc/online_doc.htm

resolution of 0.05˚ by 0.05˚; providing spectral boundaries to an intermediate SWAN nest, extending over the southern North Island with a resolution of 0.005˚ by 0.005˚. Wellington Harbour was modelled using a high-resolution SWAN domain (0.0006˚ by 0.0004˚), which included high resolution tidal flow and elevation fields, along with local wind wave generation forced from the WRF hindcast.

2.3.3. Output and post-processing

Gridded wave statistics were calculated over the entire high-resolution Wellington Harbour SWAN domain. The data were stored in yearly files at three-hour intervals over the 10-year hindcast period. For each modelled frequency-direction wave spectrum $S(f,\theta)$, a one-dimensional frequency spectrum $S(f)$ was calculated as:

$$S_n(f) = \int_{-\pi}^{\pi} E_n(f,\theta)d\theta \tag{2.1}$$

where E is the energy density. The peak frequency f_p was identified as the frequency corresponding to the peak in $S(f)$. The significant wave height H_s, mean direction at peak energy D_{pm} and peak wave period T_p were defined as:

$$H_s = 4\sqrt{\int_0^{\infty} S_n(f)df}$$

$$D_{pm} = \arctan\frac{\int_{-\pi}^{\pi} E_n(f_p,\theta)\sin(\theta)d\theta}{\int_{-\pi}^{\pi} E_n(f_p,\theta)\cos(\theta)d\theta}$$

$$T_p = 1/f_p \tag{2.2}$$

Wave statistics for the swell and sea wave components were also calculated. The two-dimensional wave spectra were split at 8 s period with spectral energy above and below the partition classified as swell and sea, respectively.

2.3.4. Wave model validation

The local scale wave model was first validated with historical wave data measured adjacent to Baring Head by a waverider buoy (see Figs. 2.3 and 2.4). The following quantitative measures of accuracy were calculated from the measured x_m and hindcast, x_h data:

Mean absolute error (MAE): $\overline{|x_h - x_m|}$ (2.3)

RMS error (RMSE): $\sqrt{\overline{(x_h - x_m)^2}}$ (2.4)

Draft for public consultation

Mean relative absolute error (MRAE):

$$\overline{\left|\frac{x_h - x_m}{x_m}\right|} \qquad (2.5)$$

Bias:

$$\overline{x_h - x_m} \qquad (2.6)$$

Scatter Index (SI):

$$\frac{\sqrt{\overline{(x_h - x_m)^2}}}{\overline{x_h}} \qquad (2.7)$$

The overall agreement between model predictions and measurements (Figs. 2.5 and 2.6) indicates the model correctly reproduces the variability of the local wave climate south of the entrance. Shortcomings of the model include a slight under-prediction of the larger events over 3 m. However, the quantitative accuracy measures remain reasonable, with a MAE of 0.28 m and a bias of 0.11 m.

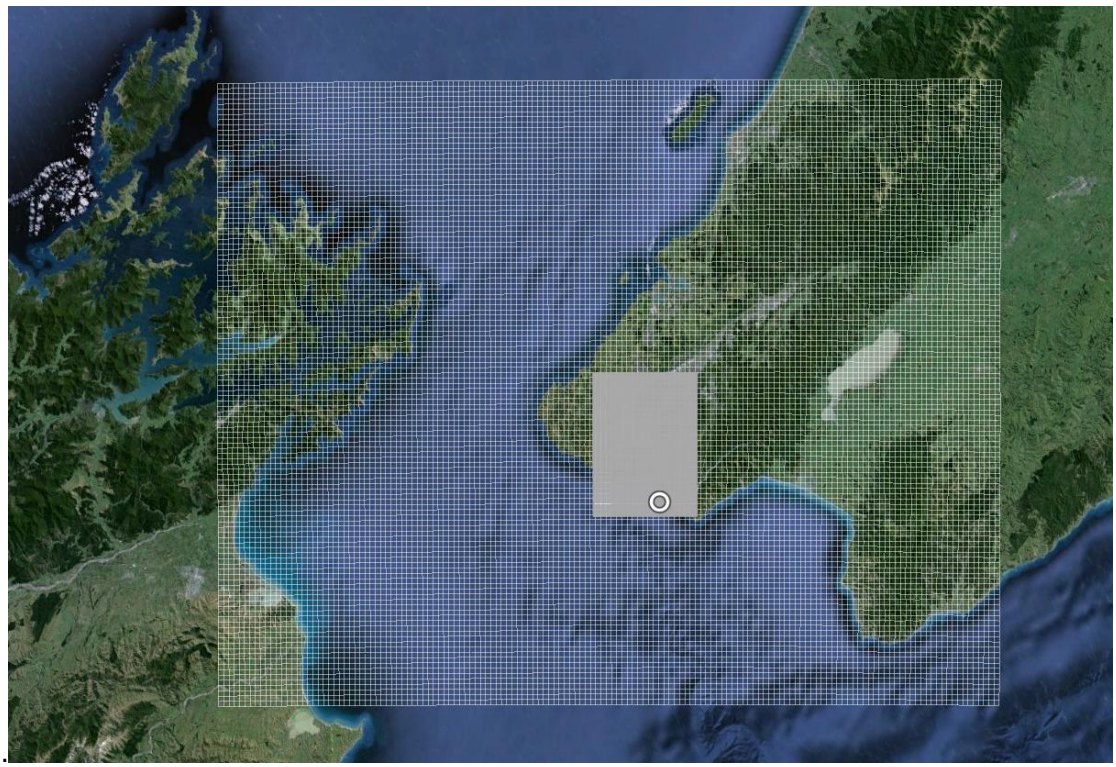

Figure 2.3 The two nested SWAN domains implemented for the study. The white circle shows the position of the Baring Head waverider buoy.

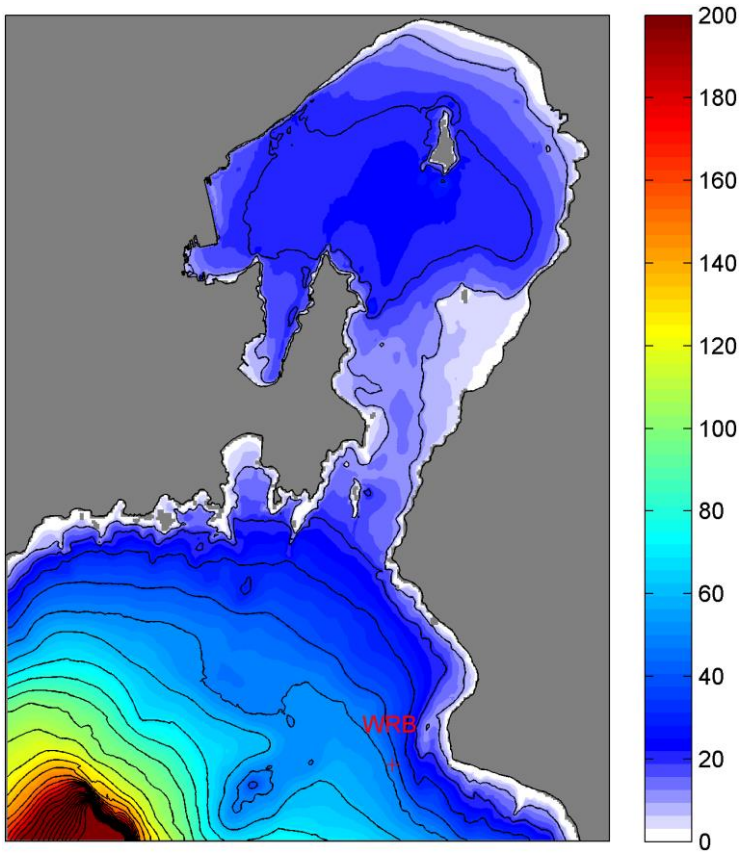

Figure 2.4 Bathymetry of the high resolution Wellington Harbour SWAN domain. The Baring Head waverider buoy (WRB) position is shown in red.

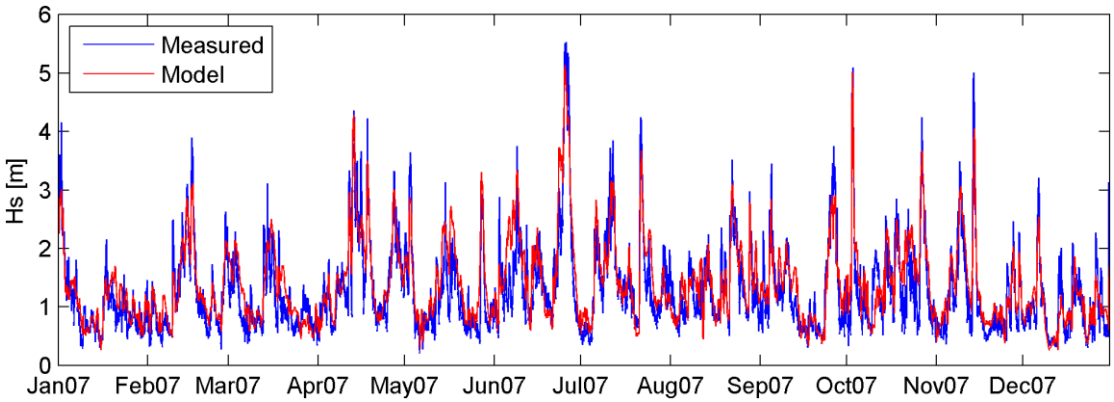

Figure 2.5 Comparison of the measured and modelled significant wave heights at the Baring Head waverider buoy during 2007.

Draft for public consultation

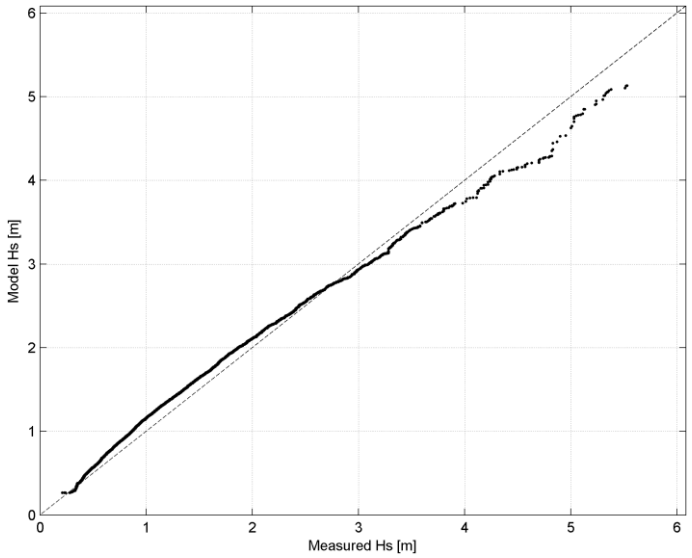

Figure 2.6 Quantile-quantile plot of measured and modelled significant wave heights at the Baring Head waverider buoy during 2007.

Table 2.1 Accuracy measures of the hindcast based on a comparison with measured significant wave heights at Baring Head.

MAE [m]	0.28
RMSE [m]	0.38
MRAE [%]	0.27
Bias [m]	0.11
SI	0.30

A program of wave measurement was undertaken within the Wellington Harbour Entrance (Figure 2.7) to provide an empirical basis to the modelled wave transformation processes, plus confirm the tidal modulation effects on the harbour wave climate due to the local hydrodynamics. While the measurement period was not included in the model hindcast interval, these contemporary data still allow a quantitative validation to be made because the measured spectral transformation (i.e. from waverider buoy to the inshore wave meters) can be compared with modelled values under similar conditions.

The time series of total and swell partition (Tp>8 s) significant wave heights measured at the 7 sites are shown in Figure 2.8 and Figure 2.9. The deployment period included a range of energetic events with significant wave heights exceeding 2 m. The tidal modulation is clearly evident in the measured wave data, both inside and outside the entrance.

The ability of the model to replicate the wave dynamics inside the harbour entrance was investigated by comparing the ratios of significant swell wave heights at the W1, W2, E1, S1, S2 and S3 positions to that at the WRB i.e. $H_{s,swell}$ (W1,W2,E1,S1,S2,S3) / $H_{s,swell}$ (WRB). Note the analysis focused on the low-frequency component of the wave field since the transformations of the short-period sea are not expected to be significantly affected by the tidal flows, and local wind-sea generation may obscure the effects. Further, the

pressure attenuation effects with depth on the wave meters effectively negate a portion of the sea frequency range.

The measured wave conditions were partitioned into a range of wave height, period, and directional bins for which average ratios were computed. The modulation of the wave field by wave period, wave direction, tidal elevation and tidal flow were assessed by comparing the ratio values to a range of these parameters. These significant swell wave height ratios are presented in Figure 2.10 - Figure 2.15.

The incoming wave direction and wave period have a clear influence on the swell wave ratios. For example, at W1 on the eastern side of the entrance, the south to south-westerly waves generally result in wave heights 10-20 % larger compared with south to south-easterly conditions. Increasing wave period also produces larger waves due to increased refraction.

The strong tidal flows in the entrance region are expected to modulate the local wave climate and amount of energy penetration through the entrance. The time-varying water depth can also modulate refraction patterns as well as energy dissipation by friction or breaking. Currents that are co-linear with the incident wave field may induce a relative steepening (opposing flow) or flattening (same-direction flow) of the incident waves, as well as causing localised refraction.

Comparison of measured swell wave height ratios at site W1 with the concurrent tidal flow through the entrance shows a trend of enhanced wave height for opposing flow and reduced heights for same-direction flow, with height variations of the order 10-15 %. The tidal water levels also appear to play a role in the wave height modulation with larger height ratios observed for lower water levels and vice versa. Magnitudes of the wave height modulation in this manner are slightly larger, in the range 10-30 %, and enhanced wave refraction along the sides of the entrance are responsible.

Further inside the entrance on the west side at site W2, the swell wave height ratios are much smaller, generally around 0.2. That is, only 20 % of the significant height penetrates to this location, compared with around 80% at site W1 on the other side. This location at W2 experiences more dissipation by friction and dispersal of the wave energy to the sides of the entrance through diffraction and refraction, and the swell wave height modulation is much less evident. Some response to the incident wave direction and period is present; consistent with the W1 site observations, although in much smaller proportions. Tidal modulation effects are also much less evident, but the most notable trend is a relative ratio increase for higher water level. This contrasts with W1 and likely due to modified refraction patterns and reduced frictional effects over high tide.

At E1 on the eastern side but further inside the entrance, the swell wave height ratios are around 0.3. As for W2, this indicates smaller wave heights due to dissipation and transformation processes. Although E1 is located further inside the Harbour than W2, wave heights on the eastern side are typically much higher.

Along Seatoun Beach (sites S1, S2 and S3) the swell wave height ratios are very low, around 0.08. Seatoun Beach is well sheltered from incoming

Draft for public consultation

southerly waves, and the Steeple Reef limits the propagation of swell waves to this region. Typically, this location is dominated by the locally-generated wind-sea waves.

The measured data and resultant ratios provide an opportunity to validate the wave modelling technique for reproducing these complex interactions. Using data from the 10-year high-resolution wave hindcast, ratios from the same seven measurement locations have been produced and are presented in Figure 2.16 - Figure 2.21.

For site W1, the main features of the modulation of the swell wave energy penetration in the harbour with respect to offshore wave direction and tidal conditions (elevation and flow) are generally well reproduced by the model. The modelled range of 0.6-0.8 is consistent with the measured ratios, and similar modulation trends.

At W2, while the modelled ratio is slightly larger than the measured ratios by ~10 %, the model still correctly reproduces the tidal modulation effect. The overestimation of wave penetration at W2 may be due to inaccurately defined bathymetry and bottom friction over rocky reef areas, or related to a slight spatial offset in refraction and wave penetration patterns in the model that result in strong height gradient in the area, as well as possible limits in the model ability to fully reproduce diffraction effects along the depth gradients on the sides of the channel, particularly along its western flank.

At site E1, the modelled ratio is lower than the measured ratios by ~10%. At S1, S2 and S3, comparing modelled and measured wave height ratios suggest that the model ratios are within ~20% of the measured values. It is probable that the wave model does not fully resolve the physical processes occurring around Steeple Reef, but the absolute magnitudes are reasonable and transformation outcomes within 20% error are acceptable in the context of the complex non-linear and time-varying processes in play.

Maps of the wave height ratio fields for several events (Figure 2.22) clearly illustrates the variations in swell energy penetration with subtle changes in offshore direction as well as the important wave height gradients developing in the entrance region where the W1 and W2 wave meters where located.

Draft for public consultation

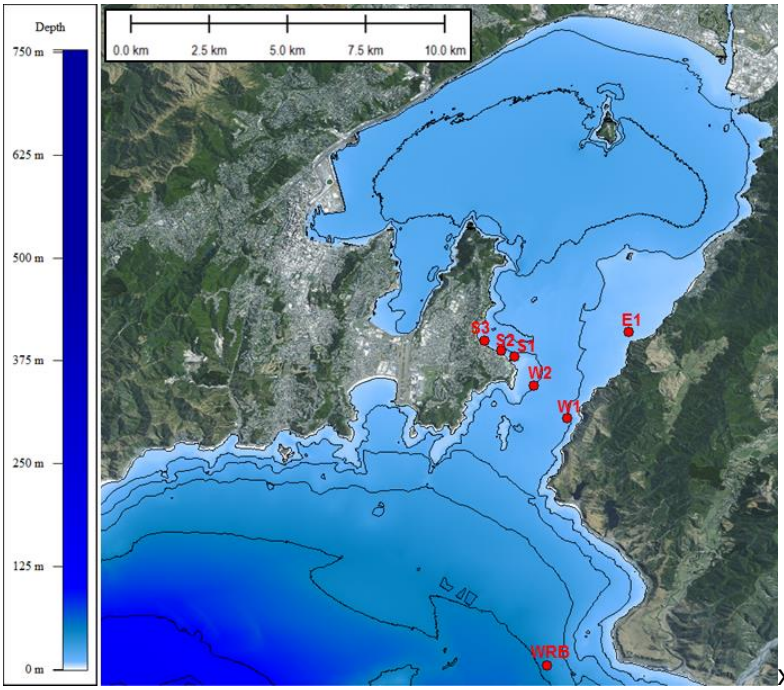

xx

Figure 2.7 Positions of wave measurements within the Wellington Harbour entrance. Water depths at the instruments WRB, W1, W2, E1, S1, S2 and S3 are 50, 10.5, 11, 5, 5.5, 5.5 and 5.5 m to Mean Sea Level, respectively. The grey square indicates the position at which the tidal flow time series were calculated for correlation with the wave height ratios.

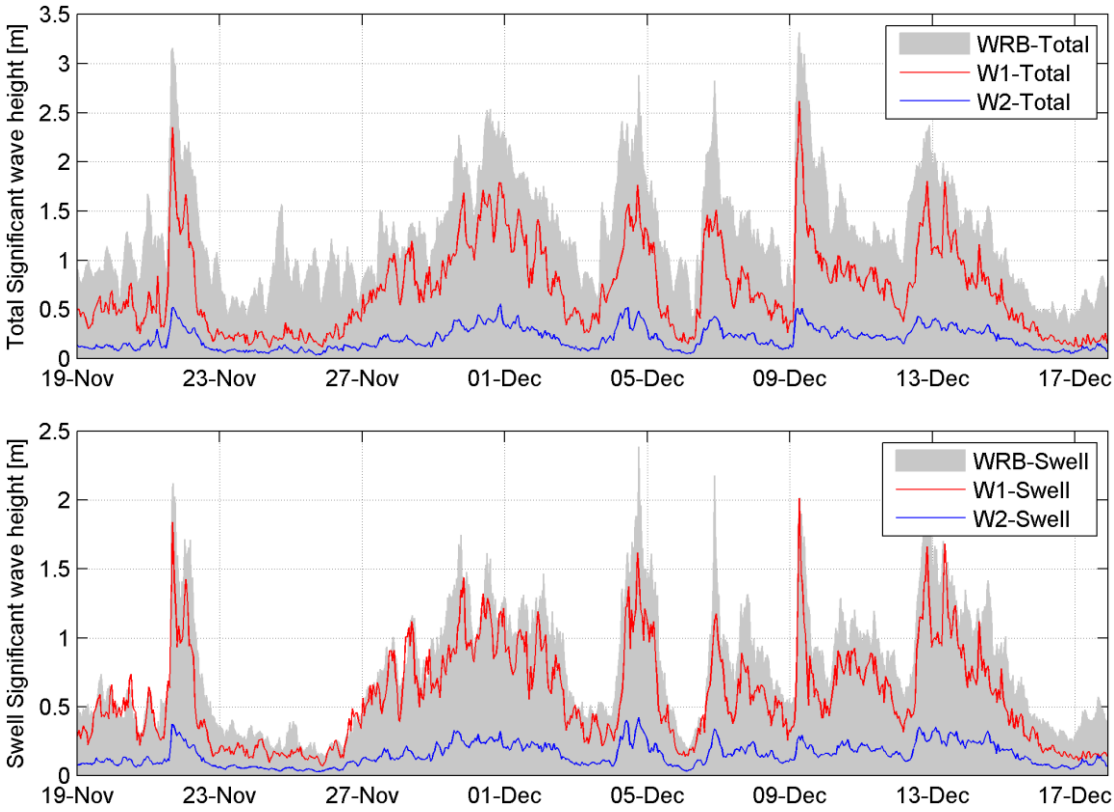

Figure 2.8 Measured total and swell (Tp>8s) significant wave heights at the Baring Head waverider buoy (WRB), W1 and W2.

Draft for public consultation

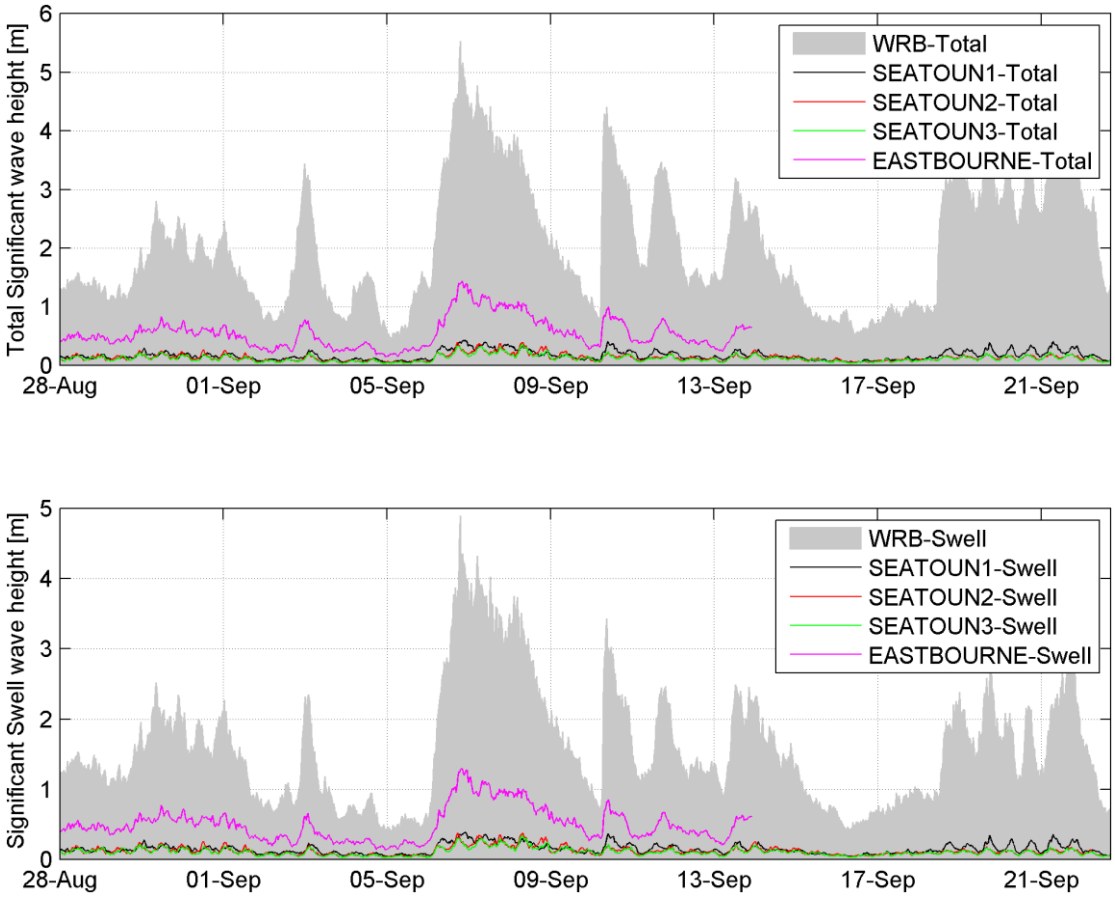

Figure 2.9 Measured total and swell (Tp>8s) significant wave heights at the Baring Head waverider buoy (WRB), Eastbourne 1 (E1), Seatoun 1 (S1), Seatoun 2 (S2) and Seatoun 3 (S3).

Draft for public consultation

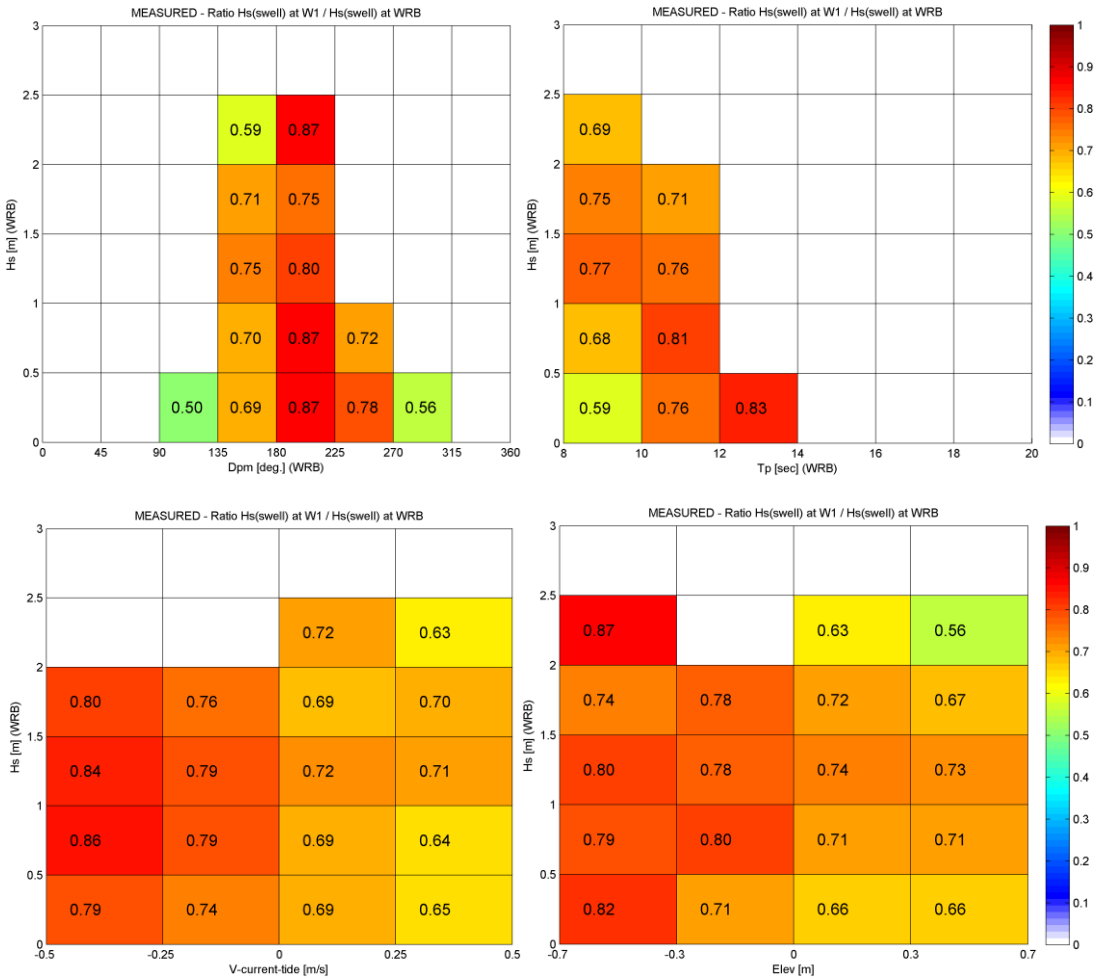

Figure 2.10 Measured significant swell wave height ratios $H_{s\ swell}$ (W1) / $H_{s\ swell}$ (WRB) as a function of the wave direction and wave period at WRB (top), and tidal elevation and tidal flow through the entrance (bottom) at W1.

Draft for public consultation

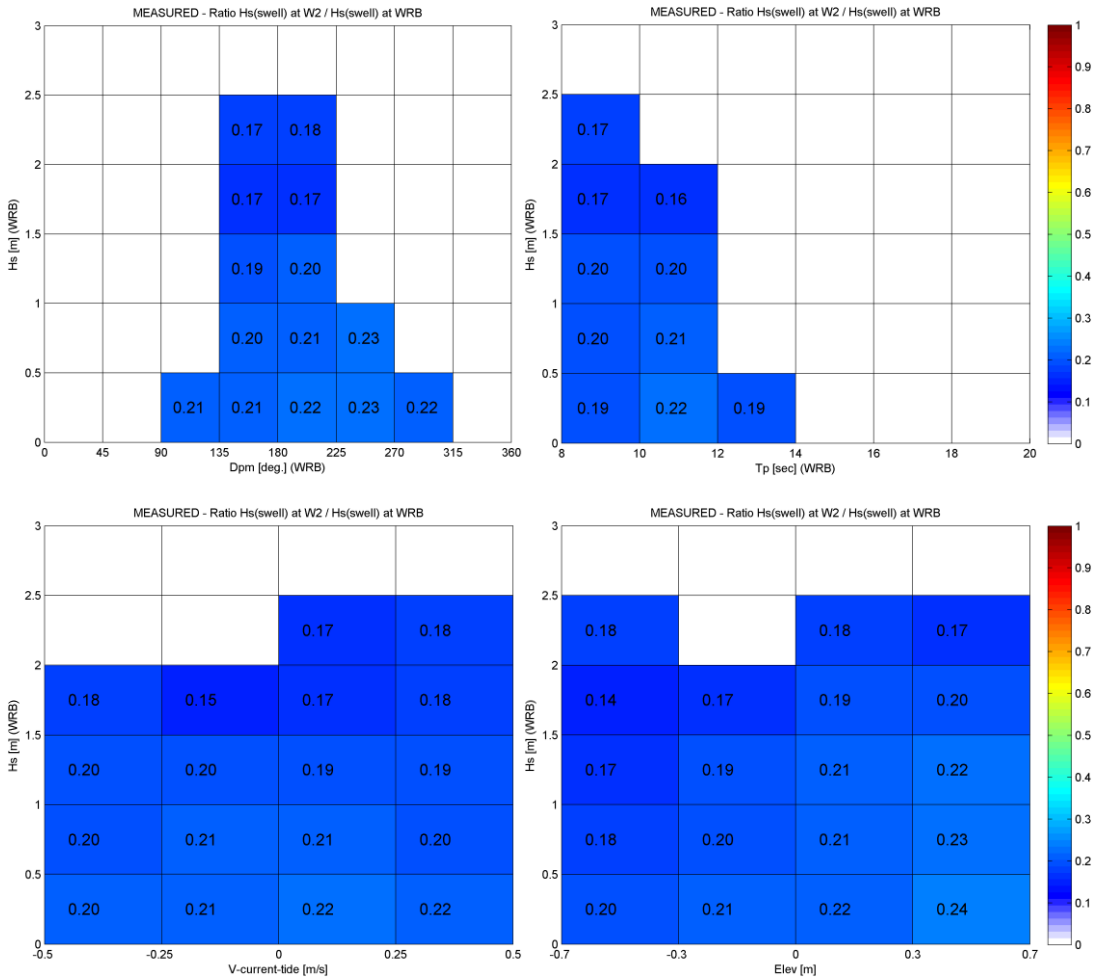

Figure 2.11 Measured significant swell wave height ratios $H_{s\ swell}$ (W2) / $H_{s\ swell}$ (WRB) as a function of the wave direction and wave period at WRB (top), and tidal elevation and tidal flow through the entrance (bottom) at W2.

Draft for public consultation

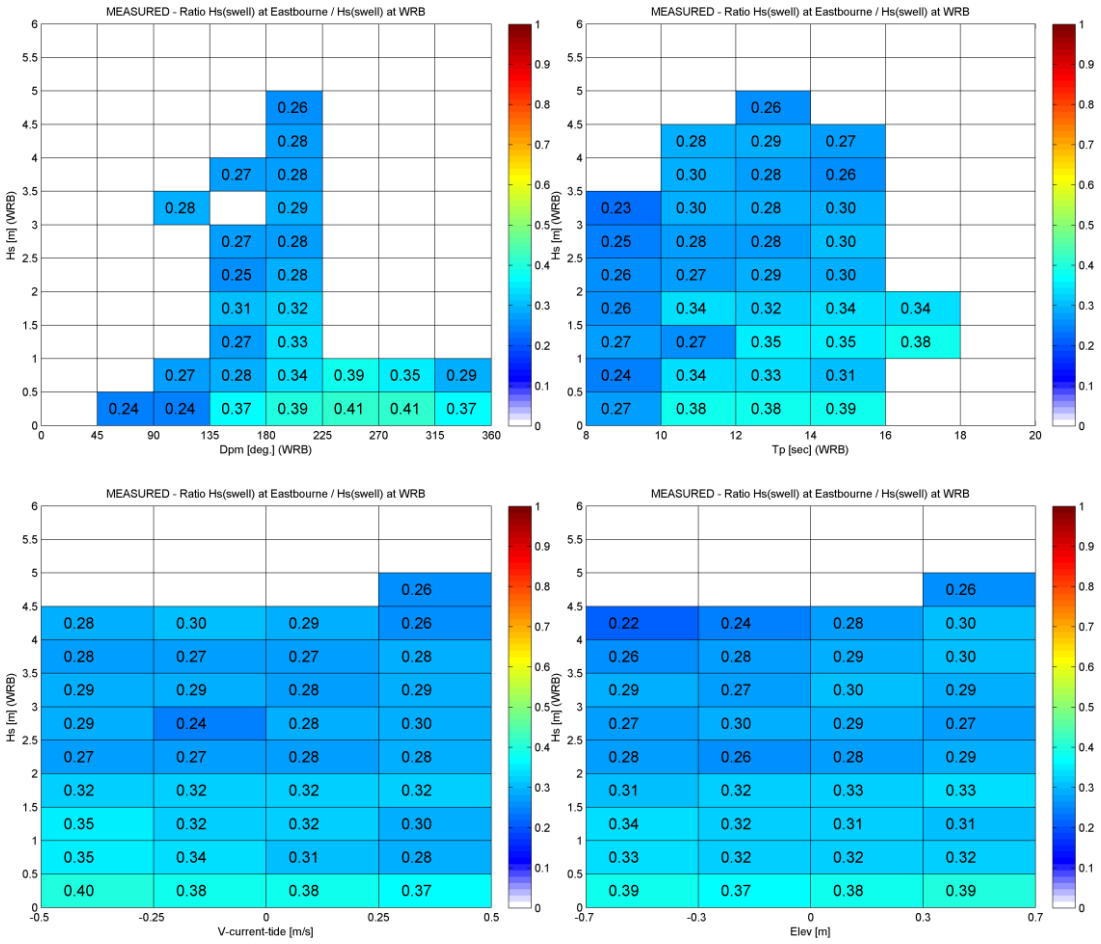

Figure 2.12 Measured significant swell wave height ratios $H_{s\ swell}$ (E1) / $H_{s\ swell}$ (WRB) as a function of the wave direction and wave period at WRB (top), and tidal elevation and tidal flow through the entrance (bottom) at Eastbourne.

Draft for public consultation

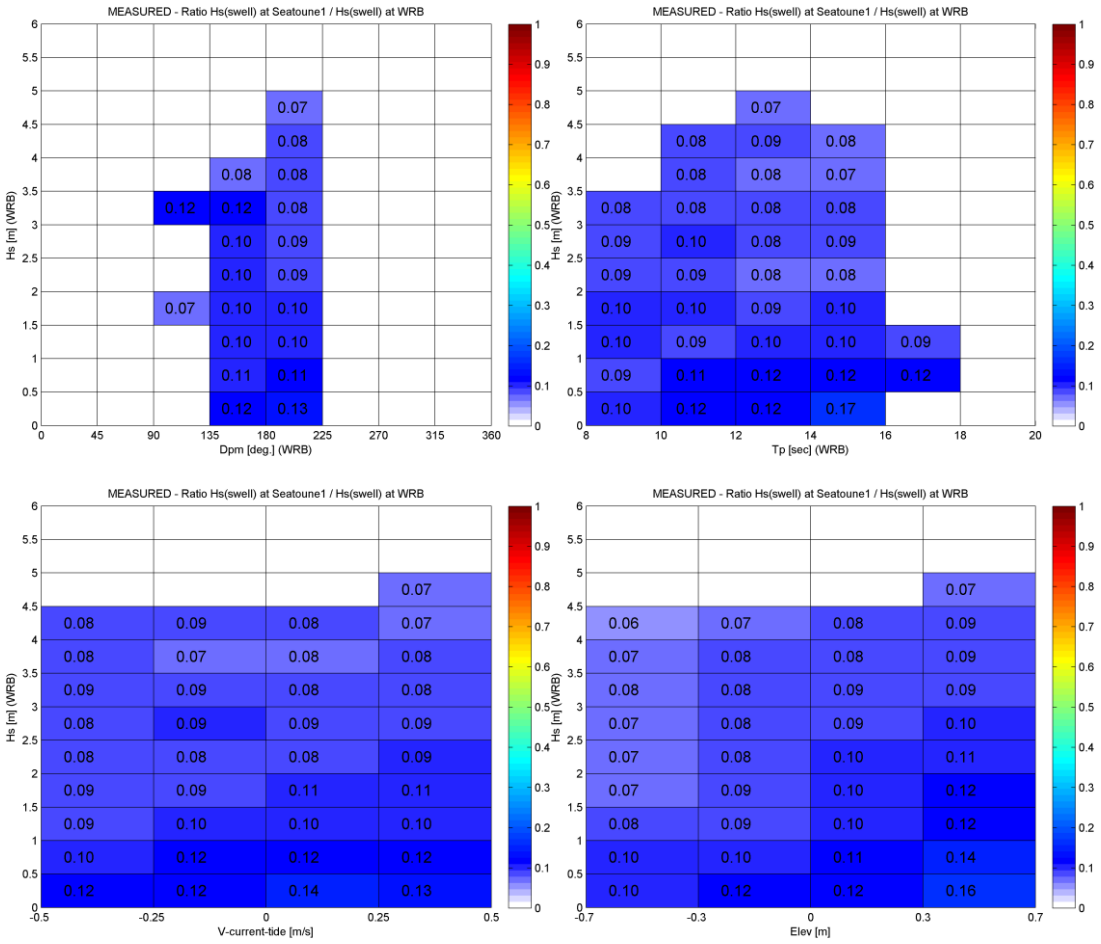

Figure 2.13 Measured significant swell wave height ratios $H_{s\ swell}$ (S1) / $H_{s\ swell}$ (WRB) as a function of the wave direction and wave period at WRB (top), and tidal elevation and tidal flow through the entrance (bottom) at S1.

Draft for public consultation

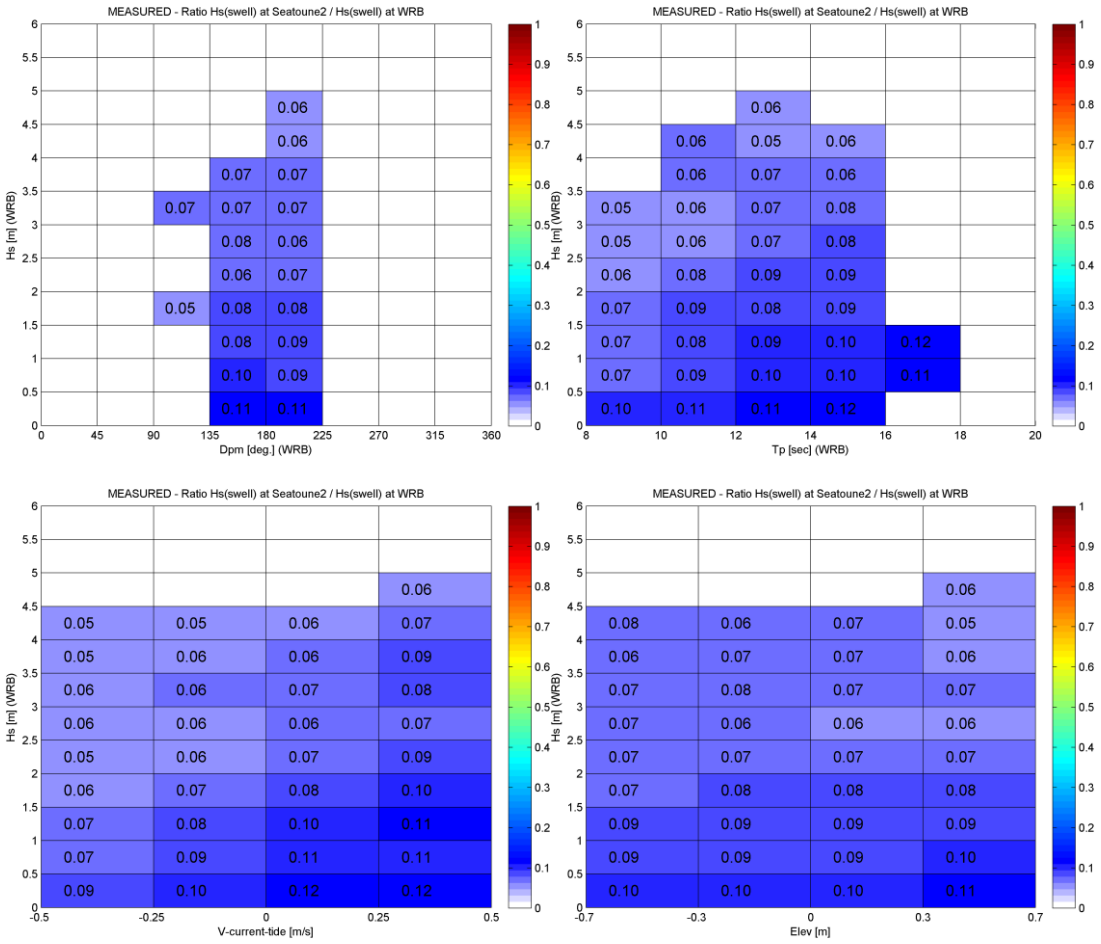

Figure 2.14 Measured significant swell wave height ratios $H_{s\ swell}$ (S2) / $H_{s\ swell}$ (WRB) as a function of the wave direction and wave period at WRB (top), and tidal elevation and tidal flow through the entrance (bottom) at S2.

Draft for public consultation

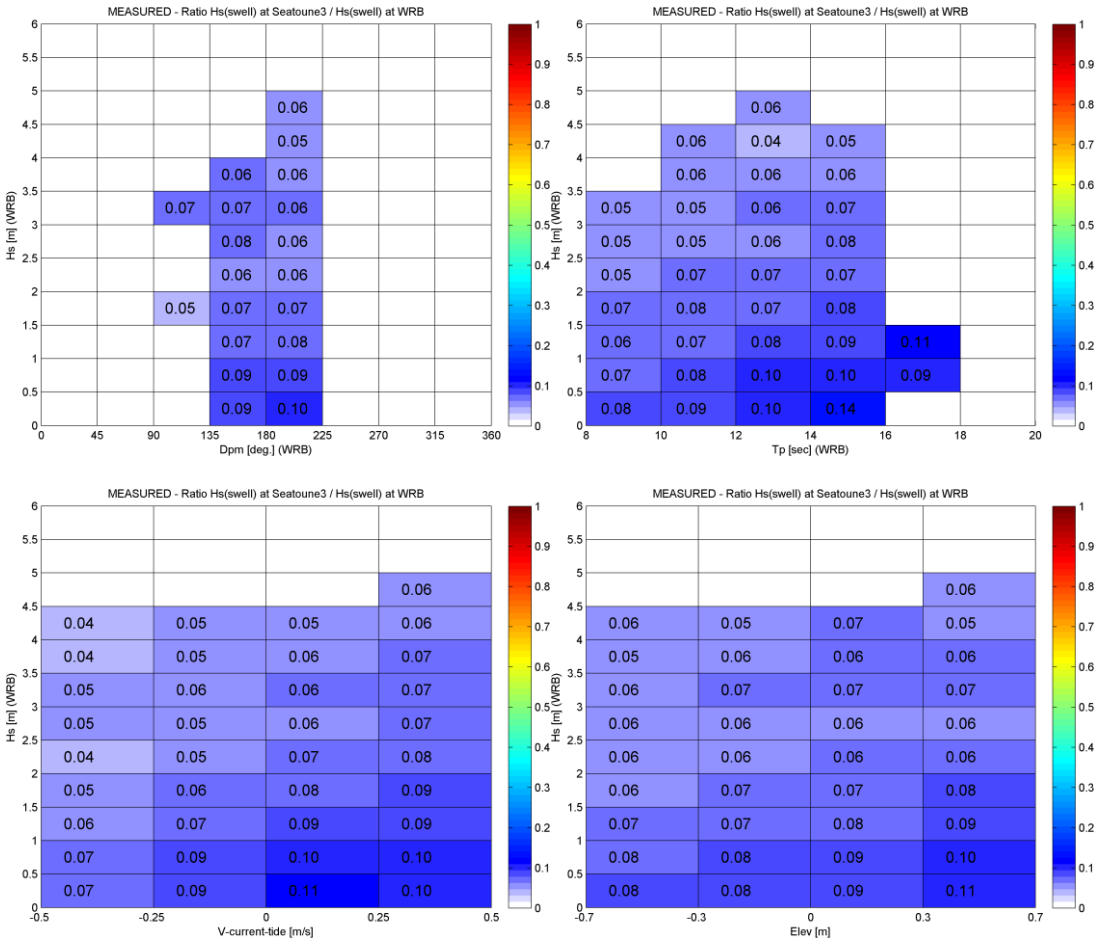

Figure 2.15 Measured significant swell wave height ratios $H_{s\ swell}$ (S3) / $H_{s\ swell}$ (WRB) as a function of the wave direction and wave period at WRB (top), and tidal elevation and tidal flow through the entrance (bottom) at S3.

Draft for public consultation

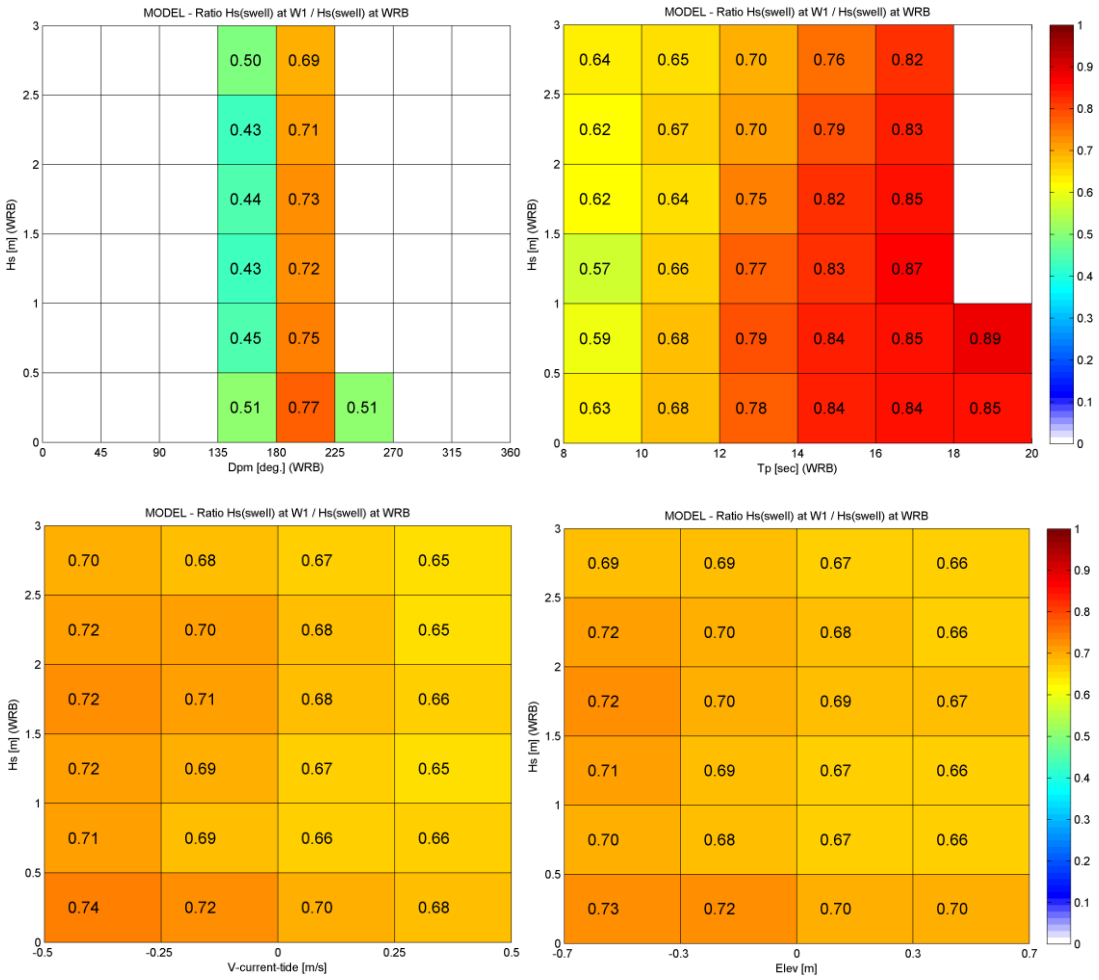

Figure 2.16 Model significant swell wave height ratios $H_{s\ swell}$ (W1) / $H_{s\ swell}$ (WRB) as a function of the wave direction and wave period at WRB (top), and tidal elevation and tidal flow through the entrance (bottom) at W1.

Draft for public consultation

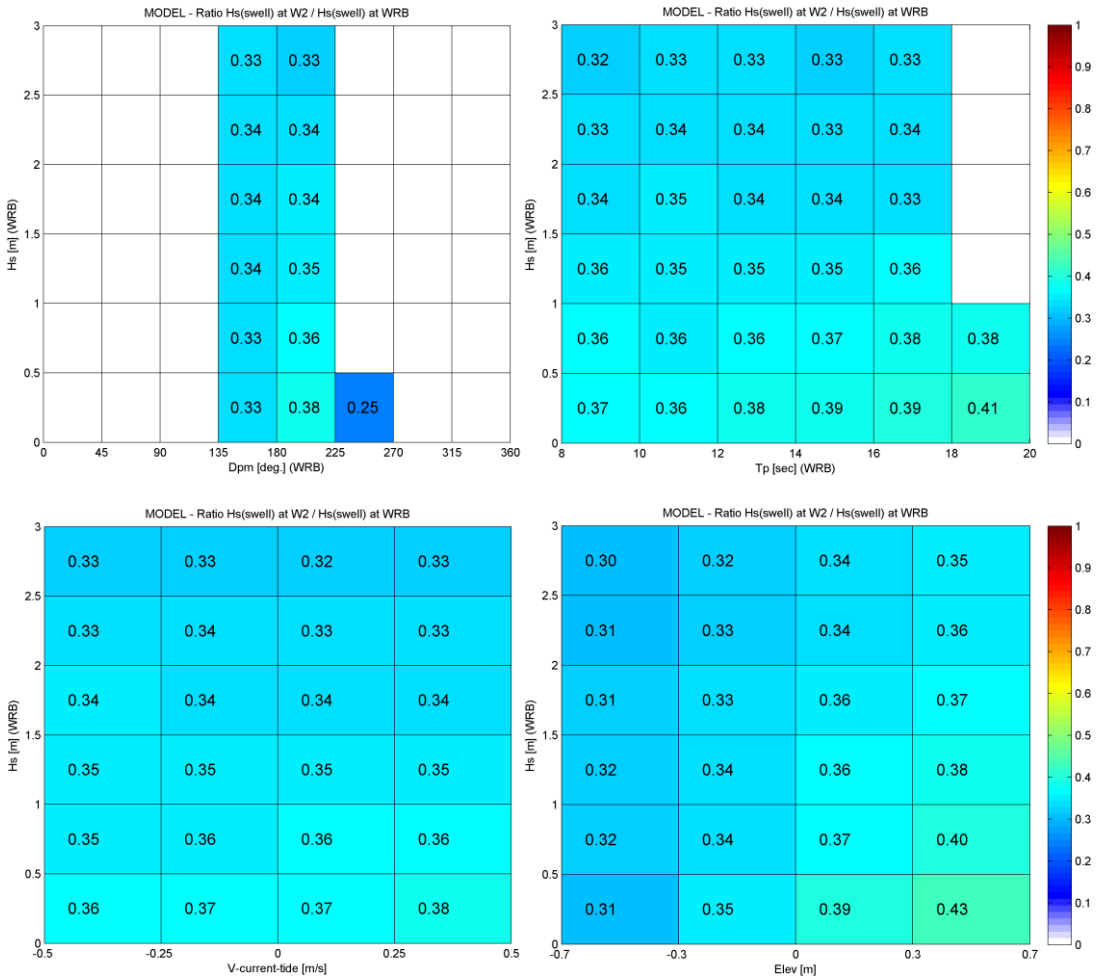

Figure 2.17 Model significant swell wave height ratios $H_{s\ swell}$ (W2) / $H_{s\ swell}$ (WRB) as a function of the wave direction and wave period at WRB (top), and tidal elevation and tidal flow through the entrance (bottom) at W2.

Draft for public consultation

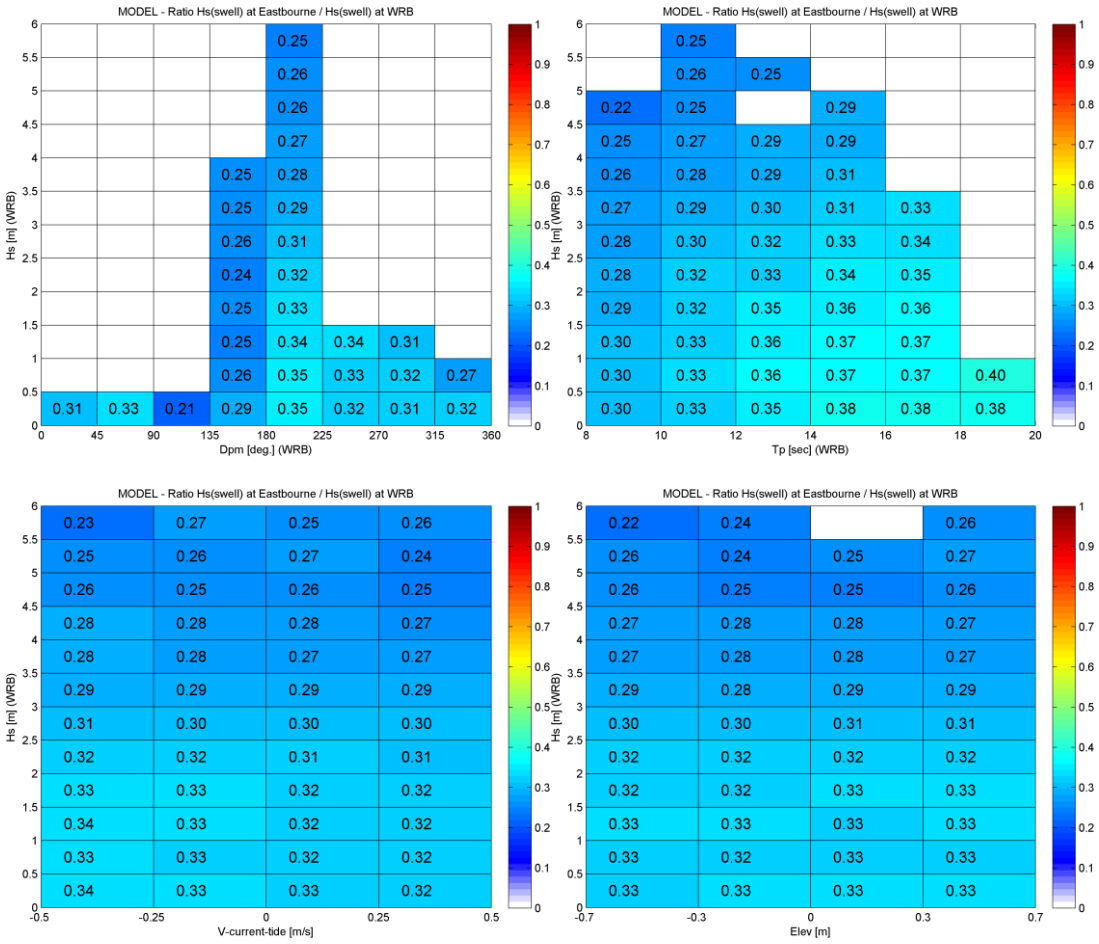

Figure 2.18 Model significant swell wave height ratios $H_{s\ swell}$ (E1) / $H_{s\ swell}$ (WRB) as a function of the wave direction and wave period at WRB (top), and tidal elevation and tidal flow through the entrance (bottom) at E1.

Draft for public consultation

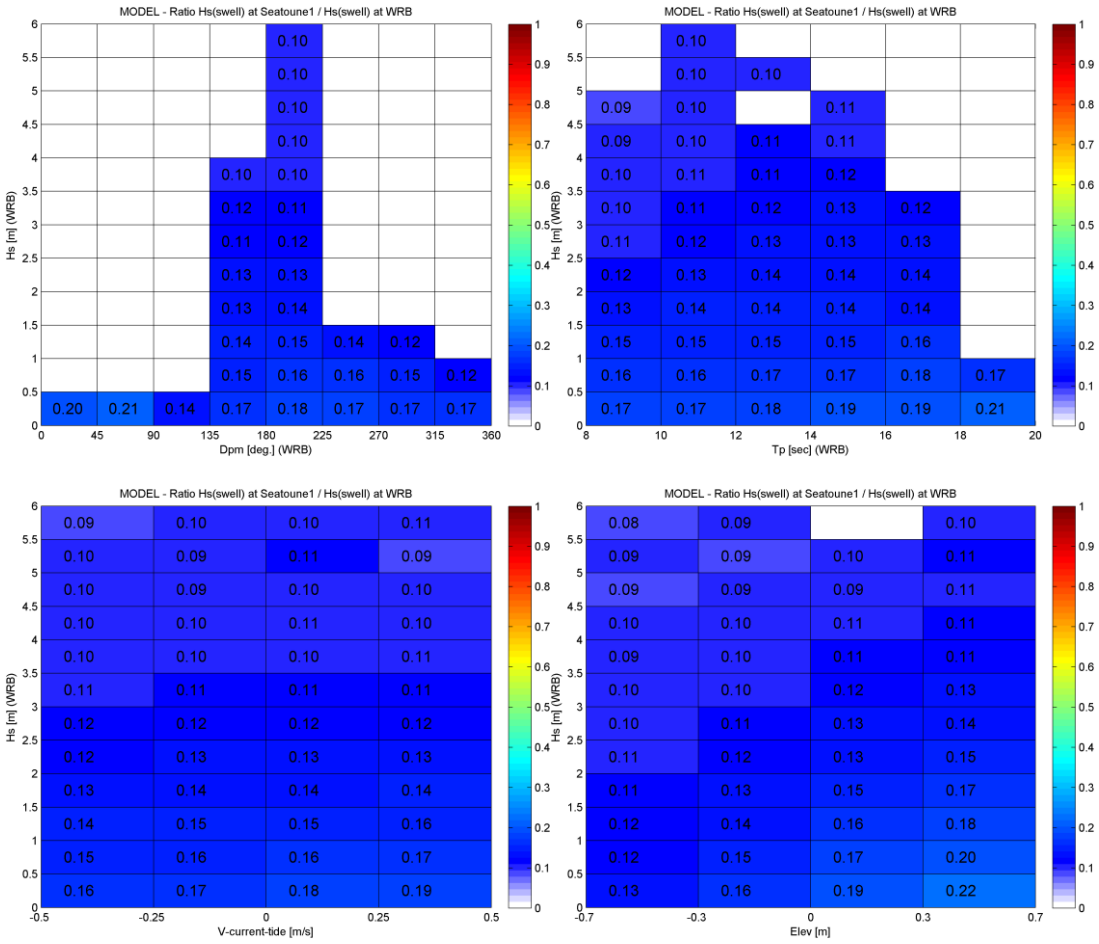

Figure 2.19 Model significant swell wave height ratios $H_{s\ swell}$ (S1) / $H_{s\ swell}$ (WRB) as a function of the wave direction and wave period at WRB (top), and tidal elevation and tidal flow through the entrance (bottom) at S1.

Draft for public consultation

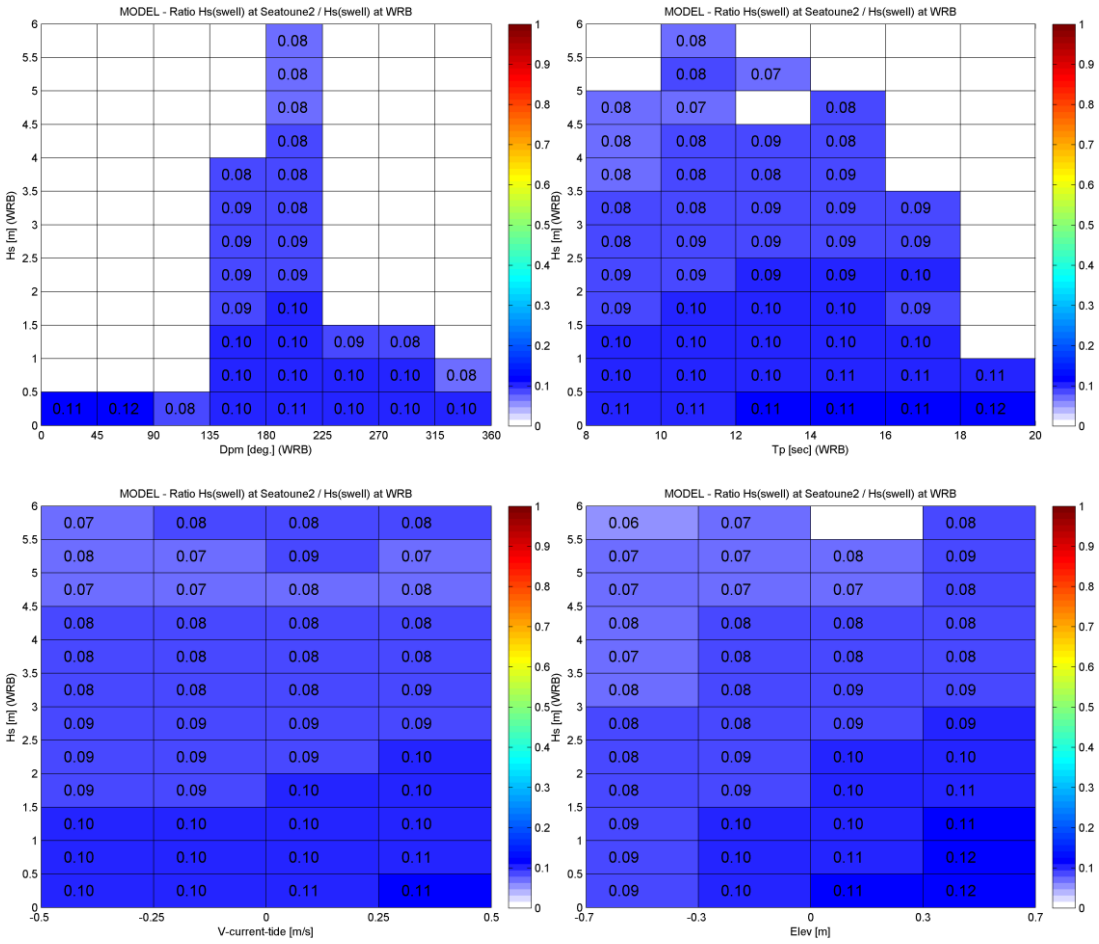

Figure 2.20 Model significant swell wave height ratios $H_{s\ swell}$ (S2) / $H_{s\ swell}$ (WRB) as a function of the wave direction and wave period at WRB (top), and tidal elevation and tidal flow through the entrance (bottom) at S2.

Draft for public consultation

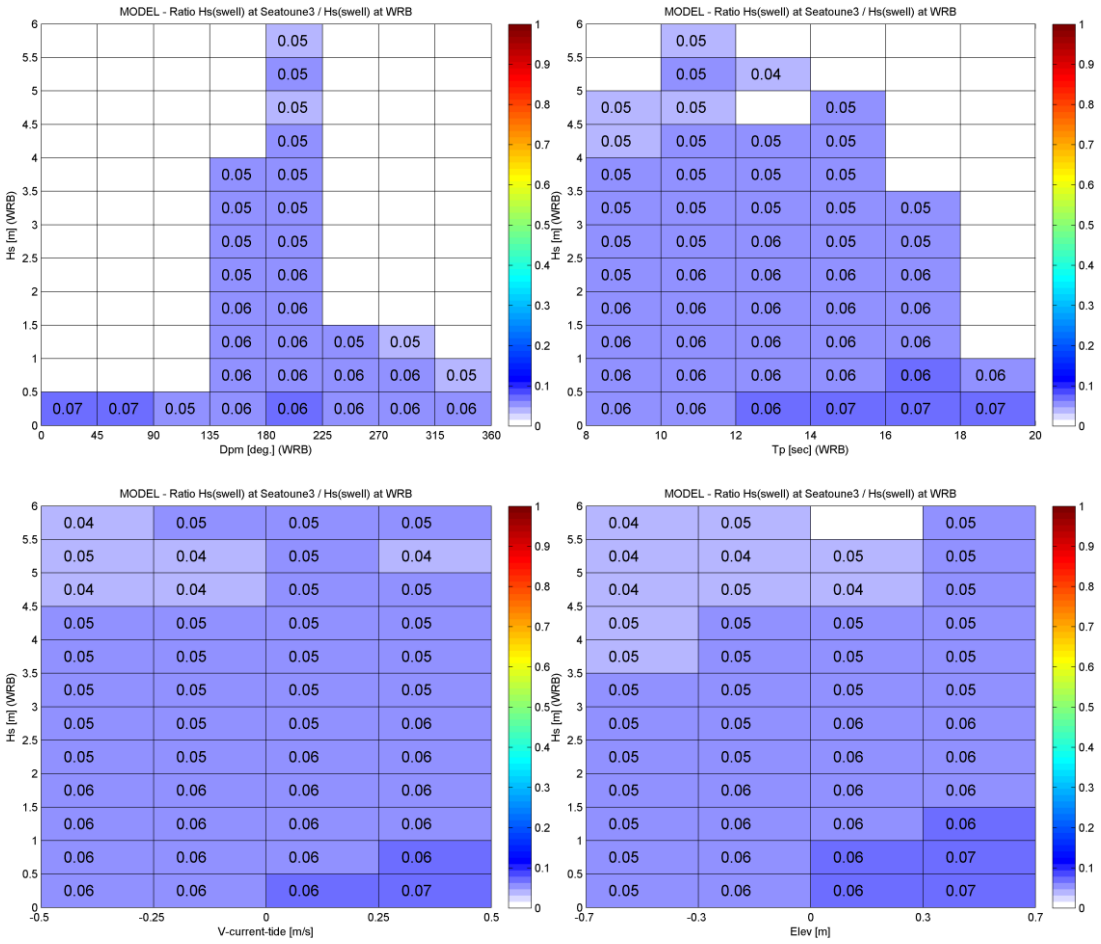

Figure 2.21 Model significant swell wave height ratios $H_{s\ swell}$ (S3) / $H_{s\ swell}$ (WRB) as a function of the wave direction and wave period at WRB (top), and tidal elevation and tidal flow through the entrance (bottom) at S3.

Draft for public consultation

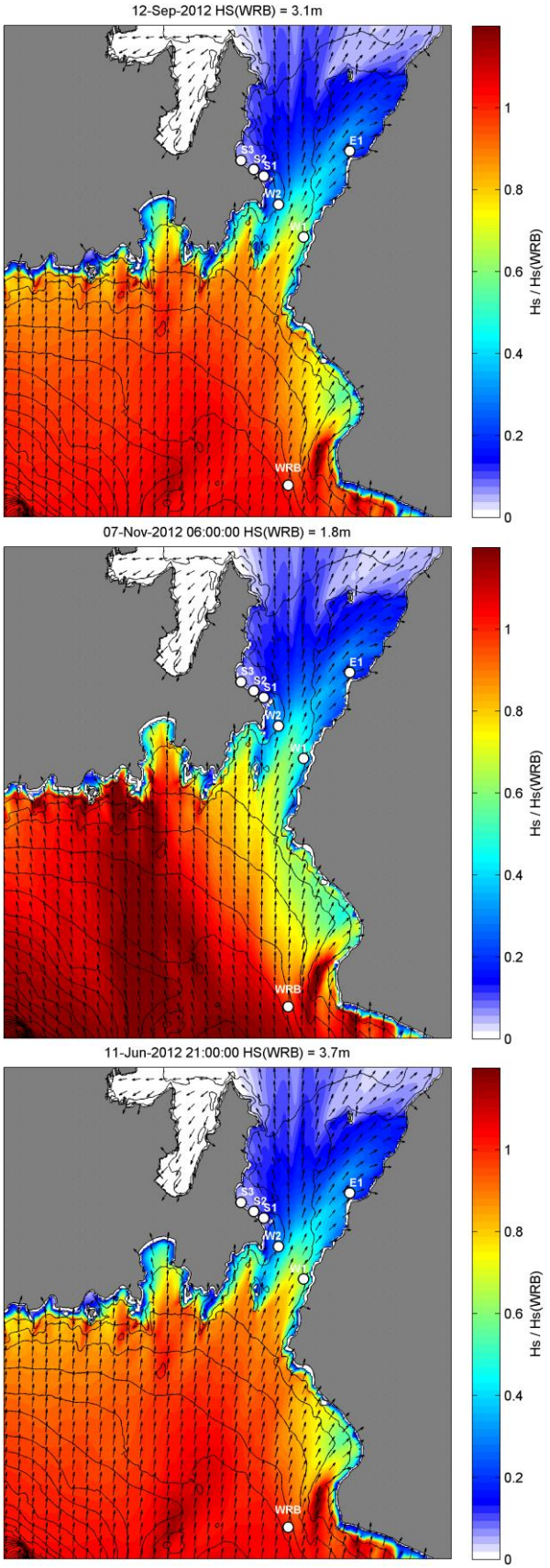

Figure 2.22 Snapshots of modelled wave height ratios throughout the Wellington Harbour entrance region for different types of wave conditions. The swell height ratio maps were obtained by normalisation to the swell height at site WRB.

Draft for public consultation

2.4. Hydrodynamics

2.4.1. The numerical model

The hydrodynamic modelling was undertaken with the finite element model SELFE. SELFE is a prognostic finite-element unstructured-grid model designed to simulate 3D baroclinic, 3D barotropic or 2D barotropic circulation. The barotropic mode equations employ a semi-implicit finite-element Eulerian-Lagrangian algorithm to solve the shallow-water equations, forced by relevant physical processes (atmospheric, oceanic and fluvial forcing). A detailed description of the SELFE model formulation, governing equations and numerics can be found in Zhang and Baptista (2008).

2.4.2. Model domains and boundary conditions

The anticlockwise motion of the tidal wave around New Zealand drives significant water levels gradients between the eastern and western sides of the country, which results in intense tidal flows throughout the Cook Strait. To effectively model this complex configuration, a two-level nesting approach was required to correctly resolve the tidal hydrodynamics of the Wellington Harbour region.

The MetOcean Solutions New Zealand tidal model (~5 km resolution) provided boundary conditions for a regional-scale SELFE model of the Greater Cook Strait region in which a high resolution domain of the Wellington Harbour region was subsequently nested (Figure 2.23). The national scale 2D tide model was established using an implementation of POM (Princeton Ocean Model) and has been validated at many locations throughout New Zealand.

The triangular mesh resolution of the SELFE domains ranged from 3-7 km for the Cook Strait domain and 20-220 m for the Wellington Harbour domain. This modelling technique applied higher resolution focusing on the shallower and complex areas, as well as over the proposed disposal ground. The bathymetry of the Wellington Harbour domain is shown in Figure 2.24. In these simulations, SELFE was run in full 2D barotropic mode over a 210-day period, with both tidal surface elevation and current velocities prescribed along the hemispheric (open) boundary. Tidal analysis was undertaken at each model node to provide tidal elevation and current amplitudes and phases of the dominant tidal constituents.

The residual flow regime throughout the region was extracted from a 10-year hindcast of all New Zealand that was implemented as a part of a national oceanic connectivity project for the Ministry of Primary Industries. This study included a comprehensive validation process using measured data from throughout New Zealand coastal and continental shelf zones. The model domain is shown on Figure 2.25; the resolution ranges from 5 km offshore to 500 m in the nearshore regions.

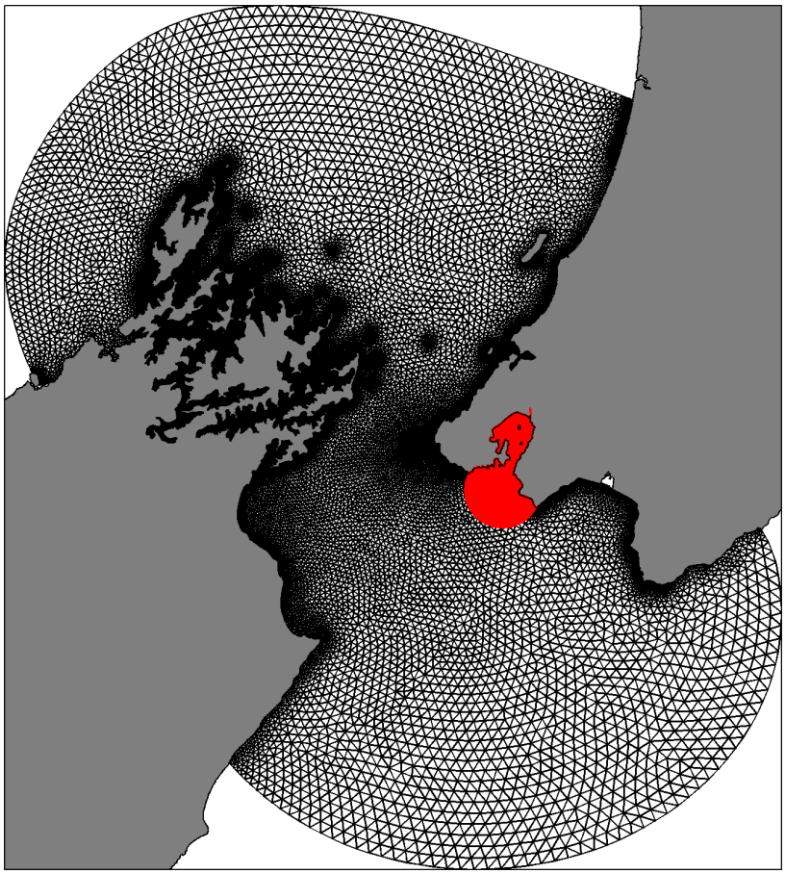

Figure 2.23 Greater Cook Strait (black) and Wellington Harbour (red) SELFE hydrodynamic model domains.

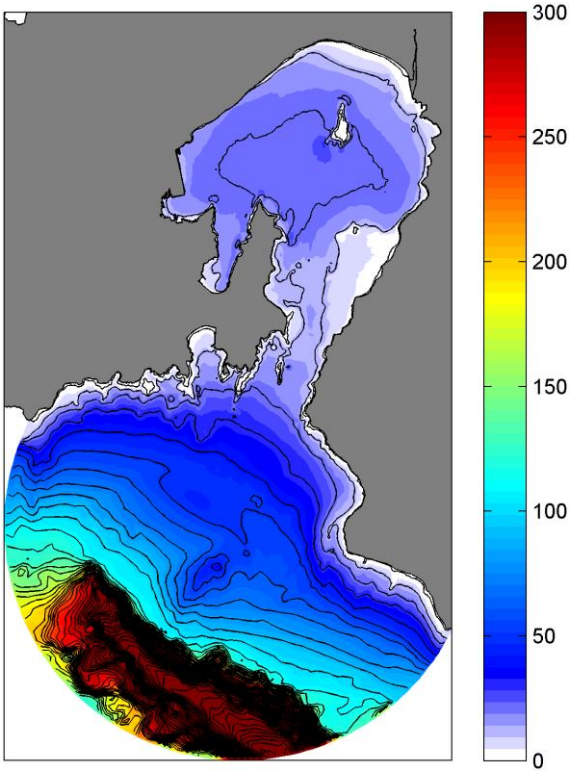

Draft for public consultation

Figure 2.24 Bathymetry (m) of the high-resolution SELFE domain for the Wellington Harbour.

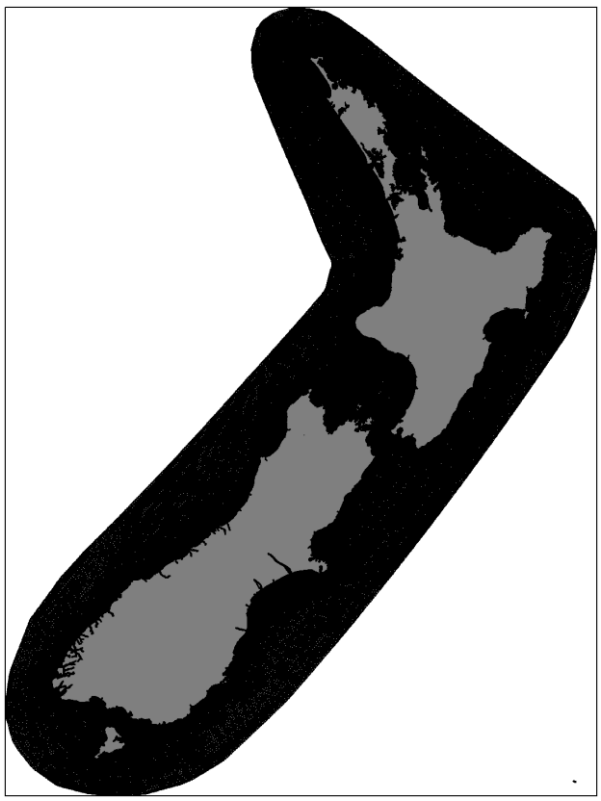

Figure 2.25 New Zealand SELFE domain used for the residual flow hindcast.

Minor edits required (e.g. decimal place after Fig. 2.23, 2.24, 2.25)

2.4.3. Hydrodynamic model validation

The tidal models were validated using archived measured datasets obtained from within the Wellington region, as well as from a contemporary measurement campaign from a current profiler deployment in the vicinity of the proposed disposal ground (Figure 2.26).

A comparison of the measured and modelled tidal flows along the main axis of the M2 constituents is provided in Figure 2.27, and tidal currents measured by the ADCP (Acoustic Doppler Current Profiler) are compared to model predictions in Figure 2.28. Modelled and measured amplitudes and phases of the dominant M2 and S2 tidal constituents are given in Table 2.2 and Table 2.3 respectively.

The agreement between model and measurements is generally very good in terms of circulation patterns and magnitudes. Some of the differences may be due to slight spatial offsets of flow patterns in the model, as well as uncertainties in the local bathymetry outside the entrance. Nonetheless, the general overall agreement indicates the model adequately resolves the complex tidal flow regime of the area.

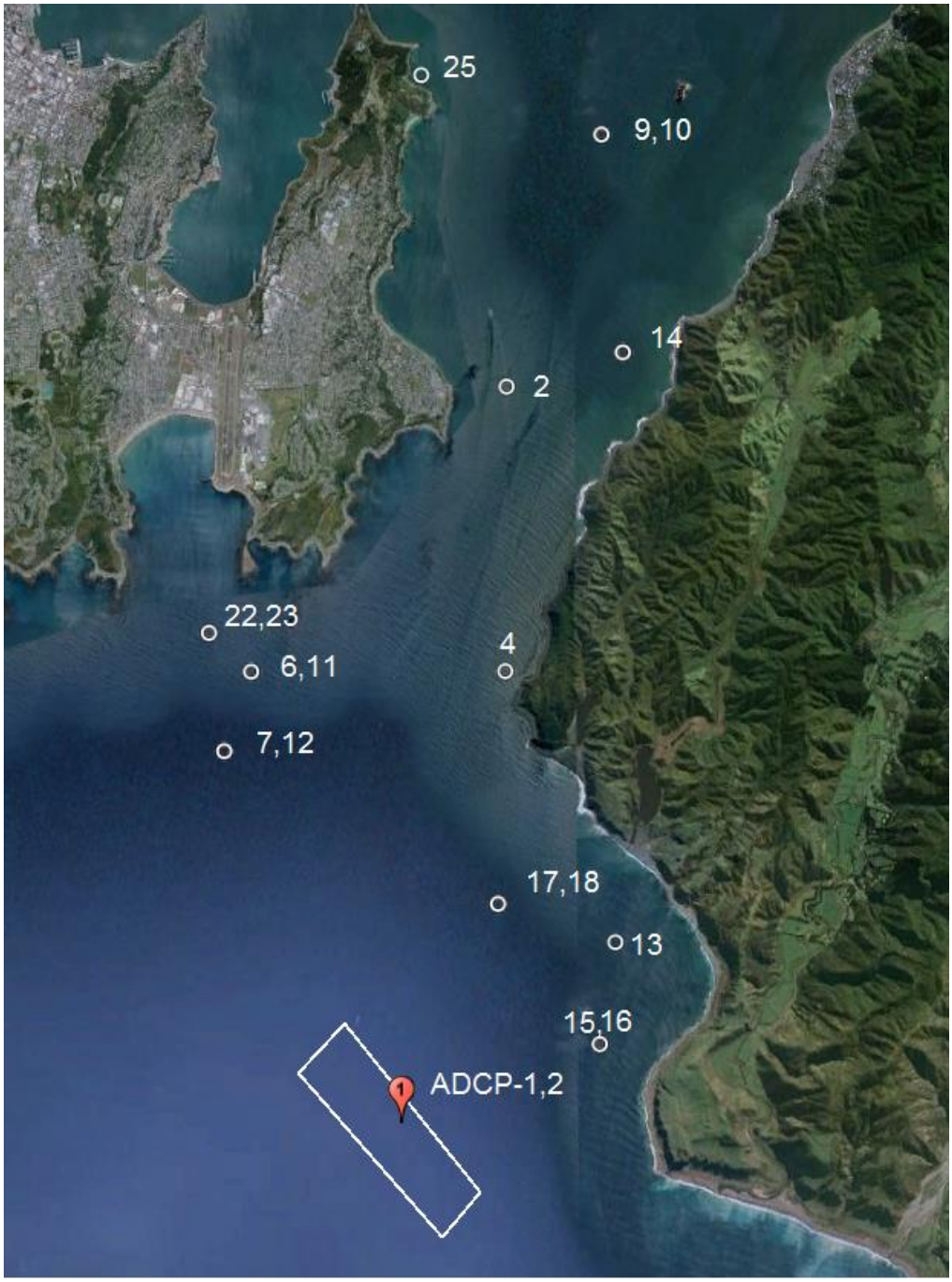

Figure 2.26 Tidal hydrodynamic model validation sites. The data location from 2014 is shown in red.

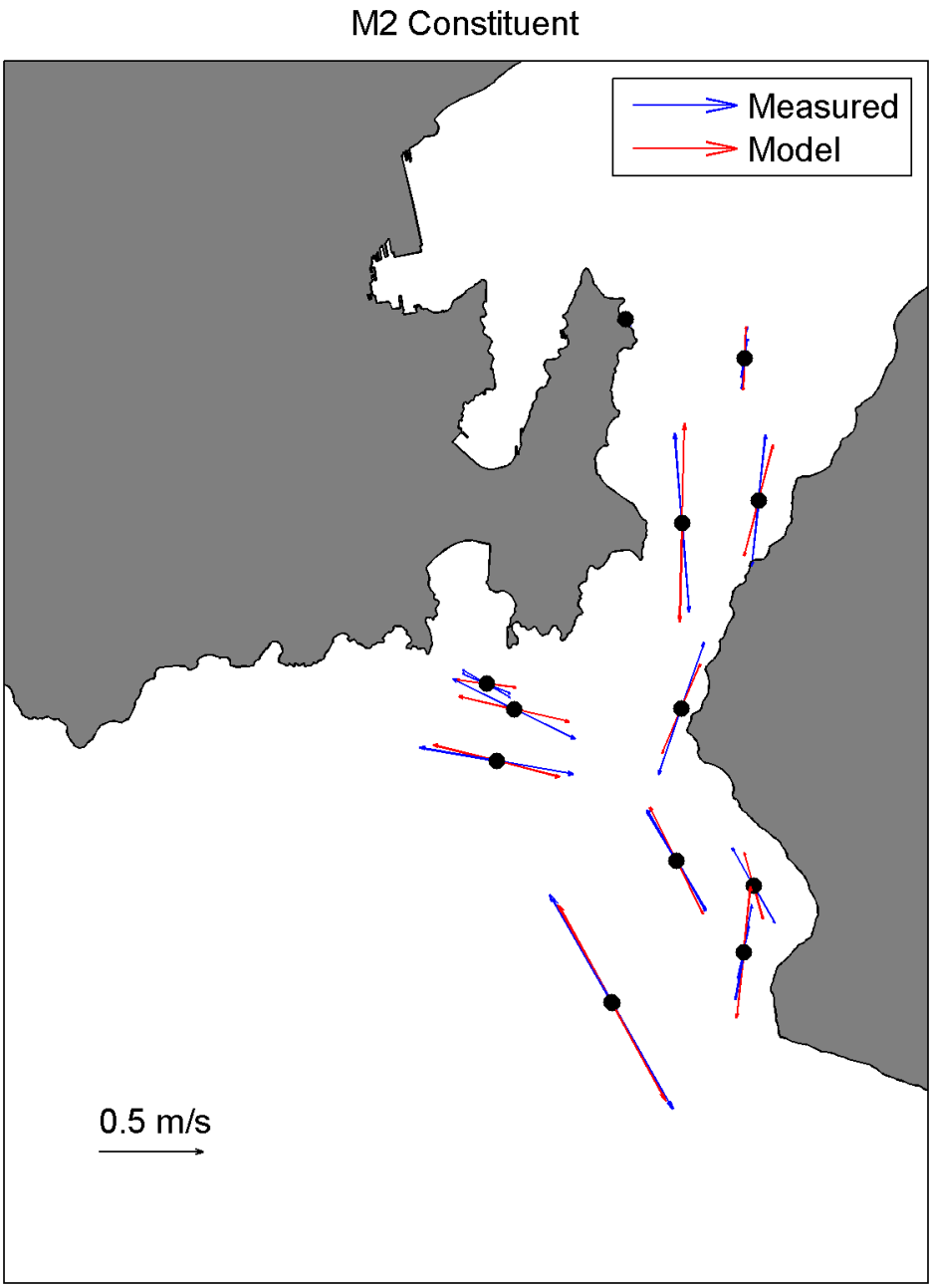

Figure 2.27 Measured and modelled tidal flows along the main axis of the M2 constituent at sites shown in Figure 2.26

Draft for public consultation

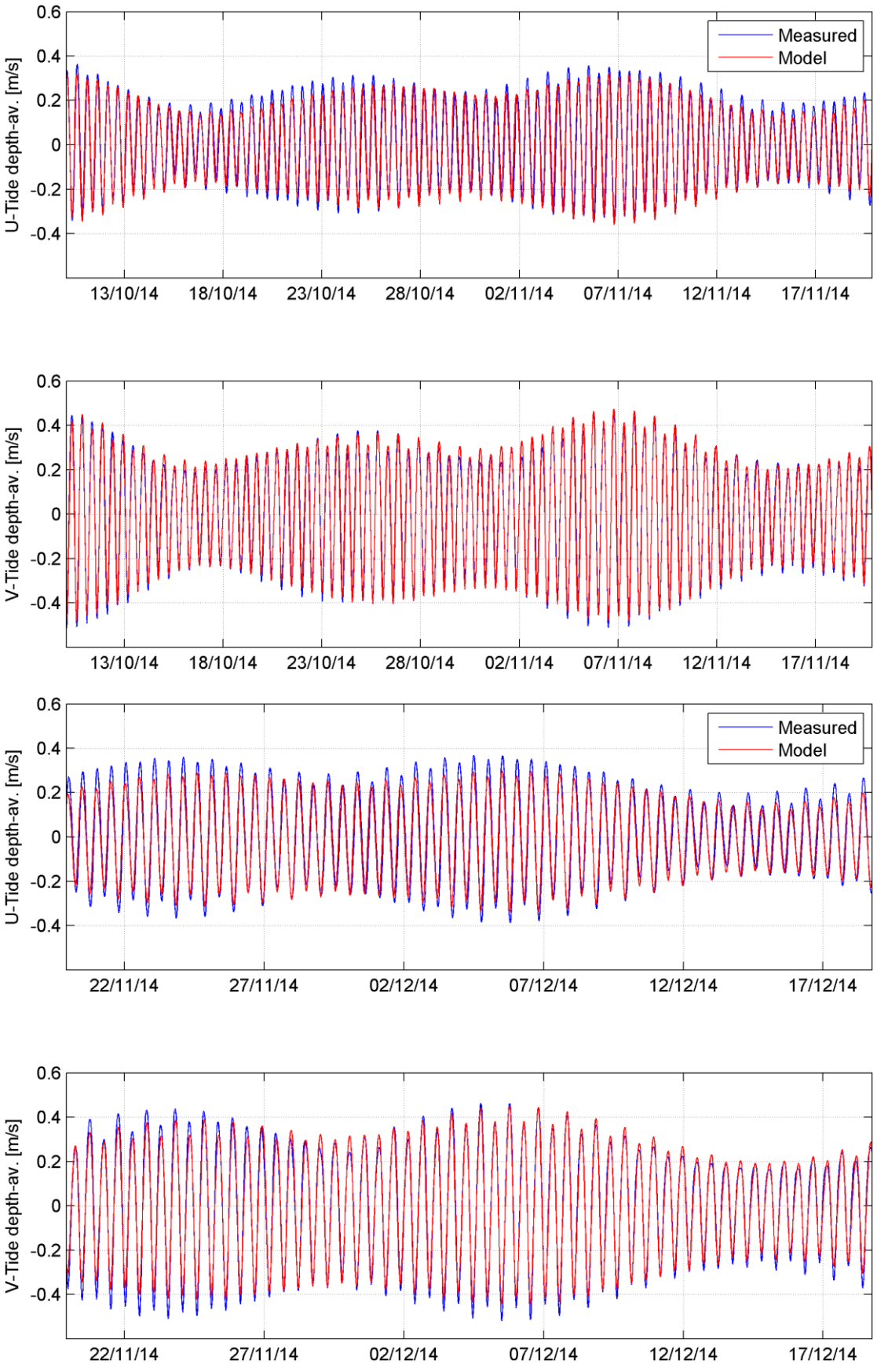

Figure 2.28 Measured and modelled tidal currents at the ADCP site within the proposed disposal ground (Figure 2.26) over the two deployment periods.

Table 2.2 Measured and modelled M2 constituent current amplitudes and phases at validation sites (Figure 2.26).

M2	u-amp [m/s]		v-amp [m/s]		u-pha [deg.]		v-pha [deg.]	
Site	**Meas.**	**Mod.**	**Meas.**	**Mod.**	**Meas.**	**Mod.**	**Meas.**	**Mod.**
2	0.0310	0.0109	0.2934	0.3259	299.66	73.00	67.00	61.00
4	0.0981	0.0830	0.2159	0.1460	69.63	66.00	80.12	76.00
6	0.2648	0.2375	0.0978	0.0417	12.36	15.00	113.81	124.00
7	0.3323	0.2725	0.0437	0.0526	39.02	21.00	188.24	164.00
9	0.0110	0.0064	0.1018	0.1045	53.01	18.00	51.44	62.00
10	0.0152	0.0064	0.0617	0.1045	76.00	18.00	63.33	62.00
11	0.2648	0.2375	0.0978	0.0417	12.36	15.00	113.81	124.00
12	0.3323	0.2725	0.0437	0.0526	39.02	21.00	188.24	164.00
13	0.0918	0.0397	0.1228	0.1083	354.68	1.00	168.79	183.00
14	0.0304	0.0627	0.2151	0.1813	345.97	61.00	67.57	60.00
15	0.0248	0.0308	0.0843	0.2159	114.48	156.00	173.73	183.00
16	0.0357	0.0308	0.1557	0.2159	155.08	156.00	168.70	183.00
17	0.1250	0.1142	0.1651	0.1742	352.71	19.00	183.81	193.00
18	0.1278	0.1142	0.1599	0.1742	348.73	19.00	181.46	193.00
22	0.1012	0.1263	0.0449	0.0126	295.52	349.00	106.91	90.00
23	0.1013	0.1263	0.0323	0.0126	295.10	349.00	118.23	90.00
25	0.0191	0.0077	0.0211	0.0143	127.76	186.00	314.40	11.00
ADCP-1	0.2576	0.2301	0.3414	0.3193	48.35	36.52	216.55	208.51
ADCP-2	0.2667	0.2306	0.3509	0.3170	45.69	36.47	214.42	208.37

Table 2.3 Measured and modelled S2 constituent current amplitudes and phases at validation sites (Figure 2.26).

S2	u-amp [m/s]		v-amp [m/s]		u-pha [deg.]		v-pha [deg.]	
Site	**Meas.**	**Mod.**	**Meas.**	**Mod.**	**Meas.**	**Mod.**	**Meas.**	**Mod.**
2	0.0089	0.0005	0.0146	0.0134	268.76	269.00	233.51	242.00
4	0.0038	0.0029	0.0154	0.0082	34.88	180.00	73.86	177.00
6	0.0443	0.0388	0.0109	0.0058	4.95	17.00	99.90	164.00
7	0.0491	0.0505	0.0064	0.0124	22.48	26.00	234.78	195.00
9	0.0038	0.0003	0.0099	0.0044	246.35	189.00	268.33	246.00
10	0.0042	0.0003	0.0127	0.0044	298.27	189.00	324.85	246.00
11	0.0443	0.0388	0.0109	0.0058	4.95	17.00	99.90	164.00
12	0.0491	0.0505	0.0064	0.0124	22.48	26.00	234.78	195.00
13	0.0180	0.0080	0.0309	0.0247	312.97	5.00	163.65	198.00
14	0.0123	0.0026	0.0153	0.0076	151.21	247.00	214.81	245.00
15	0.0094	0.0074	0.0372	0.0473	165.07	167.00	190.29	198.00
16	0.0267	0.0074	0.0696	0.0473	168.31	167.00	181.17	198.00
17	0.0477	0.0243	0.0817	0.0413	24.92	28.00	221.34	213.00
18	0.0542	0.0243	0.0701	0.0413	2.77	28.00	200.98	213.00
22	0.0191	0.0200	0.0139	0.0019	279.81	356.00	69.09	142.00
23	0.0174	0.0200	0.0099	0.0019	261.29	356.00	52.05	142.00
25	0.0032	0.0003	0.0028	0.0006	181.93	3.00	348.13	182.00
ADCP-1	0.0812	0.0504	0.0871	0.0730	65.55	55.92	244.44	225.77
ADCP-2	0.0971	0.0505	0.1148	0.0724	85.30	55.78	251.00	225.65

Draft for public consultation

3. SEDIMENT DYNAMICS MODELLING METHODS

3.1. Model description

The Delft3D numerical model system (e.g. Lesser et al., 2004) was used for the numerical simulations of the coupled wave, current and sediment transport. The modelling system consists of three modules:

- Delft3D-WAVE is a nearshore wave propagation model which simulates the evolution of the incoming wave field.
- Delft3D-FLOW is a multi-dimensional (2D or 3D) hydrodynamic model which calculates non-steady flows and transport phenomena that result from tidal, meteorological and wave forcing.
- Delft3D-MOR computes the sediment transport fluxes and the resulting morphodynamic evolution based on the combined action of currents and waves.

The three modules are fully coupled to simulate the morphodynamic feedbacks. Every coupling time step, a new flow field (depth-averaged currents and water levels) is supplied from the hydrodynamic module to the wave module. The wave module propagates waves within the domain, accounting for the ambient hydrodynamics, and in turn provides radiation stress fields and basic wave parameters that will be used as forcing by the hydrodynamic module. Delft3D-MOR computes sediment transport based on the combined wave and current action, and updates the seabed morphology, thus affecting subsequent wave and flow computations.

Note that the updating of the seabed morphology can be switched off. In that case, the sediment transport fluxes are computed, but the model bathymetry is left unchanged. This is a useful option for studying general sediment transport pathways, without the unrealistic divergence that can occur due to uncorrected non-linear feedbacks between waves, currents and morphology.

3.1.1. Delft3d-WAVE

The third-generation SWAN model (Simulating WAves Nearshore) is used as the wave module (Holthuijsen et al., 2007). SWAN computes the evolution of random, short-crested waves in coastal regions with deep, intermediate and shallow water depths. The SWAN model accounts for (refractive) propagation due to depth and current and can represent the processes of wave generation by wind, dissipation due to white-capping, bottom friction and depth-induced wave breaking, and non-linear wave-wave interactions explicitly with state-of-the-art formulations (Deltares, 2013b).

For the present work, the local wave model boundary conditions are nested 2D spectral boundaries obtained from a regional scale grid forced either by representative wave events (i.e. accelerated morphological simulations) or real hindcast conditions (i.e. real-time simulations). The nesting allows the retention of spatial variability in the incident wave field due to large scale regional refraction and sheltering effects. Bottom friction was modelled using the formulation of Collins (1972) and the default coefficient value was set to 0.015. Dissipation by friction, wave breaking and whitecapping was applied

Draft for public consultation

in the model. In these simulations, the wave conditions were updated every 60 minutes using the current field provided by the hydrodynamic module.

3.1.2. Delft3d-FLOW

The hydrodynamic module Delft3D-FLOW solves the Navier-Stokes equations for an uncompressible fluid under the shallow water and Boussinesq assumptions. The system solves the horizontal equations of motion, the continuity equation, the transport equations for conservative constituents, and a turbulence closure scheme. The details of equations and associated sub-models are fully described in Lesser et al. (2004) and the Delft3D-FLOW user manual (Deltares, 2013b).

The model was run in 2D mode, thus providing water levels and depth-averaged flows at each computational time step. The 2D mode is appropriate here as the channel and surrounding water bodies are expected to be relatively well-mixed. Bed shear stresses are computed using a standard quadratic friction law. The non-linear enhancement of the bed shear stress in the presence of waves was taken into account by means of the wave-current interaction model of Fredsoe (1984). Turbulence effects are modelled using constant background horizontal and vertical eddy viscosity and eddy diffusivity coefficients. Horizontal background eddy viscosity is set 3 $m^2.s^{-1}$ while diffusivity is equal to 1 $m^2.s^{-1}$. A value of $10e^{-6}$ is used for the vertical background viscosity and diffusivity.

Current and water elevation boundaries were prescribed at the boundaries of the different grids implemented. The tidal constituents prescribed at the model boundaries were generated from a high resolution tidal model (Section 2.4).

A time step of 3 s was used for the Delft3D-FLOW simulations, equivalent to maximum Courant numbers of less than 8. The Courant number is a numerical stability criterion that needs to be less than 10 in Delft3D-FLOW (Deltares, 2013a).

3.1.3. Delft3D-MOR

The module Delft3D-MOR combines the information provided by the flow and wave modules to compute the sediment transport fluxes at each computational time step. The seabed level can then be updated as a result of the sediment sink and sources terms and computed transport gradients.

The present study considers both cohesive sediments (mud) and non-cohesive sediments (gravel, coarse sand and medium sand) for the channel dredging simulations and only non-cohesive (medium sand) for the offshore disposal modelling.

The modelling and transport of cohesive sediment requires an approach that is fundamentally different to mobile sand transport. For very fine sediment size (i.e. silt or clay-sized), the inter-particles forces due to ionic charges becomes significant relative to the gravitational forces which strongly dominate the sand transport processes. As a result, processes including flocculation, hindered settling, and bed consolidation have important roles in the movement of cohesive particles. Description of the associated sub-models are included the Delft3D FLOW manual (Deltares, 2013a).

Draft for public consultation

The cohesive sediment transport is calculated by solving the advection-diffusion equation for the suspended sediment. Note that no bed load transport is considered for the cohesive sediment in Delft3D.

$$\frac{\partial C}{\partial t}+\frac{\partial uC}{\partial x}+\frac{\partial vC}{\partial y}+\frac{\partial (w-w_s)C}{\partial z}= \frac{\partial}{\partial x}\left(\varepsilon_{s,x}\frac{\partial C}{\partial x}\right)+\frac{\partial}{\partial y}\left(\varepsilon_{s,y}\frac{\partial C}{\partial y}\right)+\frac{\partial}{\partial z}\left(\varepsilon_{s,z}\frac{\partial C}{\partial z}\right) \quad (3.1)$$

where,

E	Mass concentration [kg.m^{-3}]
u, v, w	Velocity components [m.s^{-1}],
$\varepsilon_{s-x,y,z}$	Eddy diffusivities in the x,y,z directions [m^2.s^{-1}],
w_s	Sediment settling velocity [m. s^{-1}].

Sediment fluxes between the water phase and the bed are calculated using the Partheniades-Krone formulations (Partheniades,1965).

$$E = M.S(\tau_{cw}, \tau_{cr,erosion}) \quad (3.2)$$

$$D = w_s.c_b.S(\tau_{cw}, \tau_{cr,deposition}) \quad (3.3)$$

$$c_b = c(z = \frac{\Delta z_b}{2}, 2) \quad (3.4)$$

where,

E	Erosion flux [kg/m^{-2}.s^{-1}]
M	User-defined erosion parameter [kg/m^{-2}.s^{-1}]
$S(\tau_{cw}, \tau_{cr,erosion})$	Erosion step function:

$$S(\tau_{cw}, \tau_{cr,erosion}) = \begin{cases} \left(\frac{\tau_{cw}}{\tau_{cr,erosion}} - 1\right), & when\ \tau_{cw} > \tau_{cr,erosion} \\ 0 & ,when\ \tau_{cw} > \tau_{cr,erosion} \end{cases} \quad (3.5)$$

D	Deposition flux [kg/m^{-2}.s^{-1}]
M	User-defined erosion parameter [kg/m^{-2}.s^{-1}]
w_s	Sediment settling velocity [m. s^{-1}].
c_b	Average sediment concentration near bottom [kg.m^{-3}]

$$S(\tau_{cw}, \tau_{cr,deposition}) = \begin{cases} \left(\frac{\tau_{cw}}{\tau_{cr,deposition}} - 1\right), & when\ \tau_{cw} > \tau_{cr,erosion} \\ 0 & ,when\ \tau_{cw} > \tau_{cr,erosion} \end{cases}$$

Draft for public consultation

(3.6)

τ_{cw}	Maximum bed shear stress due to current and waves.
$\tau_{cr,erosion}$	User defined critical erosion shear stress [N. m^{-2}]
$\tau_{cr,deposition}$	User defined critical deposition shear stress [N. m^{-2}]

Erosion and deposition terms are finally used as bed boundary conditions;

$$-w_s.C - \varepsilon_{s,z}\frac{\partial C}{\partial z} = D - E\ ,\ at\ z = z_b \quad (3.7)$$

The formulation requires the specification of erosion and deposition shear stresses. The critical erosion shear stress is a widely accepted concept that is the shear stress magnitude that must be exceeded before sediment motion is initiated. In contrast, the existence of a critical deposition shear stress, which is a threshold shear stress over which no deposition can occur, is still debated. In the present study the critical deposition shears stress was set to a very large value of 1000 N.m^{-2}, which is never exceeded, so that deposition can occur continuously and without any restrictions related to the ambient shear stress.

3.1.4. Model domains

Considering the different expectations related to the dredging and discharge operations, the sediment transport modelling was performed using two independent grids combined with two different configurations of the model (IM01 & IM02).

- **Disposal ground modelling (IM01)**

Delft3D – FLOW model was implemented on a curvilinear grid focusing on the proposed disposal ground (Figure 3.1).

The domain includes the coastline from Sinclair Head to Turakirae Head and extends approximately 4 km offshore to around 120 m depth. These limits of the domain allow the model to capture the kinetic motion of the tidal flows incoming and outgoing throughout the Cook Strait, while preserving a relatively narrow depth range and thereby avoid numerical instability in the depth average simulations. Grid resolution ranges from 40-210 m, with higher resolution focused over the proposed disposal ground.

Draft for public consultation

Delft3D – WAVE model was implemented on the same local curvilinear grid as defined for Delft3D – FLOW model but considering a nesting approach with a coarser grid (Figure 3.2) in order to correctly reproduce the spectral wave transformation during the propagation of wave energy from deep to shallow water.

- **Channel modelling (IM02)**

A very high resolution curvilinear grid (see Figure 3.3) was defined in Delft3D – FLOW to perform the numerical modelling of the morphological changes induced by the channel dredging for two different channel design (100% and 98% optimisation channel), with resolution ranging from 15 m in the channel to 200 m in Fitzroy Bay (Figure 3.5 and Figure 3.6). The domain extends from Taputeranga Island to Pencarrow Head and Pencarrow Head to Kau Bay. The boundaries of the domain are located in areas of relative homogenous depths, sufficiently distant from the channel to limit numerical boundary artefact effects. Both pre- and post-dredged channel bathymetries were considered.

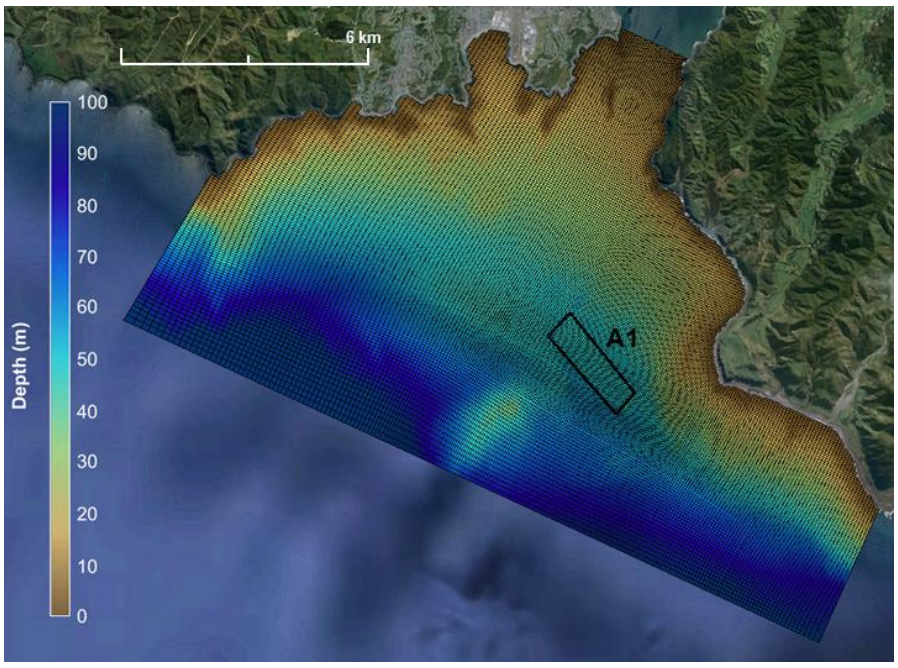

Figure 3.1 Delft3D – FLOW model grid for primary disposal ground modelling (GRID01). The proposed disposal ground area is shown in black (A1). The bathymetry interpolated on the Delft3D - FLOW grid is defined by patch colours following a positive downward convention.

Draft for public consultation

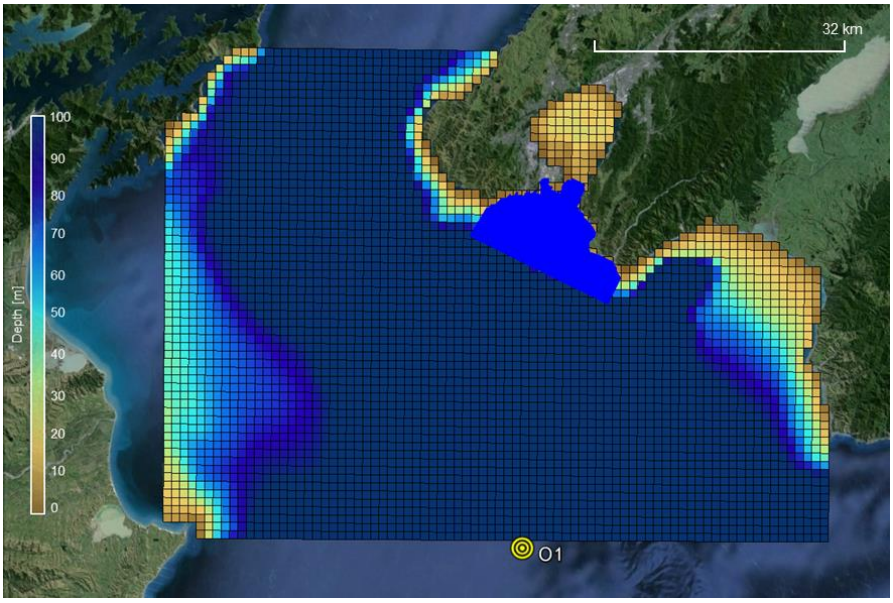

Figure 3.2 Delft3D –WAVE model grid for the proposed disposal ground modelling. Location (O1) for representative wave climate is shown at the centre of the southern boundary. The bathymetry interpolated on the Delft3D - WAVE grid is defined by patch colours following a positive downward convention.

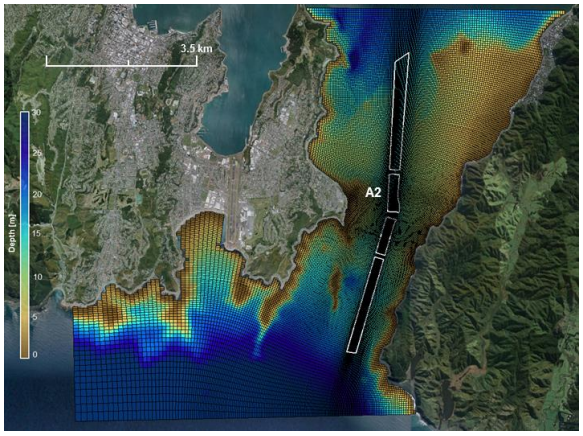

Figure 3.3 Delft3D – FLOW model grid for dredged channel modelling (GRID02). The dredging area is shown in white (A2). The bathymetry interpolated on the Delft3D - FLOW grid is defined by patch colours following a positive downward convention.

Draft for public consultation

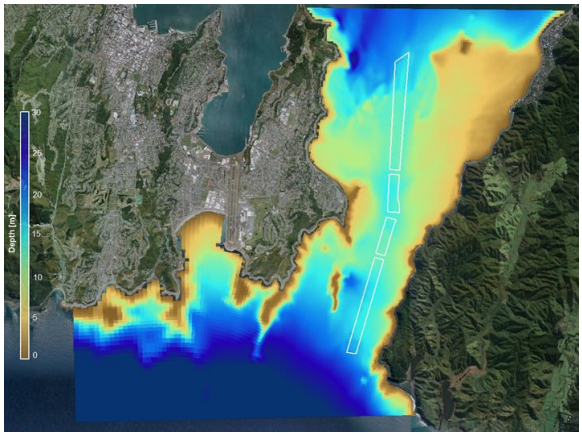

Figure 3.4 Pre-dredging bathymetry interpolated on Delft3D – FLOW grid. Depth is defined by patch colours following a positive downward convention.

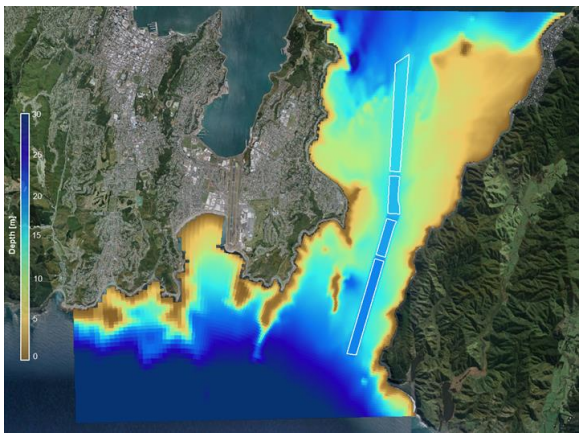

Figure 3.5 Post-dredging bathymetry (100% optimisation channel) interpolated on Delft3D – FLOW grid. Depth is defined by patch colours following a positive downward convention.

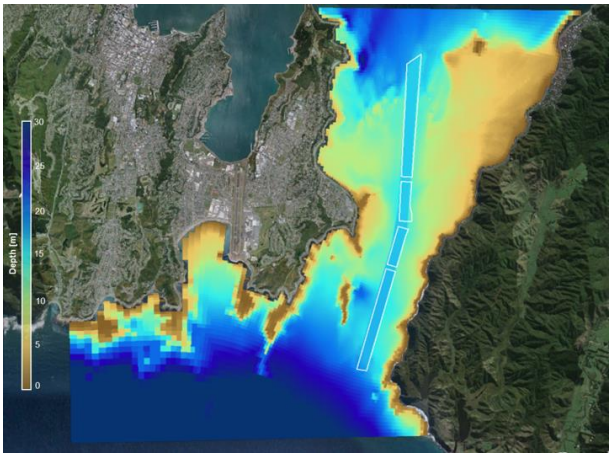

Figure 3.6 Post-dredging bathymetry (98% optimisation channel) interpolated on Delft3D – FLOW grid. Depth is defined by patch colours following a positive downward convention.

Draft for public consultation

3.1.5. Model setup

The various models require the input of a range of numerical and physical parameters that eventually control the sediment movement. A number of calibration parameters governing the sediment transport regime and resulting sedimentation patterns have been identified based on a careful sensitivity analysis of the models including erosion factors, sediment transport formulations and friction coefficients. The configurations of Delft3D for the disposal ground modelling (IM01) and the dredge channel modelling (IM02) are presented in Table 3.1 and Table 3.2, respectively. Note that the formulation integrating the horizontal diffusivity coefficient in Delft3D (Dicouv = 10, default value) is different from the formulation used in the particle track model. A factor of 5 – 10 between the horizontal eddy viscosity coefficient and the horizontal eddy diffusivity is usually prescribed in Delft3D.

The initial sediment layer thickness and the spatial distribution of sediments for the channel modelling was defined on the Delft3D – FLOW grid from different sources of information, such as backscatter data, eco-sounder data and digitalized maps of spatial distribution (Pallentin et al., 2009; Aaron and Lewis, 1993). In Delft3D-MOR, the sediment distribution is defined for each class. A unique mixed sediment layer was defined considering the proportion of the different sediment classes. Spatial distributions of sediments are shown in Figure 3.7.

Table 3.1 Delft3D model parameters for IM01.

Parameter	Description	Value
Wave		
BedFriction	Seabed friction formulation	Collins (1972)
BedFricCoef	Collins's frictions coefficient	0.015
Breaking	Depth induced breaking model	TRUE (Battjes and Janssen,1978)
BreakAlpha	Rate of dissipation	1
BreakGamma	Breaker parameter Hmax/h	0.73
WaveSetup	Wave-induced setup model	TRUE
Whitecapping	Dissipation by whitecapping	TRUE
Hydrodynamics		
Dt	Computational time step	3 s.
DryFlc	Minimum depth for drying/flooding	0.1
Vicouv	Horizontal background eddy viscosity	1
Dicouv	Horizontal background eddy diffusivity	10
Vicoww	Vertical background eddy viscosity	1.00E-06
Dicoww	Vertical background eddy diffusivity	1.00E-06
Rouwav	Model for bottom stress formulation due to combined wave and current action	#FR84# (Fredsoe, 1984)
Roumet Ccofu,Ccofv	Manning Coefficient	#M# 0.026
Sediment transport		
Non – Cohesive Sediment		
RhoSol	Sediment density [kg/m3]	2650
SedTyp	Sediment type	sand
SedDia	Median sediment diameter (D50)	1.0E-04 2.0E-04 3.0E-04
CDryB	Dry bed density [kg/m3]	1600
IniSedThick	Initial sediment layer thickness [m]	4.50 (Disposal area)
FacDSS	FacDss * SedDia = initial suspended sediment diameter.	1
IFORM	Sediment transport formulation	-2 (Van Rijn, TR2000)

Table 3.2 Delft3D model parameters for IM02.

Parameter	Description	Value
Wave		
BedFriction	Seabed friction formulation	Collins Collins (1972)
BedFricCoef	Collins's frictions coefficient	0.015
Breaking	Depth induced breaking model	TRUE (Battjes and Janssen,1978)
BreakAlpha	Rate of dissipation	1
BreakGamma	Breaker parameter Hmax/h	0.73
WaveSetup	Wave-induced setup model	TRUE
Whitecapping	Dissipation by whitecapping	TRUE
Hydrodynamics		
Dt	Computational time step	3 s.
DryFlc	Minimum depth for drying/flooding	0.1
Vicouv	Horizontal background eddy viscosity	1
Dicouv	Horizontal background eddy diffusivity	10
Vicoww	Vertical background eddy viscosity	1.00E-06
Dicoww	Vertical background eddy diffusivity	1.00E-06
Rouwav	Model for bottom stress formulation due to combined wave and current action	#FR84# (Fredsoe, 1984)
Roumet Ccofu,Ccofv	Manning Coefficient	#M# 0.026
Sediment transport		
Non – Cohesive Sediment		
RhoSol	Sediment density [kg/m3]	2650
SedTyp	Sediment type	Gravel, Coarse & Fine sand
SedDia	Median sediment diameter (D50)	2.0E-03, 8.0E-04, 1.8E-04
CDryB	Dry bed density [kg/m3]	1600
IniSedThick	Initial sediment layer thickness [m]	Non - homogeneous
FacDSS	FacDss * SedDia = initial suspended sediment diameter.	1
IFORM	Sediment transport formulation	-2 (Van Rijn, TR2000)
Cohesive Sediment		
RhoSol	Sediment density [kg/m3]	2650
SedTyp	Sediment type	Mud
TcrSed	Critical bed shear stress for sedimentation	1000 N/m^2
TcrEro	Critical bed shear stress for erosion	0.0484 N/m^2

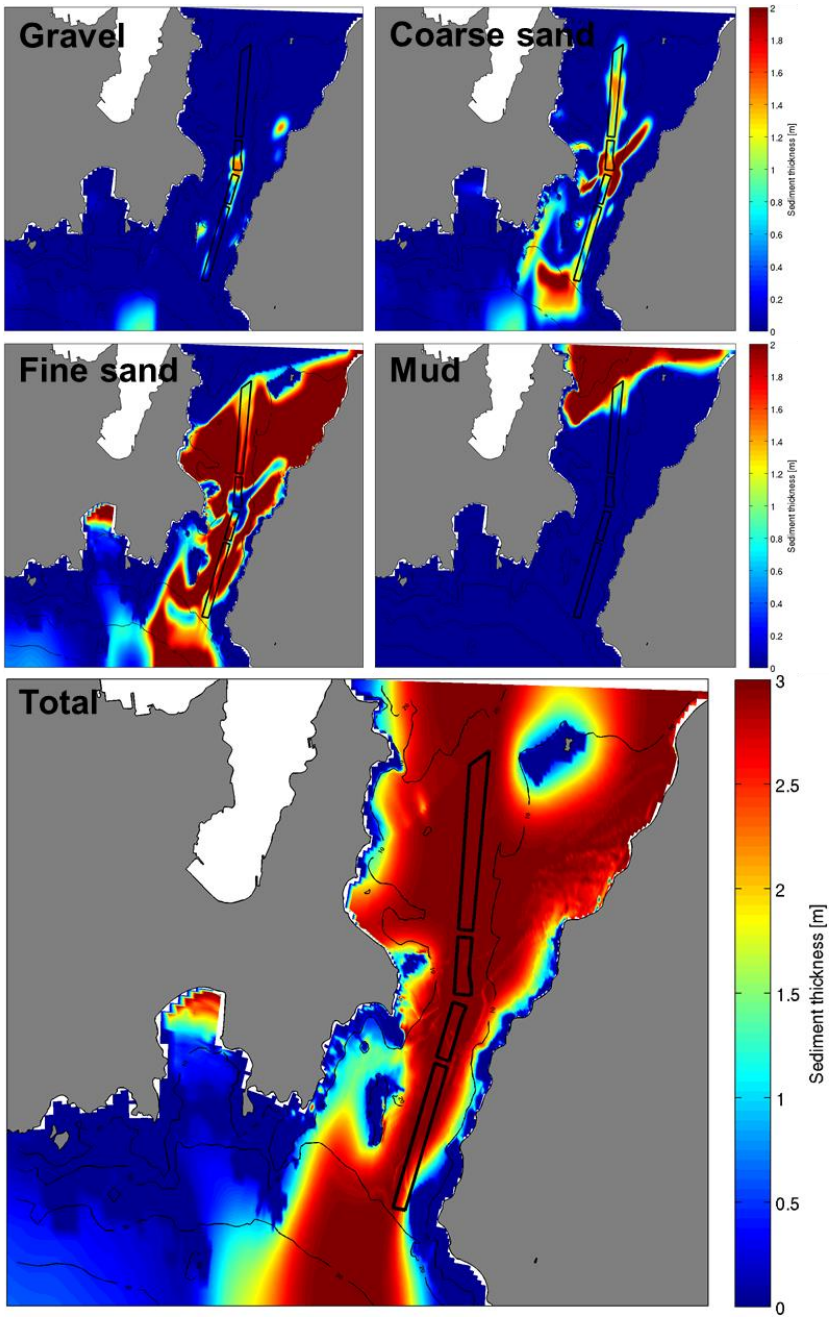

Figure 3.7 Sediment thickness of gravel, coarse sand, fine sand, mud and total interpolated on the Delft3D-FLOW grid in the channel. Zero sediment thickness indicates a rocky area where no erosion is possible.

Draft for public consultation

3.2. Medium-term morphological modelling

The main challenge with applying process-based models to predict morphological evolution is that the morphology of coastal systems generally develops over time scales several orders of magnitude larger than the time scale of the hydrodynamic fluctuations driving the sediment transport (i.e. hours to days versus years to decades and more). This means that a model system that is able to predict the time series of instantaneous hydrodynamics and sediment transport will require an unfeasibly long period of time to compute a multi-year real time simulation. Instead, several strategies are commonly used to simplify and accelerate the modelling of medium to long term morphological evolution (i.e. de Vriend et al., 1993, Roelvink, 2006). The approach employed here combines the reduction of the input forcing (i.e. wave, tides, current residuals) with the use of morphological factors, which is one of the most commonly applied method (e.g. Dastgheib, 2012; Grunnet et al., 2004; Lesser, 2009).

Input reduction essentially means selecting a limited number of representative forcing conditions (i.e. tide and wave) that will reproduce the medium-term residual sediment transport patterns and associated morphological evolution (de Vriend et al., 1993). The morphological factor is a technique to improve computational efficiency by accelerating computed morphological evolution. The application of these techniques to the present study is explained in the following sections.

3.2.1. Tidal input reduction

Astronomical tides are deterministic and can therefore be accurately predicted for any period of time. However tidal oscillations exhibits significant long-term modulations (e.g. spring/neap, yearly and nodal cycles), which make chronological simulations of such cycles computationally demanding.

The basis for tidal input reduction is to find a *representative* tide that most closely reproduce the net and gross sediment transport as the naturally varying tides over the region of interest and for the time period considered. In the present study, the *representative* tide was determined following the approach of Latteux (1995), which is commonly applied (e.g. Brown and Davies, 2009, Dastgheib, 2012, Grunnet et al., 2004). Given the duration of the simulations that will be undertaken (i.e. 1 year), the main concern is to capture the residual effects of the spring-neap oscillations, so a time period of 12 cycles (~1 year) or longer was considered necessary.

Tidal signals at a reference point located at the centre of the disposal ground (see Figure 3.8 and Table 3.3) were generated from a high resolution tidal constituents grid, and time series of sediment transport were estimated using a simple power law $Q=A.u^{b}$ (Q is the transport flux, A is a constant factor, u is current velocity, b=5 following Engelund and Hansen (1967)). The single tide best reproducing the net and gross transport magnitude was identified and used in the accelerated simulations. The representative tide is compared to M2 tidal signals in Figure 3.9.

The representative tide at site S1 (Fig. 3.8) has a period of 12.25 hours which is similar to the M2 component period and an elevation range of 1.03 m, which is ~1% larger than the mean range. The representative tide at site

Draft for public consultation

S2 has a period of 12.35 and an elevation range of 1.05 m, which is ~7% larger than the mean range.

Table 3.3 Location of the control site (S1) used to define the best representative tide.

Site S1			
Geographic (deg.)		**NZTM (m)**	
Longitude	Latitude	X	Y
174.8308	-41.4058	1753028.2	5414576.4

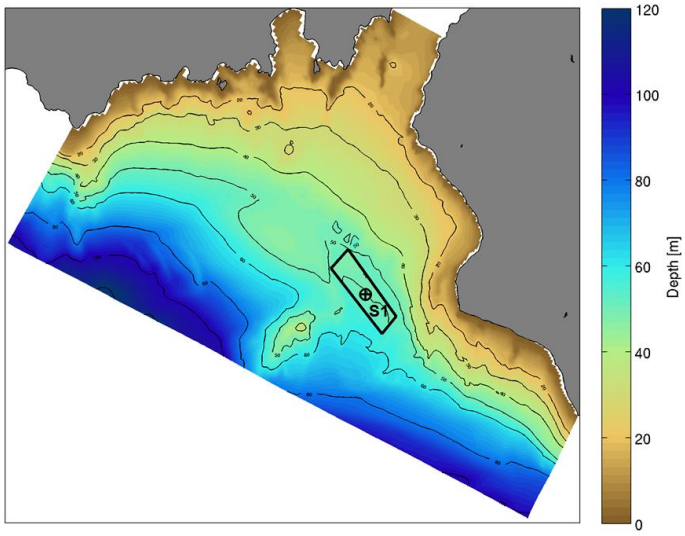

Figure 3.8 Reference site at the centre of the disposal ground used for the definition of the representative tide. The location of the control site (S1) used for the tidal input reduction is detailed in the Table 3.3.

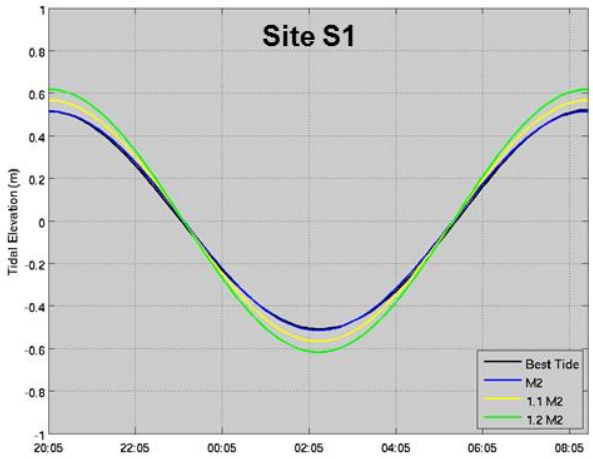

Figure 3.9 Comparison of the best tide, pure M2 tide, 1.1 M2 and 1.2 M2 tide curves at the control site (S1) located at the centre of the disposal ground area (see Table 3.3 and Figure 3.8).

Draft for public consultation

3.2.2. Wave input reduction

The objective of wave input reduction is to define a set of offshore wave boundary conditions which reproduce the same residual sediment transport patterns and morphological evolution as the real time forcing over a given time period. The approach employed here follows the input reduction framework provided in Lesser (2009) and Walstra et al. (2013).

The first step is the selection of a reduction period, which is the length of real-time wave time series that is used to define the representative conditions. This is typically governed by the time scale of the morphological evolution of interest (e.g. monthly, seasonal, annual behaviour). In the present study, the reduction was undertaken based on a 10 year hindcast wave climate obtained from SWAN simulations to define an average annual wave climate. The wave conditions time-series was extracted at the middle of the southern boundary of the wave model domain.

In a second step, a set of representative wave classes is defined by distributing the discrete wave data points into a finite number of height and direction bins, and computing a *representative* value for each bin.

The basic method to determine a *representative* value within a bin is to use a weighted average of the data points by their frequency of occurrence:

$$F_{rep,j} = \frac{\sum_{i=1}^{n} f_i . F}{\sum_{i=1}^{n} f_i} \tag{3.8}$$

where *F* represents the wave height, period or direction, *f* is the frequency of occurrence of the wave condition *i* and n is the number of data points within a bin.

To account for the non-linear dependence of sediment transport on wave height, an additional weighting can be applied for the computation of the representative height:

$$H_{s,rep,j} = \left(\frac{\sum_{i=1}^{n} f_i . H_{s,i}^{p}}{\sum_{i=1}^{n} f_i} \right)^{1/p} \tag{3.9}$$

where *p* is the power to which the sediment transports are assumed to be related to the wave height. Typically *p* is set to 2 to 3. The exponent ensures that larger waves will have a relatively greater contribution in the computation of the representative wave height.

Here Eq. 3.9 was used with a value of p = 2.5 which corresponds with the CERC formula for longshore transport (CERC, 1984) and is frequently used to estimate the morphological impact of waves. Associated representative periods and directions were determined using the same weighting as the wave height.

The initial wave data binning is relatively arbitrary and can be equidistant or non-equidistant (i.e. varying bin size). In the non-equidistant case, bins can be defined following either (subjective) scientific judgment or more objective approaches. Here, the height and direction bins were defined so that the relative "morphological impact of waves" was similar in each bin (Dastgheib, 2012; Lesser, 2009).

Draft for public consultation

The morphological impact of waves of a given wave class was estimated according to:

$$M_j = p_j \,.\, H_{s,rep,j}^{2.5} \tag{3.10}$$

where p_j is the probability of occurrence of the bin j, and $H_{s,rep,j}$ the representative wave height of that bin (Lesser, 2009). Note that this is equivalent to "potential sediment transport" indicator used in Dastgheib (2012).

To automate the determination of bin limits, this indicator was initially computed for a joint probability of wave height and direction with very fine equidistant bins (ΔH=0.1 m, ΔDir=2 deg.). Based on the number of directional and wave height bins to be used for the classification, the directional bin limits are determined first, in a way that the sum of the morphological impact of waves M_j within each bin is (approximately) equal. The same principle is then used within each of these directional bins to define the wave height bin limits. This way, the "morphological impact of waves" is similar in each bin.

The wave climate classification used in the following morphological simulations was defined using 4 directional bins and 3 wave height bins. The general classification obtained for the average annual wave climate at the reference site reproduces the three main groups of wave events from the south, southeast and northeast direction (Figure 3.10) experienced at the site.

The wave height delimitations are relatively consistent with a first class having a significant wave heights below 2 m (which occurs most frequent), a second with wave heights from 2.0 – 2.5 to 3.0 – 3.5 m and the highest energy group for wave heights larger than ~3.5 m (Figure 3.11).

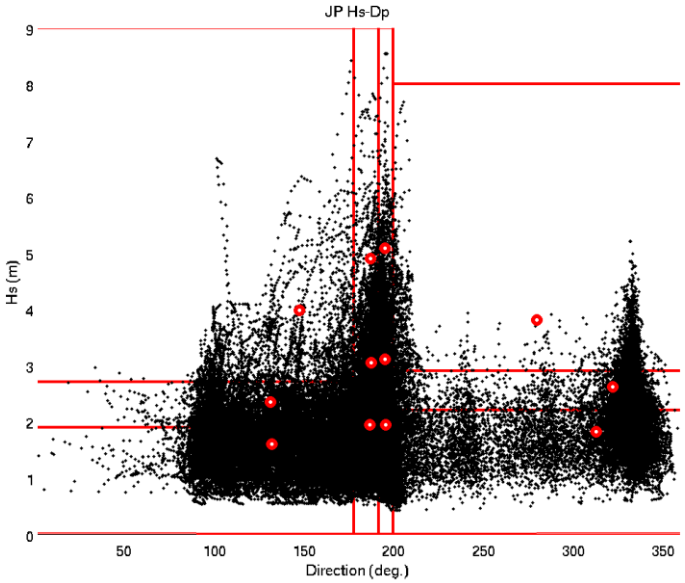

Figure 3.10 Scatter plot of wave heights as a function of wave directions for the 10-year time series, with delimitation of bins (red). Red dots are the representative conditions of each bin.

Draft for public consultation

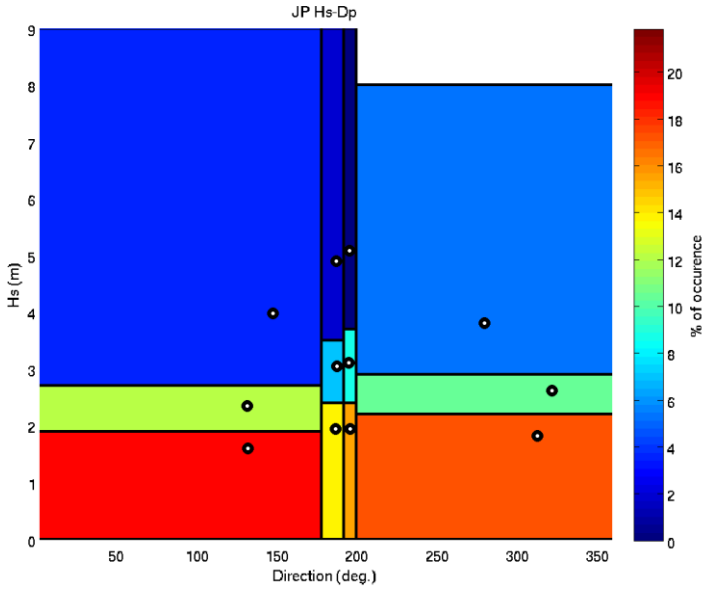

Figure 3.11 Reduced average annual wave climate based on the 10-year wave hindcast using 4 directional bins and 3 wave height bins (i.e. 12 wave classes). Colours indicate the probability of occurrence of a given class. The white dots are the representative wave condition of each wave class. Wave classes are summarized in Table 3.6.

3.2.3. Residual current input reduction

The input reduction technique used for the residual component of the current is a simple average of the hydrodynamic conditions (non-tidal component) associated with the wave classes summarized in Table 3.6. This approach was implemented at the centre of the Delft3D – FLOW boundaries. Water Elevations are prescribed at the southern boundary while current velocities are prescribed to the northern, western and eastern boundaries. Details of residual forcing are presented in Table 3.4.

Table 3.4 Residual current associated with each wave class.

Wave classes	P1 - Northern Boundary			P2 - Western Boundary		
	Current Speed (m/s)	Current Dir (deg.)	Elevation (m)	Current Speed (m/s)	Current Dir (deg.)	Elevation (m)
1	0.001	164.0	0.072	0.107	278.9	0.050
2	0.002	171.5	0.094	0.125	279.4	0.070
3	0.004	187.2	0.128	0.188	281.3	0.089
4	0.002	173.4	0.078	0.111	279.2	0.056
5	0.002	170.5	0.096	0.127	280.5	0.069
6	0.003	168.6	0.131	0.144	282.7	0.092
7	0.001	163.6	0.069	0.104	278.9	0.048
8	0.002	168.7	0.085	0.101	279.8	0.062
9	0.004	148.6	0.126	0.111	283.2	0.087
10	0.001	159.7	0.053	0.072	276.6	0.036
11	0.001	75.7	0.041	0.041	270.4	0.028
12	0.002	62.1	0.054	0.022	263.5	0.040
Wave classes	**P3 - Southern Boundary**			**P4 - Eastern Boundary**		
	Current Speed (m/s)	Current Dir (deg.)	Elevation (m)	Current Speed (m/s)	Current Dir (deg.)	Elevation (m)
1	0.018	2.3	0.080	0.019	270.5	0.081
2	0.026	339.1	0.103	0.027	280.0	0.105
3	0.078	315.0	0.129	0.058	297.6	0.134
4	0.021	350.4	0.086	0.020	274.8	0.088
5	0.032	333.0	0.101	0.023	291.7	0.102
6	0.039	335.5	0.124	0.017	319.4	0.124
7	0.017	5.9	0.078	0.014	268.4	0.078
8	0.018	40.3	0.091	0.004	190.7	0.090
9	0.023	42.1	0.116	0.015	92.0	0.114
10	0.033	91.1	0.064	0.017	147.1	0.063
11	0.069	106.0	0.056	0.048	129.5	0.053
12	0.090	109.3	0.065	0.065	126.3	0.060

3.2.4. Wind input reduction

The wind input reduction was performed following the same approach as used for the residual current reduction. The wind conditions associated with each wave class were calculated by averaging the wind speed and direction at the control point located at the centre of the disposal area. This approach was used in Lesser (2009) based on the partial correlation existing between the offshore wind and wave conditions. Such correlation reaches 57% in the present study which justifies the use of this approach.

Draft for public consultation

The reduction was performed using a 10 year hindcast dataset provided by a 4 km resolution implementation of the model WRF (Weather Research and Forecasting model) to characterize the annual wind climate. Wind time series were extracted at the centre of the disposal ground. Representative wind conditions associated with wave classes are presented in Table 3.5. Common statistics and wind rose are presented in Table 5.1 and Figure 5.2.

Table 3.5 Wind conditions associated with each wave class.

class	U-wind (m/s)	V-wind (m/s)	Speed (m/s)	Dir (deg.)
1	-0.85	-1.41	1.65	31
2	-0.49	-0.03	0.49	86
3	-0.04	7.27	7.27	180
4	-0.44	-1.05	1.14	23
5	1.08	3.23	3.41	198
6	4.28	9.46	10.38	204
7	-0.12	-1.69	1.69	4
8	2.78	1.61	3.21	240
9	7.27	9.72	12.14	217
10	1.83	-5.68	5.97	342
11	4.07	-8.92	9.81	336
12	5.32	-6.87	8.69	322

3.2.5. Morphological acceleration factor

The morphological acceleration factor (morfac) is a technique to bridge the gap between hydrodynamic and morphological timescales (Lesser et al., 2004). This technique consists in multiplying the calculated depth changes over a hydrodynamic time step $\Delta t_{hydrodynamic}$ by a constant factor f_{MOR}, effectively predicting morphological changes over a given period:

$$\Delta t_{morphology} = \Delta t_{hydrodynamic} \cdot f_{MOR} \quad (3.11)$$

Such an approach obviously has limits and involves many implicit assumptions. However it has been successfully applied on many studies to estimate medium-term morphological evolutions of tidal (e.g. Van der Wegen and Roelvink, 2008) and mixed tide and wave environments (e.g. Grunnet al., 2004; Lesser, 2009; Reniers et al., 2004). This acceleration method was combined with the reduced tide and wave forcing outlined above to simulate the morphological evolution of the study area over an annual period (i.e. 365 days).

To account for the random phasing between waves and tides that occurs naturally, each of the representative wave conditions was simulated for the duration of one complete tidal cycle. A morphological acceleration factor specific to each wave class was defined so that the morphological duration of the wave class matches its probability of occurrence within the period considered. The morphological factor is computed following.

Draft for public consultation

$$f_{MOR} = \frac{p_j \,.\, Period\ Duration}{T_{morph\ tide}} \quad (3.12)$$

where p_j is the probability of occurrence of wave conditions falling in the wave class (or bin) j (Figure 3.11), "Period Duration" is the total duration to be simulated, and $T_{morph\ tide}$ is the duration of the representative morphological tide. The wave climate reduction and associated morfacs obtained for a 1-year simulation based on the average annual wave climate are given in Table 3.6. Morfacs range from 9.3 to 154 for high to low wave energy events respectively.

The model system is run for each different wave class, one after the other, over a complete tidal cycle using the appropriate morphological factor. The final bathymetry of each wave class simulation is used as the initial bathymetry for the next simulation. Running each wave class separately rather than using time-varying wave forcing and morfacs over a single continuous simulation suppresses any risk of discontinuities that can potentially develop in suspended sediment concentrations when the morfacs are changed after a given wave class simulation (see Lesser, 2009).

Table 3.6 Wave classification and associated morphological factors for a 1 year period, based on an average annual wave climate defined from a 10-year hindcast dataset.

Wave class	Representative Hs (m)	Representative Tp (s)	Representative Dp (deg.)	Probability of occurrence (%)	MORFAC equivalent 1 year
1	1.596	10.06	132.2	23%	154
2	2.342	10.57	131.7	9%	60.51
3	3.974	10.67	147.7	3%	19.44
4	1.942	10.89	186.8	13%	93.08
5	3.049	11.34	187.5	4%	30.1
6	4.896	11.35	187	1%	10.56
7	1.941	11.9	195.7	14%	99.06
8	3.111	11.49	195.2	4%	31.66
9	5.085	10.64	195.4	1%	9.357
10	1.826	6.534	312.8	18%	130.1
11	2.623	6.738	322.1	7%	46.12
12	3.81	8.245	279.7	3%	21.2

Draft for public consultation

3.2.6. Suitability of the technique for the project location

The reduction techniques outlined in the previous section involves many implicit assumptions which inevitably introduce errors in the estimates of morphological evolution, and these may have important limits depending on the site and the time scale of interest. Therefore it is stressed that the application of reduction methods should be coupled to the formulation of an objective (de Vriend et al, 1993; Lesser, 2009). In other words, there is presently no generic approach to reproduce correctly all features of a coastal system morphologic behaviour on the medium term, especially when exposed to both tides and waves. Instead, a reduction strategy needs to be optimised for a given study objective to serve as guide on what processes or features must be conserved and what simplifications can be made.

Given the lack of detailed morphological measurements that would be required to provide any quantitative validation of the model, the objective of the present study is to establish a model that can qualitatively simulate the fate of the sediment dredged from the new proposed channel and disposed within the ground. In that sense, it may be assumed that the interaction of the wave, tidal, and residual current forcing on an annual basis is of primary importance. In the disposal ground where the depth is 40-50 m, the tidal action is expected to have a dominant role on the morphological changes as the wave orbital velocities are generally low, except under storm conditions. The effect of the wind on the residual current is expected to be significant during strong southerly events. However, residual current velocities are relatively small compared to the daily tidal flows, and thus have less influence on the net direction of sediment dispersion. In that sense, the input reduction approach based on the morphological evolution during tides cycles is expected to be particularly well adapted. The simulations of discrete events with different wave and current conditions should confirm the highly dominant effect of tides on sediment transport.

In terms of temporal scales, it is assumed that a reduced wave climate reproducing the annual potential for sediment transport should be suitable to assess morphological impacts with respect to the fate of the disposed sediment. Therefore a representative annual wave climate was used to force the model and no particular seasonal partitioning was considered. Further, as we are mainly concerned with reproducing the cumulative effects of discrete events on the medium term morphological evolution, the event chronology was not expected to be of critical importance. The sequence of wave classes within a complete simulation was thus randomly assigned, with each condition being simulated once, rather than trying to reproduce a realistic wave climate history as a combination of successive representative classes (e.g. Walstra et al., 2013).

3.3. Long-term morphological modelling

As for the medium-term morphological modelling, an input reduction approach was employed to simulate the sediment transport at the disposal ground for a period of 10 years. Unlike the previous case, the reduction of the input forcing was performed year by year thus retaining the inter-annual variability of the wave, wind and residual current climates.

Draft for public consultation

3.4. Historical simulations

3.4.1. Disposal ground

The accelerated morphological simulations were supplemented by a series of historical simulations featuring two high-energy storm events with opposing wind directions (i.e. south directed and north directed). These events took place in 2004 and 2006, and had offshore significant wave heights greater than 5 m and residual current magnitudes in the range 0.1 – 0.3 m/s. An additional simulation of low wave energy and high current flow (from 2000) was run with current velocities around 0.6 m/s at the centre of the disposal ground. Wave significant height and wind magnitude reached 1.4 m and 2.5 m/s respectively during this event.

These simulations allowed investigation of detailed variations in sediment transport patterns due to different wave, wind and residual current forcing that cannot be examined in the reduced-model configuration. The simulations also provide a basis to verify the reduced models overall robustness in terms of predicted net transport patterns and morphology. For the three real events simulated, tides, residual currents and 2D wave spectra boundary conditions were fully nested from the regional wave and current hindcast described in sections 2.3 and 2.4.

Table 3.7 Wave, wind and total current conditions during historical events.

	Event 1	Event 2	Event 3
Start Time	02-Jul-2000 01:00	16-Aug-2004 01:00	10-Jun-2006 01:00
End Time	06-Jul-2000 01:00	20-Aug-2004 01:00	14-Jun-2006 01:00
	Conditions during storm peak		
Hs [m]	1.4	8.4	5.2
Dp [deg. From]	175	176	332
Tp [s]	9.7	11.6	9.1
Wind Speed [m/s]	2.5	26.7	16.4
Wind Dir. [deg. From]	110	195	0
Current Speed [m/s]	0.62	0.29	0.14
Current Dir. [deg. going to]	332	151	338

3.4.2. Entrance channel modelling

The sediment dynamic modelling in the entrance channel has been performed with a set of 48-hour historical events to predict the depth changes induced by the increased depth due to dredging. Seven events have been identified based on the analysis of the directional and wave height time series.

Draft for public consultation

Firstly, time series of wave height have been split in three distributions defined for three different sectors of wave propagation:

- From 112.5 to 157.5 degrees.
- From 157.5 to 202.5 degrees.
- From 202.5 to 247.5 degrees.

Then, the percentiles 50th, 95th and 99th have been calculated for each distribution to obtain in total 9 classes of wave conditions. Finally, real events have been identified based on these representative classes (H_s and D_p) spanning a period of 48 hours. Wave events with H_s and D_p outside the class ranges for a period of 24 hours or more are not considered. No event corresponding to the classes 8 and 9 have been identified for a period of at least 24 hours. The historical events are presented in Table 3.8.

Table 3.8 Wave conditions defined for the channel modelling during historical events selected for study.

Dp [deg.]	Hs [m]	Occurrence [%]	Period	Period with representative conditions on a 48h total period
112.5 - 157.5	0.95	6.26	06/05/2008 08/05/2008	48h
112.5 - 157.5	1.8		21/09/2005 23/09/2005	38h
112.5 - 157.5	2.02		25/11/2005 25/11/2005	41h
157.5 - 202.5	1.27	81.24	20/02/2005 22/02/2005	48h
157.5 - 202.5	2.45		22/07/2006 29/07/2006	43h
157.5 - 202.5	3		10/07/2007 12/07/2007	28h
202.5 - 247.5	0.99	4.72	18/08/2006 20/08/2006	29h
202.5 - 247.5	2.23		-	-
202.5 - 247.5	2.83		-	-

Draft for public consultation

4. PLUME MODELLING METHODS

4.1. Trajectory modelling

A Lagrangian particle model developed by MSL was used to simulate the trajectories of sediments released into the water column at the various disposal or dredging sites considered in the Project. The model consists of a trajectory scheme applied here to the 2D Eulerian current field $(\tilde{u},\tilde{v})$(see section 2.4) solving for the motion of discrete particles.

$$\frac{du_p}{dt} = \tilde{u}(x,y,z,t) + u_t$$
$$\frac{dv_p}{dt} = \tilde{v}(x,y,z,t) + v_t \qquad \text{(4.1 a,b,c)}$$
$$\frac{dw_p}{dt} = -w_s + w_g + w_t$$

where (u_t,v_t,w_t) are the diffusion components representing turbulent motions, w_s is the particle settling velocity and w_g is a vertical velocity component accounting for bathymetric gradients.

In the horizontal plane, the model uses an Ordinary Differential Equations (ODE) solver, including a 4th order Runge-Kutta method, to calculate the trajectory of a given particle (u_p,v_p) in the time-varying derivative field.

Diffusion is treated using a random walk approach with the following equation, shown here for the u_t component:

$$\int_t^{t+\Delta t} u_t . dt = \sqrt{6 . k_{u,v} . \Delta t} \; . \theta(-1,1) \qquad (4.2)$$

where $\theta(-1,1)$ is a random number from a uniform distribution between -1 and 1, Δt is the time step of the model in seconds and $k_{u,v}$ is the horizontal eddy diffusivity coefficient in $m^2.s^{-1}$. In the present application, a constant diffusivity coefficient of 1 $m^2.s^{-1}$ was used, which is a generic value commonly used (e.g. Bell et al., 2009).

The trajectory of particles in the vertical plane is controlled by the particle's settling velocity w_s, the vertical diffusion component w_t as defined in equation 4.2 with a constant vertical eddy diffusivity coefficient k_w of 0.0001 $m^2.s^{-1}$, and a component w_g related to the bathymetric gradient to ensure that the trajectory of a particle close to the sea-floor is parallel to it (before settling and diffusion components are applied):

$$w_g = \frac{(h-z)}{h}\left(\tilde{u}(x,y,z,t)\times\frac{dh}{dx} + \tilde{v}(x,y,z,t)\times\frac{dh}{dy}\right) \qquad (4.3)$$

where z is the particle elevation above the seabed, h is the water-column height at the particles' horizontal location (x,y), $(\tilde{u},\tilde{v})$ is the 3D current field

Draft for public consultation

from equation 4.1 and $\left(\frac{dh}{dx}, \frac{dh}{dy}\right)$ is the bathymetry gradient. Note a logarithmic profile was used to extrapolate the depth-averaged current magnitudes to any water column level.

In the present model implementation any particle reaching the shoreline, the seabed, or the outside domain boundaries, remained at the position of intersection (*i.e.* 'sticky' boundaries), thus allowing no sediment re-suspension.

4.2. Simulated scenarios

A range of particle tracking simulations was undertaken to assess the effects of both dredging and disposal activities at several locations within the offshore disposal site, channel and disposal sites.

Representative particle sizes for each area were determined based on information on sediment distribution in NIWA (2014) as well as recent samples data provided for the Project. Sample positions and associated grain size characteristics for the disposal ground and channel areas are provided in Figure 4.1. The channel area is characterised by a mixture of different sediment with sizes mostly in the fine to coarse sand ranges (d_{50} >100-150 µm), which are expected to settle relatively quickly after disturbance during dredging throughout the channel or disposal at the proposed offshore ground. The disposal areas generally exhibit finer sediments with several sampled d_{50} in the 50 µm range and also include a fraction of very fine silt material with some sampled d_{10} < 10 µm.

One representative class was selected for the particle tracking simulations:

- Fine sand, d=100µm, w_s =6.67e^{-03} m/s , offshore disposal site and channel regions

Settling velocities were computed using relationships provided in Van Rijn (1993) with a specific gravity of 2.65 for the grain density and a volumetric mass of 1025 kg/m^3 for seawater. Note these relationships do not take into account the flocculation effects of cohesive sediments (silt) that would increase the fall velocities due to the formation of larger flocs. Empirical methods may be used to estimate flocculation effects (e.g. Van Rijn, 2007), but it was chosen to follow a conservative approach and keep the uncorrected velocities.

The release depths for the dredging and disposal simulations were chosen assuming the use of a large trailing suction hopper dredger (TSHD). Dredging activities in the channel assumed concurrent releases at ~ 8m below sea surface (overflow) and 1 m above sea bed (drag head disturbance and propeller wash) while disposal (offshore disposal ground) consisted of a single release at 8 m below sea surface.

Disposal and dredging activities within the channel area were simulated over a complete spring neap-cycle tidal cycle (~28 days) assuming constant material release over time. The approach allows capturing the tidal variability over time scales that are consistent with the dredging works to be undertaken and provide robust estimations spatial plumes dispersion. The

Draft for public consultation

disposal of sediment at the offshore ground becomes more exposed to the variability in the wind and residual current forcing and was therefore simulated over a complete 1 year period with both tidal and residual forcing prescribed from the high resolution tidal constituent grid and a 10-year hydrodynamic hindcast respectively. Note the wind forcing is included in simulations through the wind-driven flows included in the residual current forcing rather than direct effect on the particles. Considered release sites for the different areas are shown in Figure 4.2.

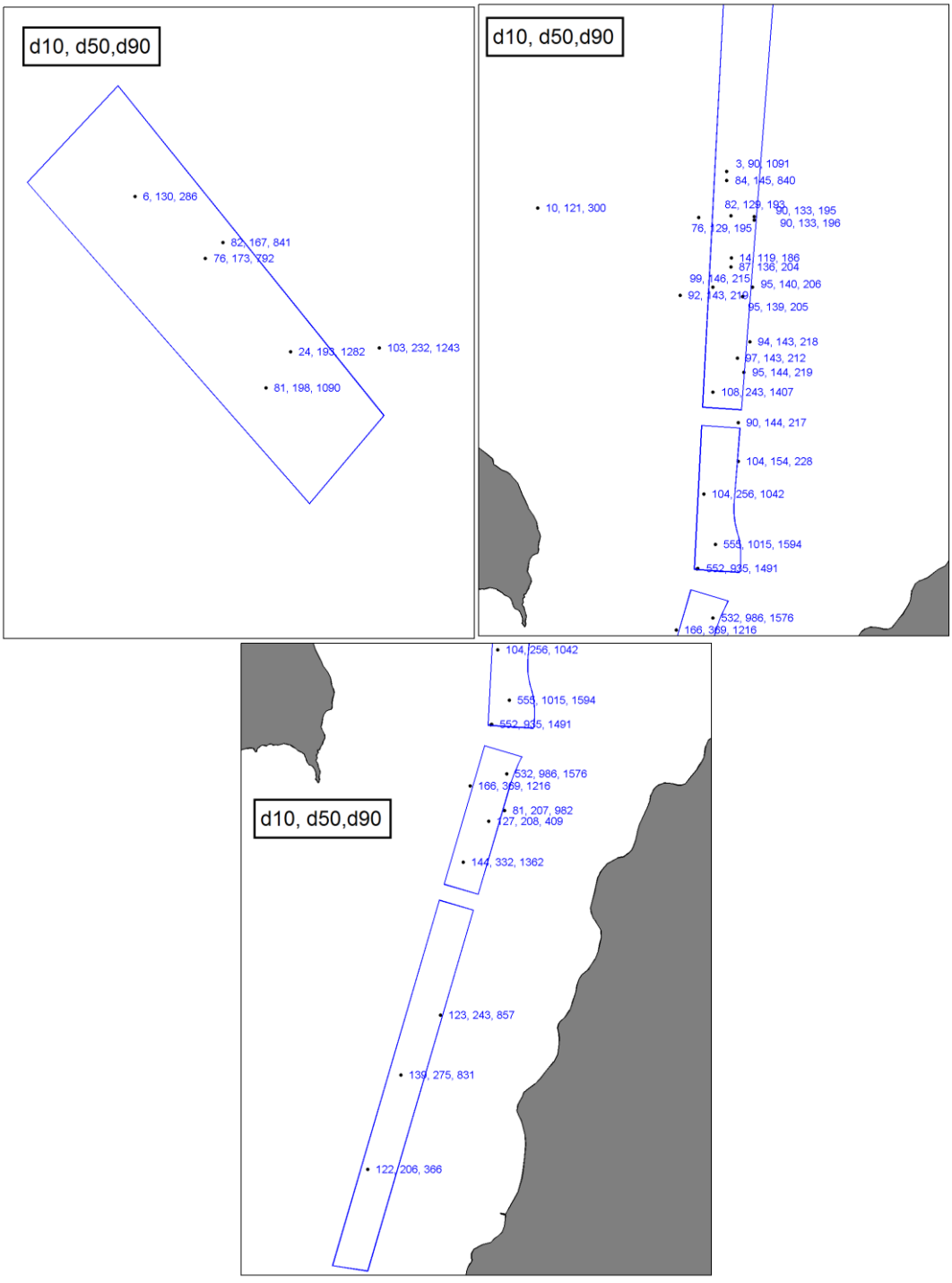

Figure 4.1 Sediment grain size characteristics (d_{10},d_{50},d_{90}) at the sample sites throughout the offshore disposal site and channel zones.

Draft for public consultation

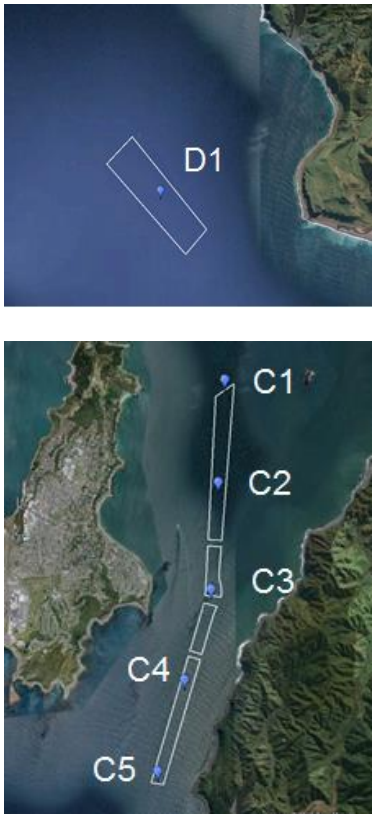

Figure 4.2 Release sites considered in particle tracking simulations at the proposed offshore disposal site and entrance channel.

Draft for public consultation

4.3. Post-processing methods

The results of the particle tracking simulations were post-processed to produce maps of the mean suspended sediment plumes. The general methods employed to reconstruct concentration fields from the model outputs are outlined below.

4.3.1. Concentration computation

To reconstruct concentrations from the particle tracking simulations at chosen receptors, a kernel method with variable bandwidth was used. The use of a variable bandwidth (kernel size) attempts to represent true variability of spatial concentration, while minimizing statistical variability that inevitably occurs away from the source due to a necessarily finite number of particles. A small kernel is used in regions gathering a high number of particles, where it is statistically appropriate to infer relatively small scale changes in concentration. Conversely, a larger kernel is used in regions presenting a low number of particles, so as to prevent unrealistically high concentrations around the precise (but partially random) locations of a few isolated particles.

In practice, the concentration *C* at a given receptor location (x,y) is computed as:

$$C(x,y) = \sum_{i=1}^{n} \frac{m_i}{\lambda_x(x,y)\lambda_y(x,y)} K\left(\left|\frac{x_i - x}{\lambda_x}\right|\right) K\left(\left|\frac{y_i - y}{\lambda_y}\right|\right) \qquad (4.4)$$

where (x_i,y_i) is the location of each particle i, n is the total number of particles, m_i is the loading for each particle, λ_x and λ_y are the kernel bandwidth in the x and y directions for location (x,y) and K is the kernel function.

Following Vitali et al. (2006), an Epanechnikov kernel function was used:

$$K(q) = \begin{cases} 0.75\left(1 - q^2\right), |q| \le 1 \\ 0, |q| > 1 \end{cases} \qquad (4.5)$$

where q is the ratio of the particle distance from receptor to bandwidth ($q_x=d_x/\lambda_x$, or $q_y=d_y/\lambda_y$)

A receptor-based method derived from the RL3 method in Vitali et al. (2006) was used to define the bandwidths λ_x and λ_y.

For each receptor location, a neighborhood was defined as the region enclosing the 1/20th closest particles. Then, for each direction x and y, the bandwidths λ_x and λ_y were defined as the minimum value between the maximum projected distance of the particles within the neighborhood and twice the standard deviation of the projected distances within the neighborhood. Finally, in order to prevent unrealistically elongated kernels, the aspect ratio λ_x / λ_y was limited to be no greater than 5:1, with the smaller value increased.

Draft for public consultation

In the present study, these methods were applied to produce maps of averaged suspended sediment concentrations after 24 h of continuous dredging or disposal activities, computed at three levels in the water column with a layer thickness of 3 m (surface, mid-water and bottom). The receptor grids used for the SSC plumes are provided in Figure 4.3.

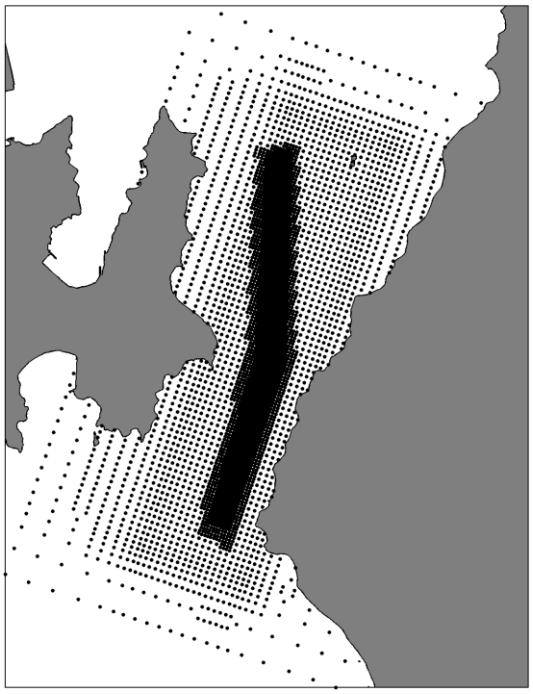

Figure 4.3 Receptor grids for the SSC plumes in the channel. The resolution ranges from 30 m to 300 m further away from the area of interest.

Draft for public consultation

5. MODEL RESULTS

5.1. Characterising the existing environment

5.1.1. Winds and hydrodynamics at the offshore disposal site

The hydrodynamic regime of the proposed disposal ground is dominated by the strong tidal flows developing within the Cook Strait, with superimposed wind-driven residual currents predominantly directed toward the northwest sector. Tidal flows at the site follow a northwest-southeast axis with an asymmetry towards the northwest and magnitudes of up to 0.6 m/s.

The wind regime is strongly bi-modal, dominated by winds from the north and south quadrants, and a relatively strong mean speed of ~8 m/s. Although northerly winds are more frequent, stronger southerly winds have a more significant effect on the long-term residual flow regime, which consists of predominant northwest-directed currents (Figure 5.2). That being said, discrete events can still drive strong residual flows in either direction (south-east or northwest directed) and velocities of up to 0.2 m/s are predicted from this forcing mechanism. A time series of depth-averaged measured currents at the current meter site and associated tidal and residual current roses are shown in Figure 5.3 and Figure 5.4 for reference. The current profile may be further examined in the time series plot on Figure 5.5. Here, the current at surface, mid-water and near-seabed are provided, along with the concurrent wave and wind conditions. The surface current responds to the local wind stress, while the mid-water and near-bed flows are reasonable coherent and generally align with the isobaths.

Snapshots of the modelled existing peak ebb and flood flows during neap and spring tides (Figure 5.7 and Figure 5.6) clearly illustrate the dominant northwest-southwest axis of the tidal flow in the vicinity of the disposal ground, and to a larger extent within the entire Fitzroy Bay. Note the stronger flow magnitudes developing within the harbour entrance due to the constriction of the ebbing and flooding tidal flows.

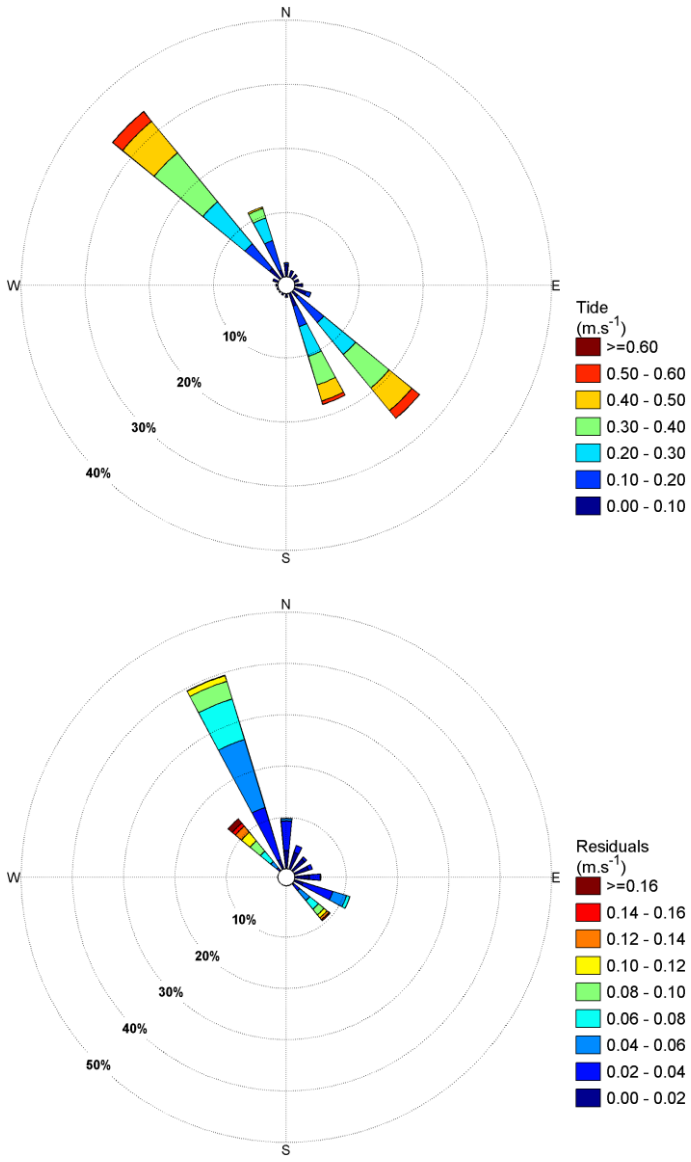

Figure 5.1 Rose plots of tidal and residual currents at the centre of the proposed disposal ground form the 10-year hindcast period. Directions are shown in the "going to" convention.

Draft for public consultation

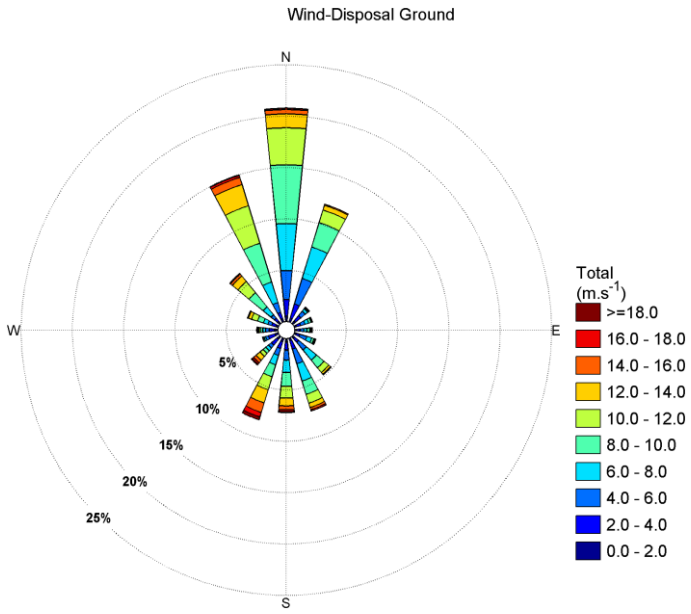

Figure 5.2 Wind rose at the centre of the proposed disposal ground form the 10-year hindcast period. Directions are "coming from".

Table 5.1 Wind speed statistics (m/s) at the centre of the proposed disposal ground for 10-year hindcast period.

m/s	min	mean	median	p90	p95	p99	max
Jan	0.19	7.82	8.05	12.21	13.24	15.38	20.86
Feb	0.18	7.58	7.73	11.77	12.95	16.19	21.19
Mar	0.17	7.57	7.66	11.99	13.28	16.27	19.55
Apr	0.09	7.12	6.99	11.85	13.48	16.33	20.41
May	0.10	7.94	7.81	12.76	14.12	17.44	22.74
Jun	0.30	8.66	8.51	13.79	15.35	18.63	23.09
Jul	0.23	7.93	7.57	13.47	15.26	18.18	21.76
Aug	0.23	8.03	7.90	13.11	15.01	18.72	26.21
Sep	0.05	8.43	8.67	12.66	13.96	16.70	19.81
Oct	0.32	8.63	8.71	13.49	14.83	18.83	23.94
Nov	0.06	8.54	8.76	13.01	14.33	17.02	21.09
Dec	0.18	8.11	8.24	12.52	13.47	15.90	22.35
2000	0.05	7.99	7.95	12.67	13.89	16.99	22.74
2001	0.06	7.73	7.70	12.26	13.71	17.55	21.92
2002	0.31	8.40	8.50	13.19	14.59	17.36	21.76
2003	0.10	7.97	7.96	12.66	13.96	16.92	23.09
2004	0.24	8.35	8.34	13.26	14.79	18.91	26.21
2005	0.17	7.64	7.72	12.09	13.44	16.07	19.81
2006	0.09	8.49	8.43	13.61	15.29	18.13	23.94
2007	0.14	7.80	7.92	12.25	13.41	15.67	21.44
2008	0.10	7.80	7.95	12.35	13.95	17.64	21.36
2009	0.20	8.13	8.17	12.94	14.20	16.76	21.94
All	0.05	8.03	8.05	12.74	14.13	17.30	26.21

Draft for public consultation

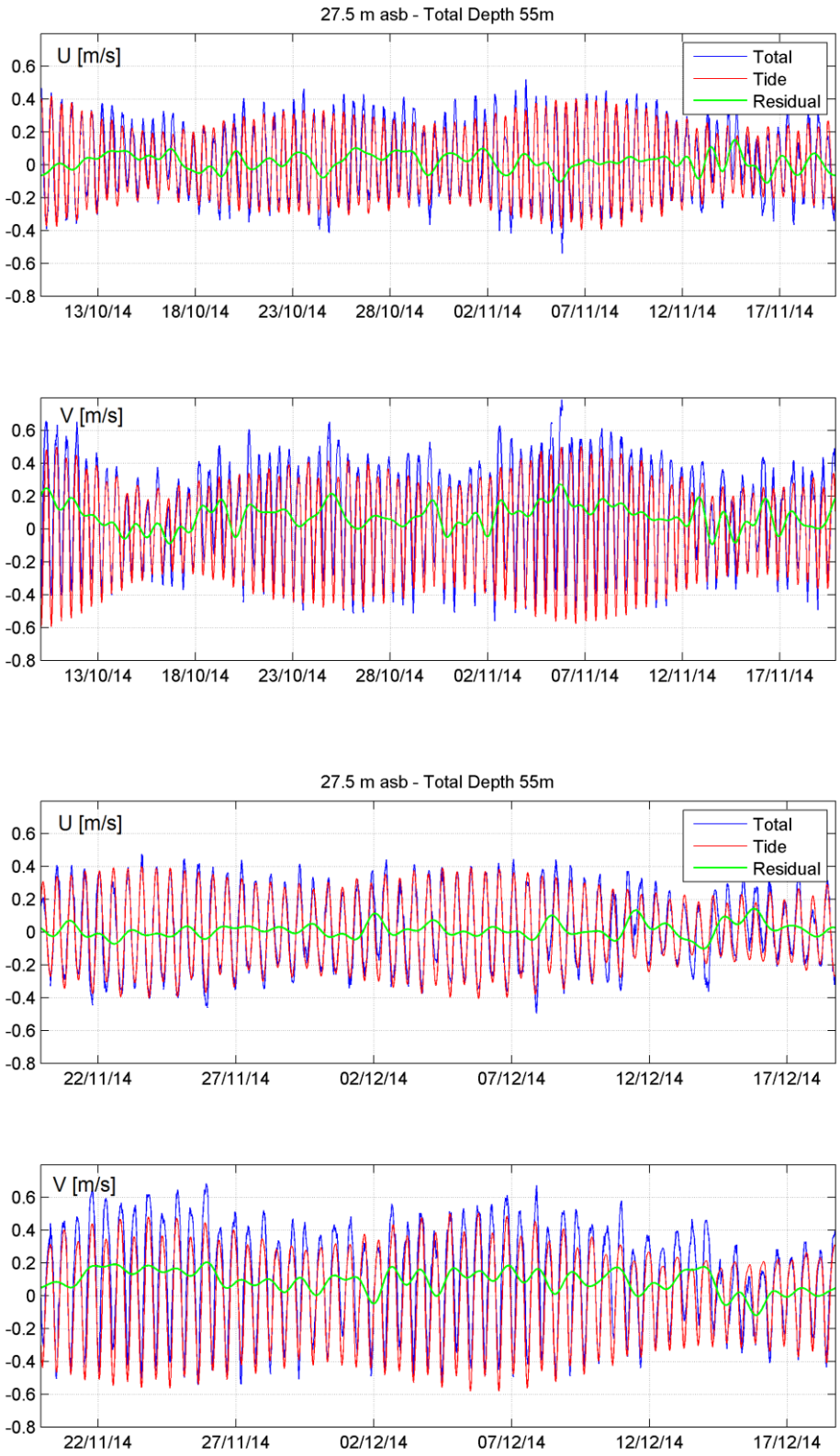

Figure 5.3 Measured currents during the two current meter deployments at the centre of the proposed disposal ground.

Draft for public consultation

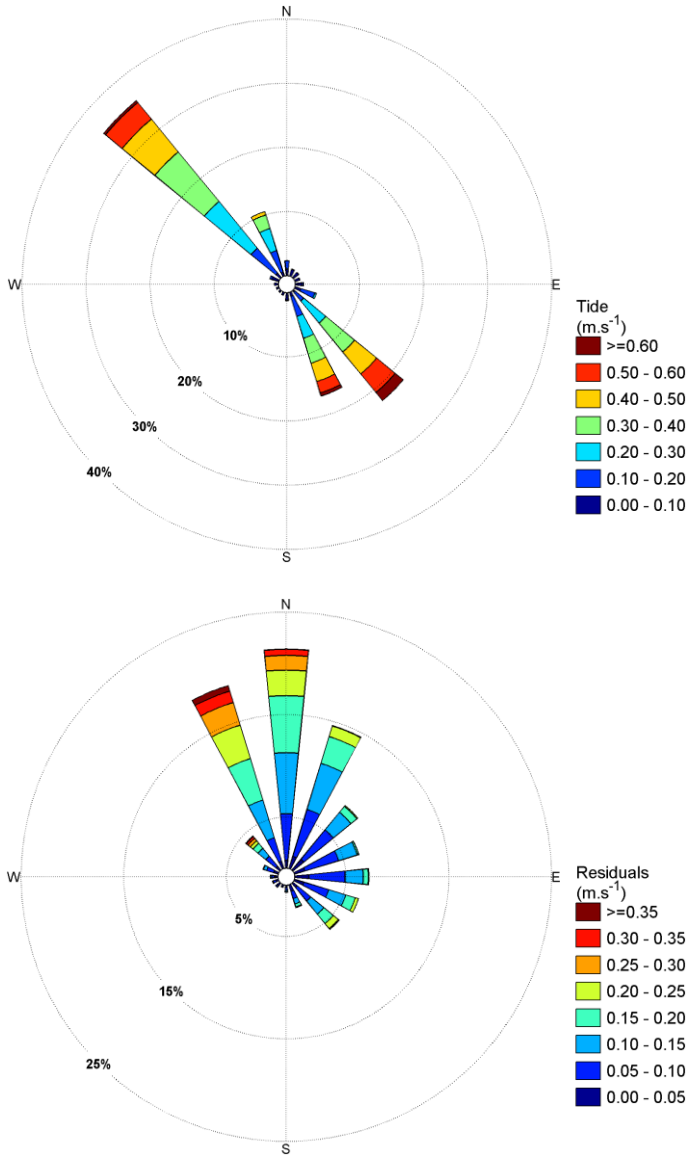

Figure 5.4 Rose plot of the measured tidal (top) and residual (bottom) currents from within the proposed disposal ground.

Draft for public consultation

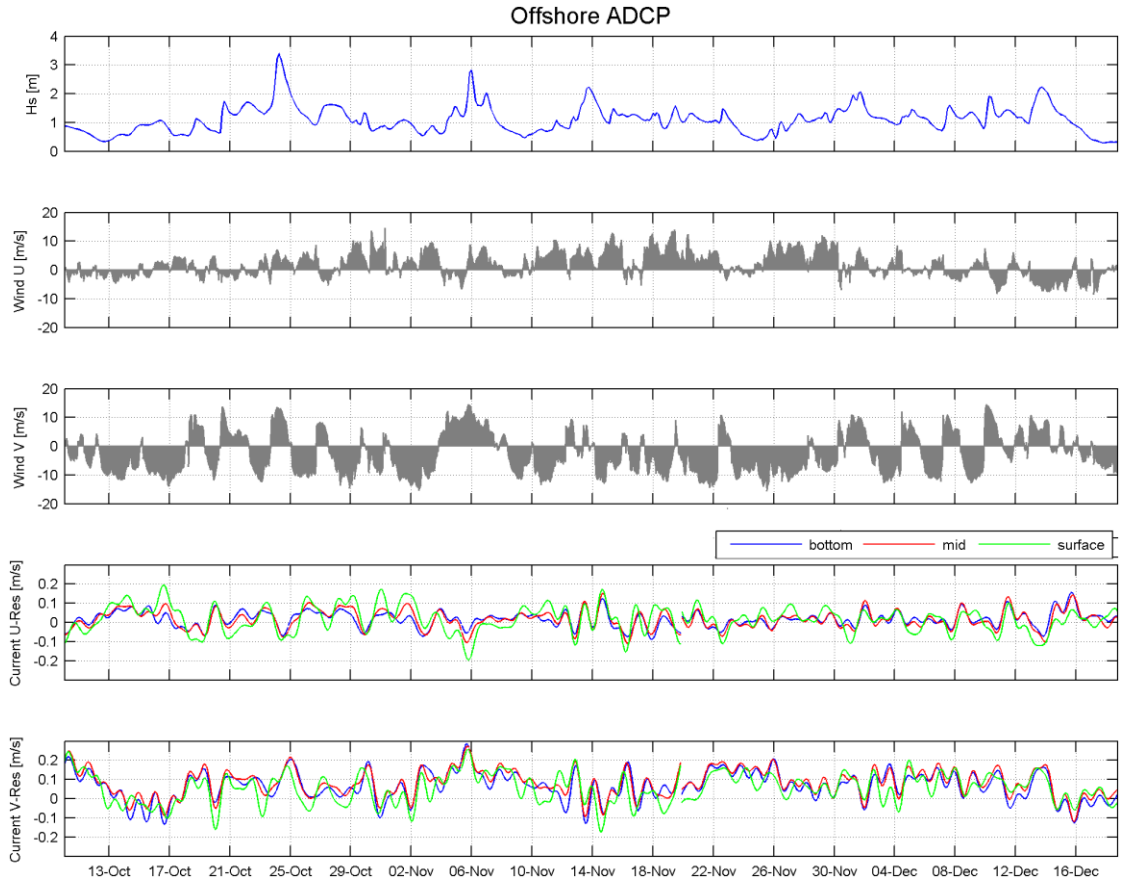

Figure 5.5 Concurrent waves, winds and measured currents at three levels in the water column.

Draft for public consultation

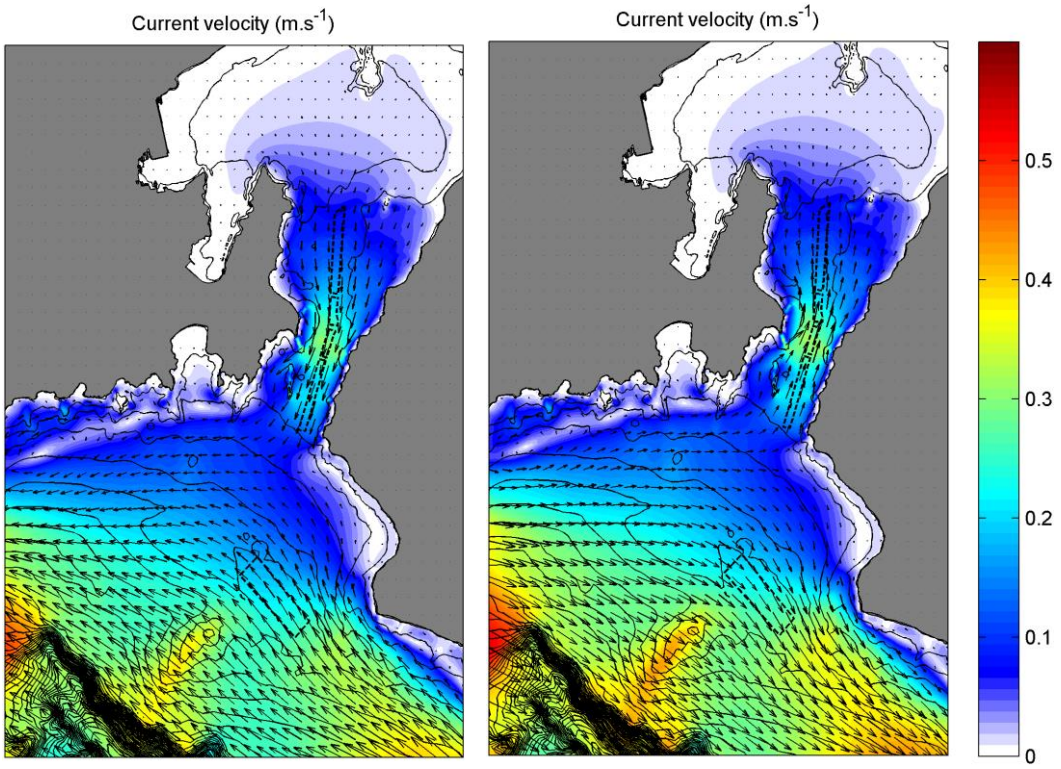

Figure 5.6 Snapshots of peak spring ebb and flood tidal flows.

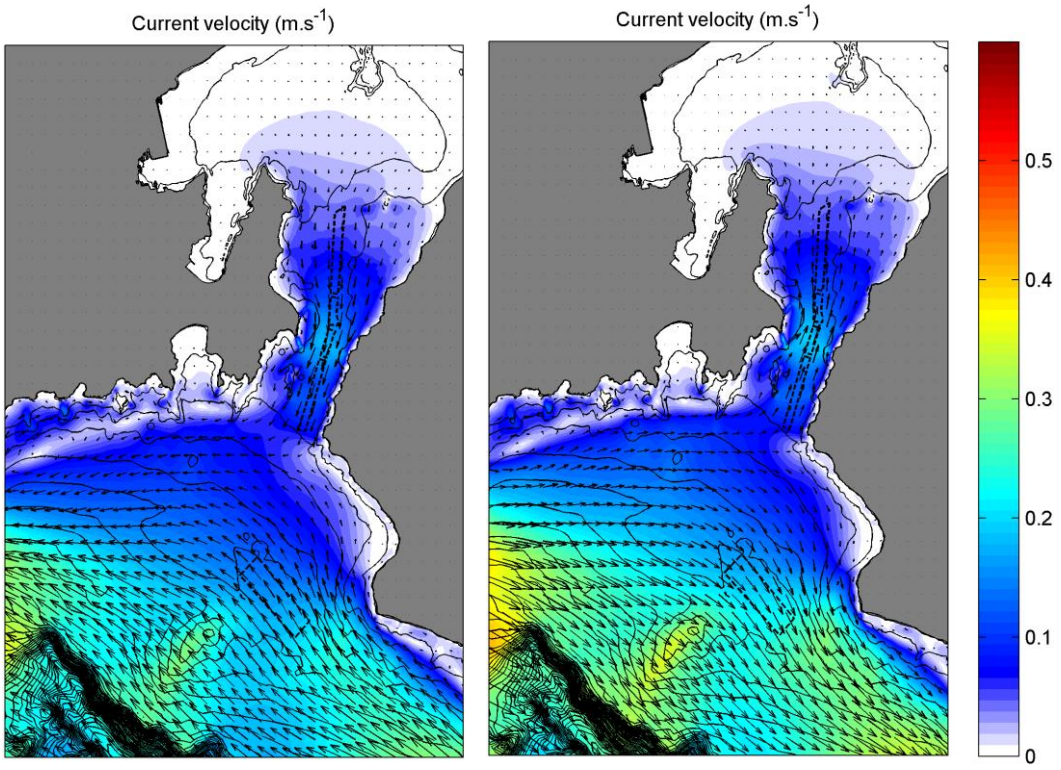

Figure 5.7 Snapshots of the peak neap ebb and flood tidal flows.

Draft for public consultation

5.1.2. Waves

Information on the wave climate at the centre of the proposed disposal ground is provided in the rose plot in Figure 5.8 and statistics in Table 5.2. The wave climate is occasionally energetic, but the average significant wave height in only 1.41 m. The region is sometimes exposed to far field swell energy from the Southern Ocean, but more frequently influenced by the shorter period conditions generated by the southerly wind fetch along the eastern seaboard of the South Island (Table 5.3).

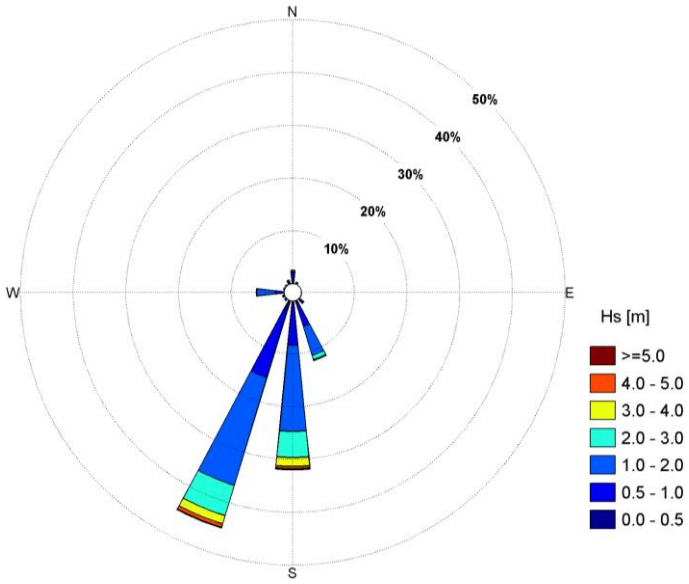

Figure 5.8 Wave rose at the centre of the proposed offshore disposal ground.

Draft for public consultation

Table 5.2 Statistics of the significant wave height at the centre of the proposed offshore disposal ground.

Hs (m)	mean	median	p90	p95	p99	max
January	1.16	1.03	1.90	2.38	3.50	5.10
February	1.23	1.09	1.93	2.42	3.57	6.01
March	1.40	1.19	2.34	2.87	3.99	5.68
April	1.41	1.28	2.35	2.88	3.89	5.65
May	1.49	1.25	2.70	3.26	4.59	6.76
June	1.85	1.61	3.36	3.97	5.08	8.23
July	1.64	1.42	2.77	3.40	4.73	7.31
August	1.41	1.19	2.43	3.18	5.15	8.07
September	1.38	1.20	2.37	2.74	3.69	5.54
October	1.48	1.30	2.41	3.08	4.19	6.27
November	1.35	1.22	2.16	2.51	3.35	5.21
December	1.17	1.03	1.93	2.47	3.96	6.03
2004	1.51	1.27	2.74	3.39	4.88	8.07
2005	1.28	1.09	2.20	2.72	3.92	5.54
2006	1.50	1.28	2.57	3.46	4.72	6.27
2007	1.38	1.22	2.33	2.77	3.76	5.15
2008	1.38	1.20	2.32	2.88	3.89	7.31
2009	1.48	1.29	2.66	3.16	4.08	6.76
2010	1.42	1.23	2.38	3.01	4.49	6.36
2011	1.46	1.29	2.48	2.97	4.28	5.65
2012	1.38	1.20	2.25	2.96	4.19	5.26
2013	1.34	1.16	2.16	2.77	4.64	8.23
All	1.41	1.22	2.41	3.02	4.35	8.23

Table 5.3 Joint probabilities (parts-per-thousand) of significant wave height and mean wave direction at peak energy at the centre of the proposed offshore disposal ground.

Hs / Dpm	0-30	30-60	60-90	90-120	120-150	150-180	180-210	210-240	240-270	270- 300	300-330	330-360	Total
> 0 <= 1	17.25	0.00	0.00	0.03	14.58	76.94	200.64	1.92	4.93	13.93	1.23	12.94	344.20
> 1 <= 2	1.88	0.00	0.00	0.03	8.86	100.32	327.31	3.08	8.83	29.30	1.44	4.62	485.60
> 2 <= 3	0.00	0.00	0.00	0.00	0.27	18.21	98.71	1.03	0.41	0.48	0.00	0.00	119.10
> 3 <= 4	0.00	0.00	0.00	0.00	0.14	4.28	30.77	0.24	0.00	0.00	0.00	0.00	35.40
> 4 <= 5	0.00	0.00	0.00	0.00	0.00	1.27	10.23	0.03	0.00	0.00	0.00	0.00	11.50
> 5 <= 6	0.00	0.00	0.00	0.00	0.00	0.31	2.70	0.00	0.00	0.00	0.00	0.00	3.00
> 6 <= 7	0.00	0.00	0.00	0.00	0.00	0.00	0.55	0.00	0.00	0.00	0.00	0.00	0.50
> 7 <= 8	0.00	0.00	0.00	0.00	0.00	0.00	0.24	0.00	0.00	0.00	0.00	0.00	0.20
> 8 <= 9	0.00	0.00	0.00	0.00	0.00	0.00	0.07	0.00	0.00	0.00	0.00	0.00	0.10
Total	19.20	0.00	0.00	0.00	23.90	201.30	671.10	6.20	14.10	43.70	2.60	17.50	1000.00

Draft for public consultation

5.2. Effects of channel deepening

The bathymetric changes from the two channel designs are shown in Figure 5.9 (as defined in MSL Report P0222-01), and the results from both are presented here. While the 98% optimisation design is proposed, the 100% optimisation design is included here for comparison purposes.

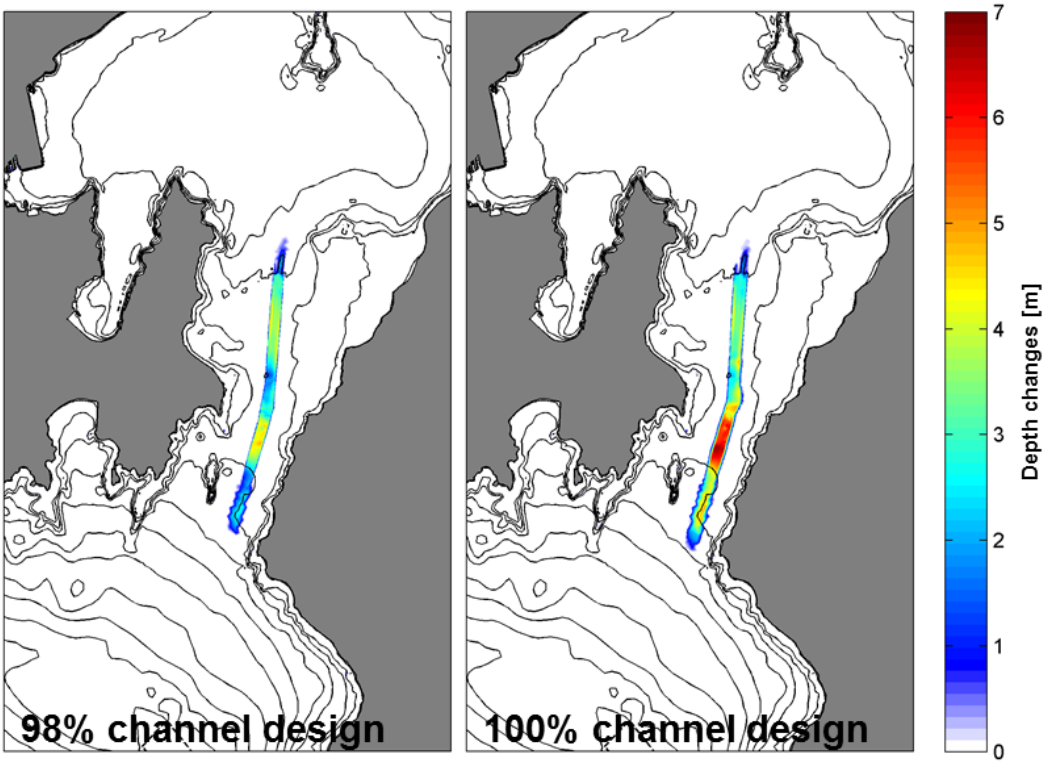

Figure 5.9 Bathymetric changes post-channel dredging (in m) for both 98% (left) and 100% (right) optimisation channel configurations. Positive depth changes indicate a deepening.

5.2.1. Effects on the tidal hydrodynamics

To assess the effect of the proposed dredging options on the tidal hydrodynamics within and offshore of the Wellington Harbour, simulations using the high resolution SELFE domain (Section 4.4) were reproduced using the two modified bathymetries. All other parameters were kept constant to allow a consistent comparison, so essentially the only difference for the simulations was an increased depth.

In the case of the 100% optimisation channel design, the differences in peak tidal flows for spring and neap tides shown in Figure 5.10 and Figure 5.12 indicate that a reduction of the tidal flow velocities by 0.02-0.04 m/s throughout the entrance region is expected. Results are shown for the ebb (outgoing) and flood (incoming) tidal stages. These magnitude difference plots should be related to snapshots of existing peak flows in Figure 5.6 and Figure 5.7, showing peak velocities of ~0.5 m/s and 0.3 m/s for the spring and neap tides respectively. This relative flow reduction translates to a slight reduction of the bed shear stress levels within the narrowest part of the entrance channel (see Figure 5.14 and Figure 5.16).

Draft for public consultation

Bed shear stress is a measure of the energy in current available to transport the seabed sediments. The bed shear stress needs to exceed a critical value, which is related to the size of the sediment grains, in order for transport to occur. The model was used predict the percentage of time that the critical bed shear stress level is exceeded, and compare the existing and dredged channel situations. The results show that a reduction of ~5% of the time is expected for the 98% optimisation case. Changes to the flow in the entrance regime have the potential over time to influence the local sediment transport regime - notably the balance of incoming and outgoing transport fluxes. These effects are considered in section 5.2.3 with an interpretation of the existing and post-dredging channel morphodynamics.

In addition to the modulation of the tidal flow velocities, the comparison of tidal flow phase fields (see Figure 5.20 for M2 constituent) indicates that deepening the channel results in a tidal flow that advances slightly in the phase within the deeper zones and slightly lags in the surrounding shallower zones (relative the existing tidal phases). However, deepening the channel does not significantly modify (0-8 % of changes) the tidal asymmetry in the channel as is shown in Table 5.4 and Table 5.5 for neap and spring tidal conditions.

For the 98% optimisation channel design, the differences in peak tidal flows for spring and neap tides shown in Figure 5.11 and Figure 5.13 indicate that a reduction of the tidal flow velocities by 0.01-0.03 m/s throughout the entrance region is expected. Positive and negative changes in phase in the channel and in shallow waters, respectively, are also predicted with amplitudes up to 5 degrees.

Draft for public consultation

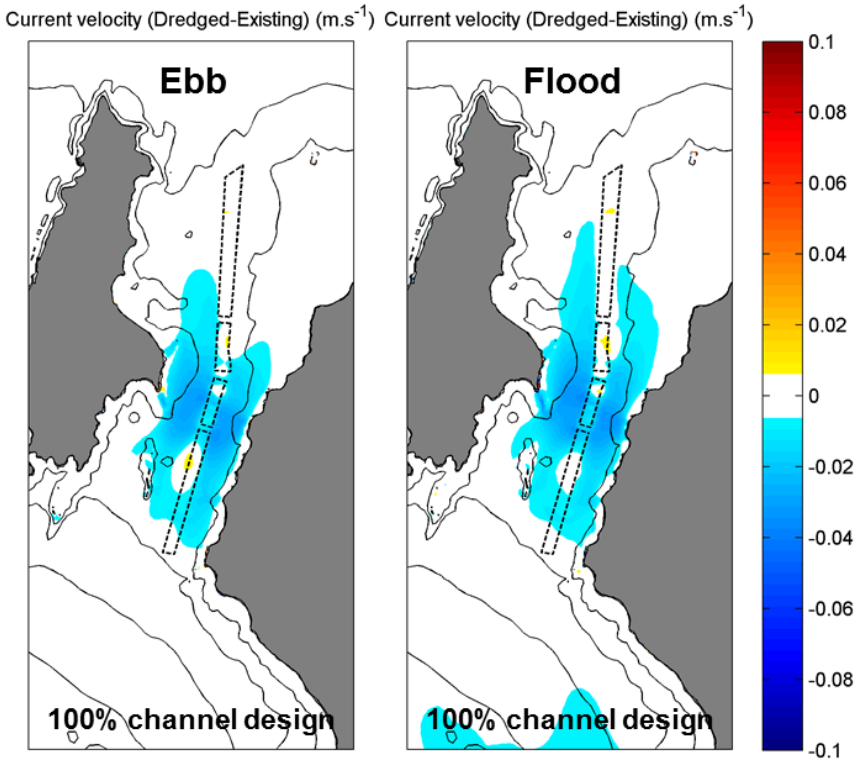

Figure 5.10 Difference in tidal flows post dredging (100% optimisation channel) during peak spring ebb and flood stages. Negative values indicate flows smaller in the post-dredging bathymetry.

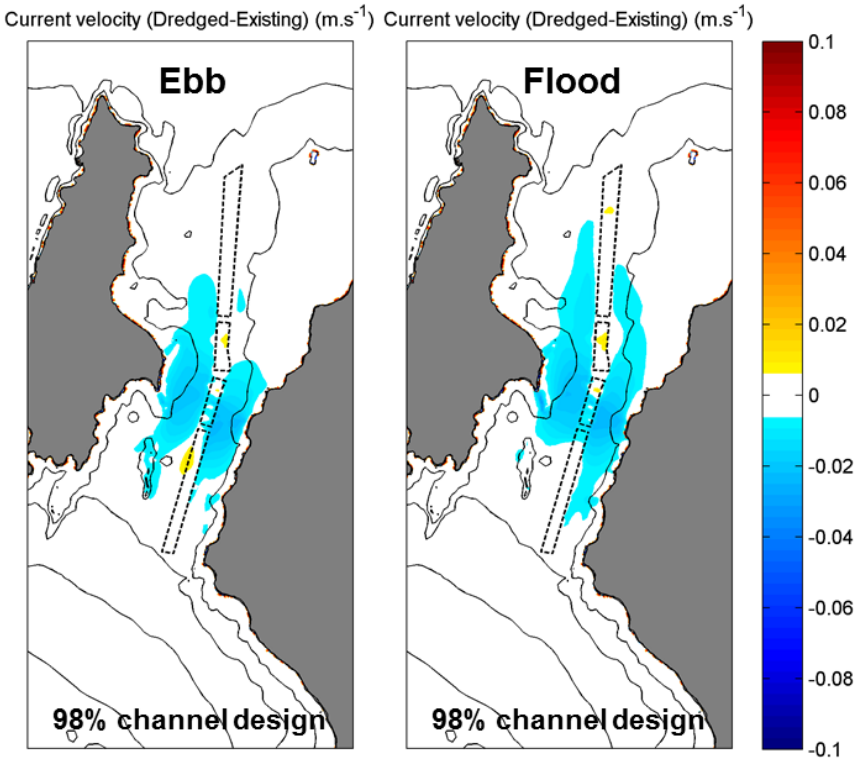

Draft for public consultation

Figure 5.11 Difference in tidal flows post dredging (98% optimisation channel) during peak spring ebb and flood stages. Negative values indicate flows smaller in the post-dredging bathymetry.

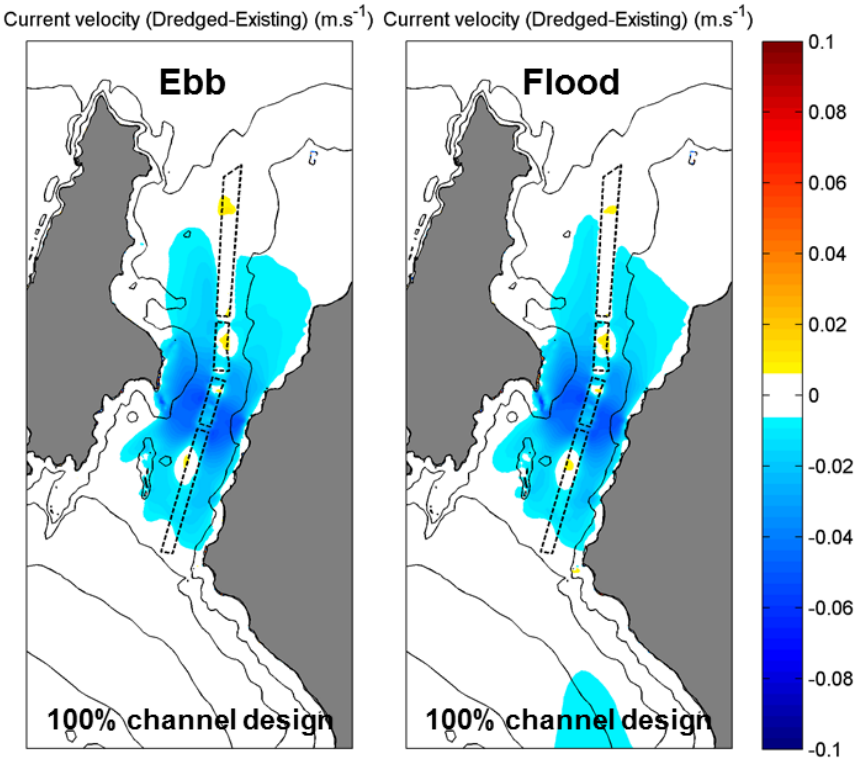

Figure 5.12 Difference in tidal flows post dredging (100% optimisation channel design) during peak neap ebb and flood stages. Negative values indicate flows smaller in the post-dredging bathymetry.

Draft for public consultation

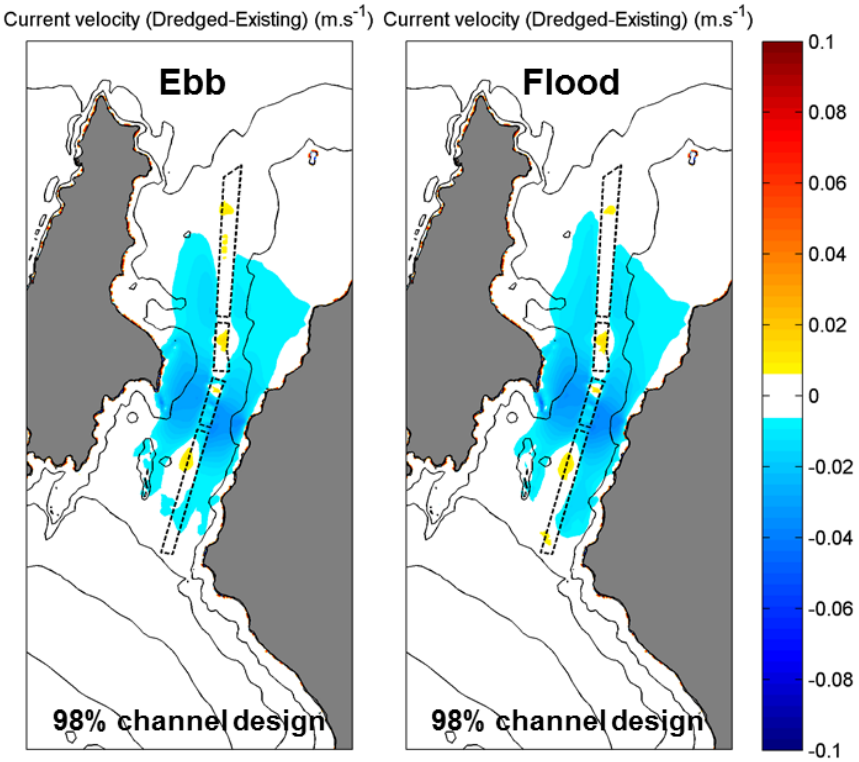

Figure 5.13 Difference in tidal flows post dredging (98% optimisation channel design) during peak neap ebb and flood stages. Negative values indicate flows smaller in the post-dredging bathymetry.

Draft for public consultation

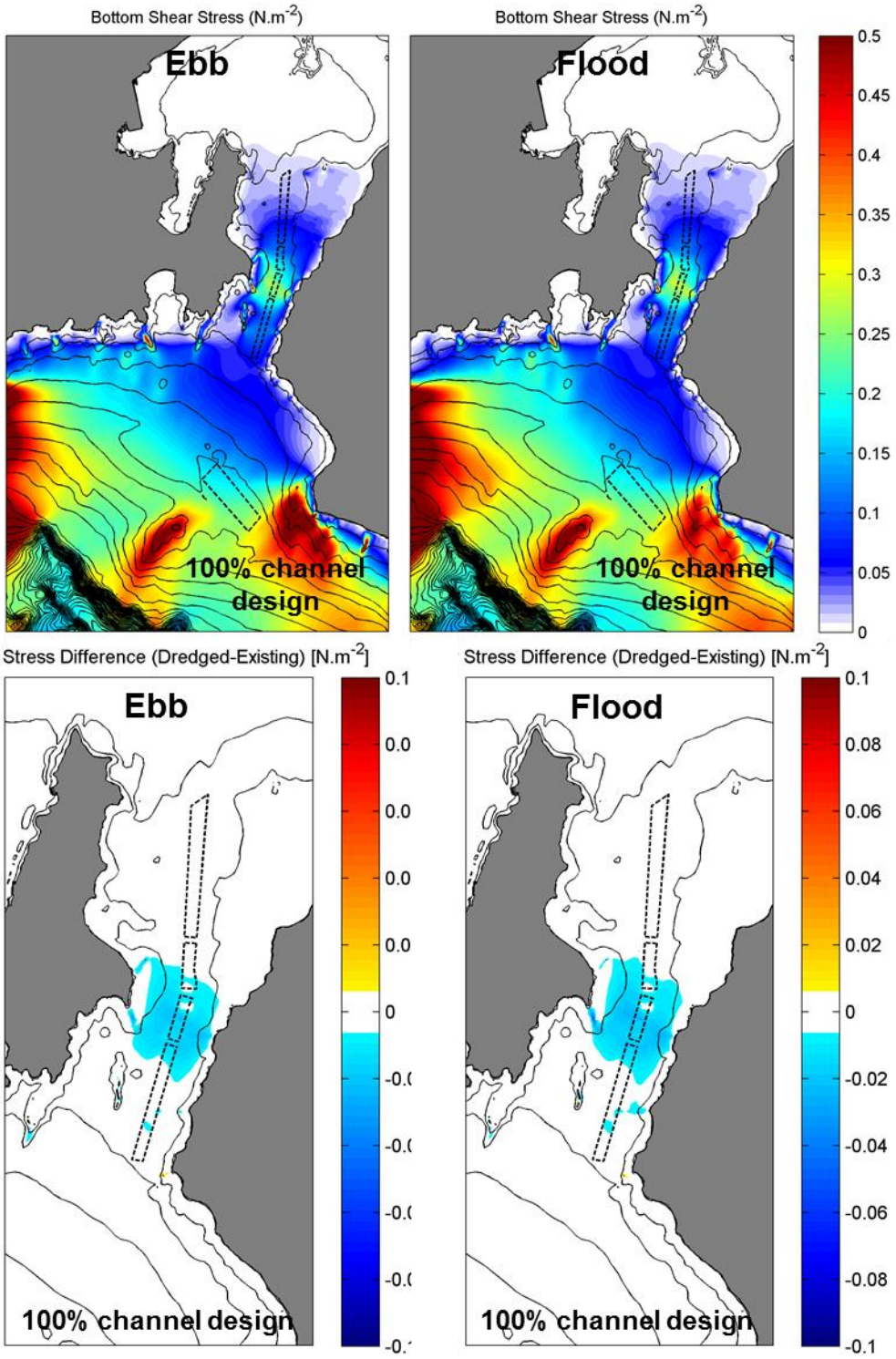

Figure 5.14 Bed shear stress fields during spring ebb and flood stages over the existing bathymetry and difference post dredging (100% optimisation channel configurations). Negative shear stress differences indicate reduction of the shear stress magnitudes post dredging.

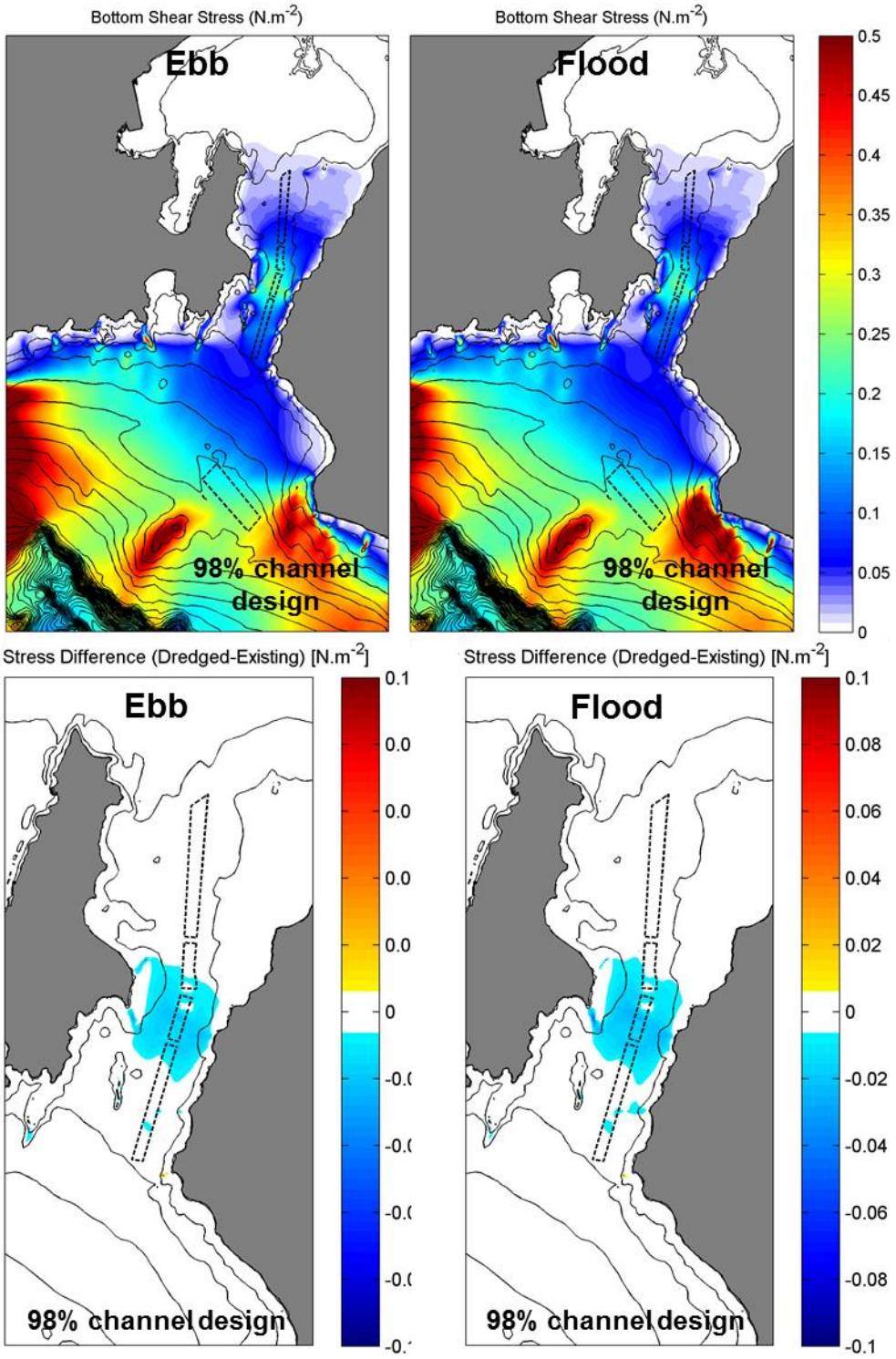

Figure 5.15 Bed shear stress fields during spring ebb and flood stages over the existing bathymetry and difference post dredging (98%optimisation channel configurations). Negative shear stress differences indicate reduction of the shear stress magnitudes post dredging.

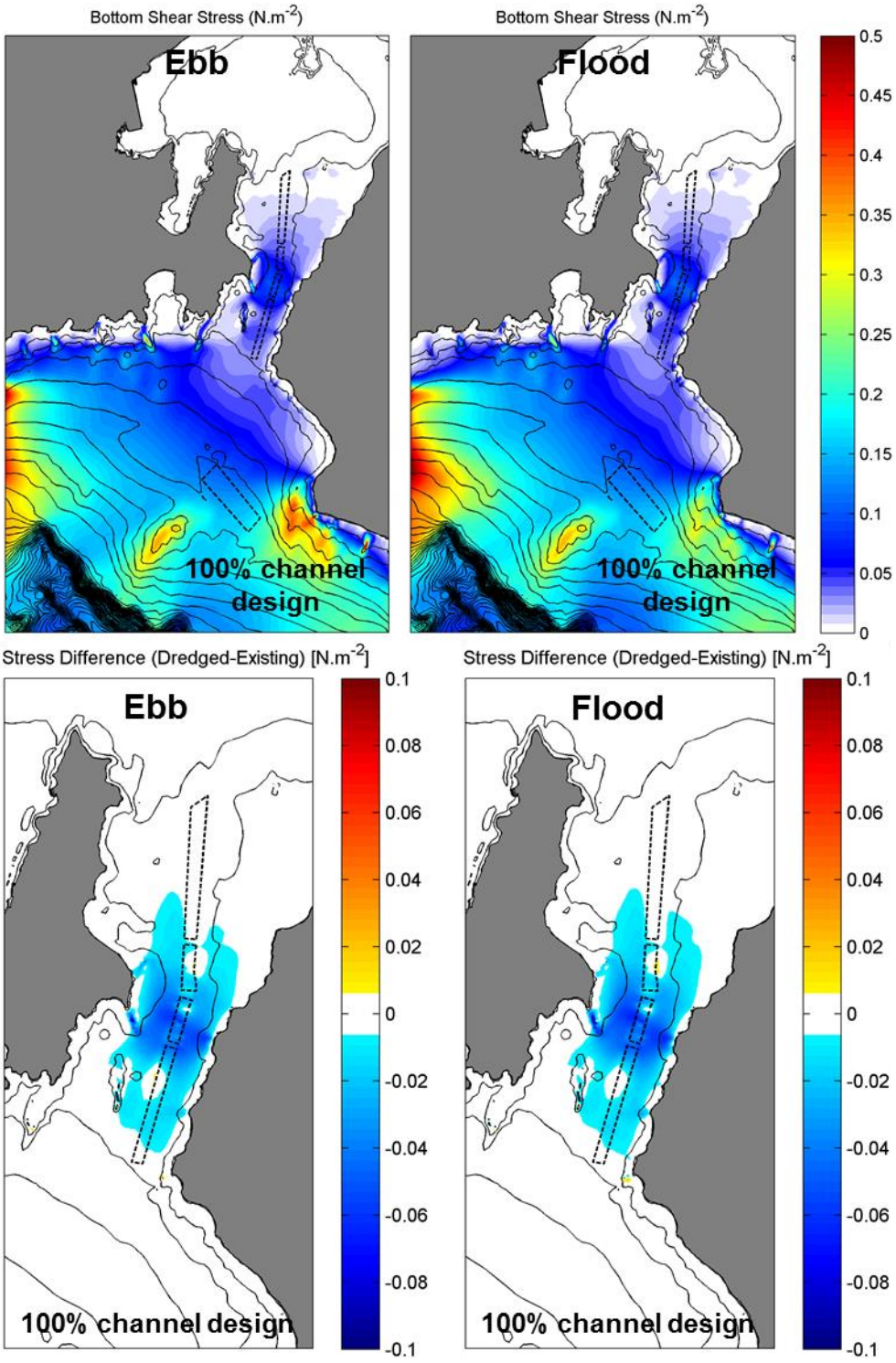

Figure 5.16 Bed shear stress field during spring ebb and flood stages over the existing bathymetry and difference post dredging (100% optimisation channel configurations). A negative shear stress differences indicate a reduction of the shear stress magnitudes post dredging.

Draft for public consultation

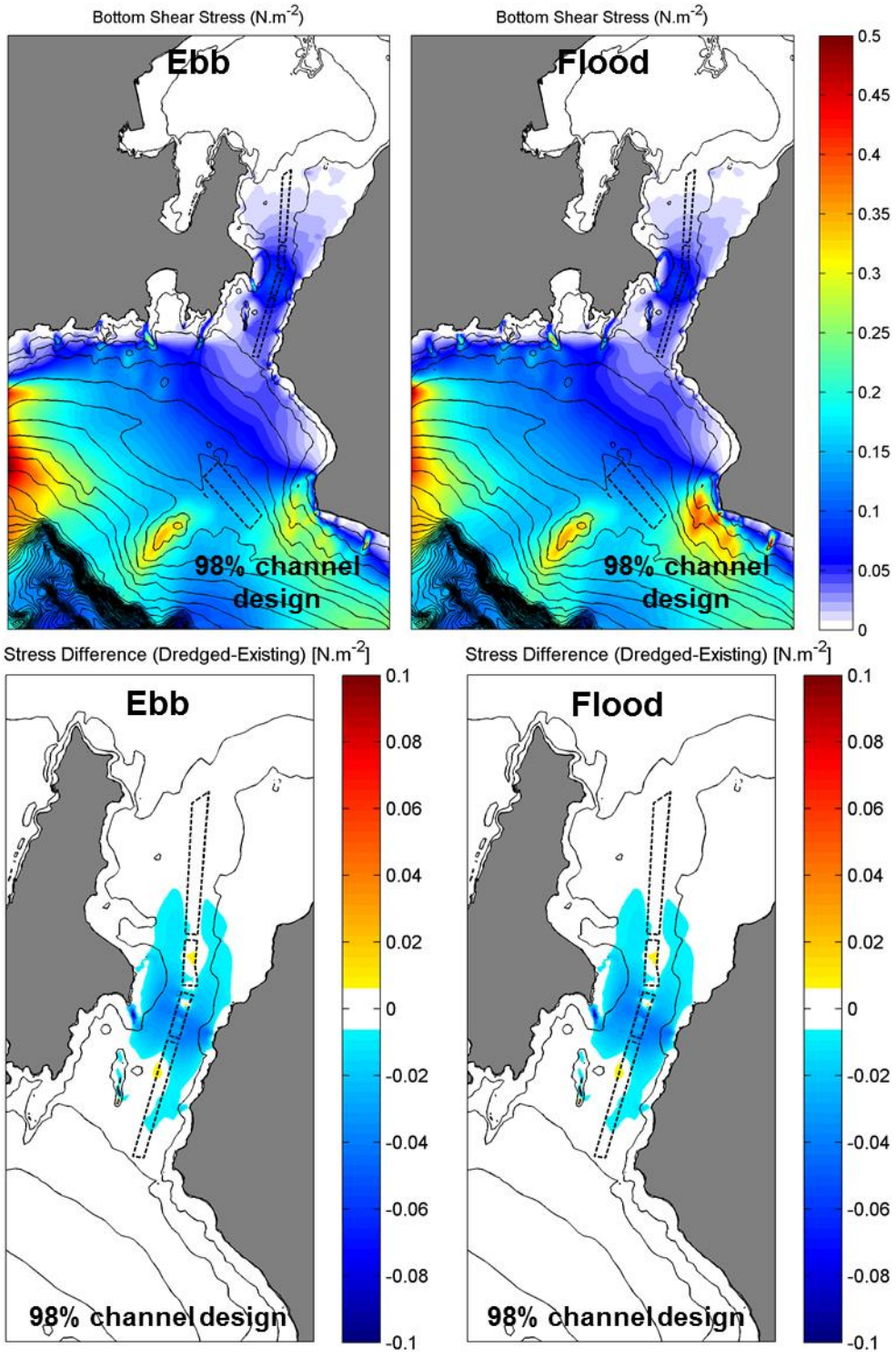

Figure 5.17 Bed shear stress field during spring ebb and flood stages over the existing bathymetry and difference post dredging (98%optimisation channel configurations). A negative shear stress differences indicate a reduction of the shear stress magnitudes post dredging.

Draft for public consultation

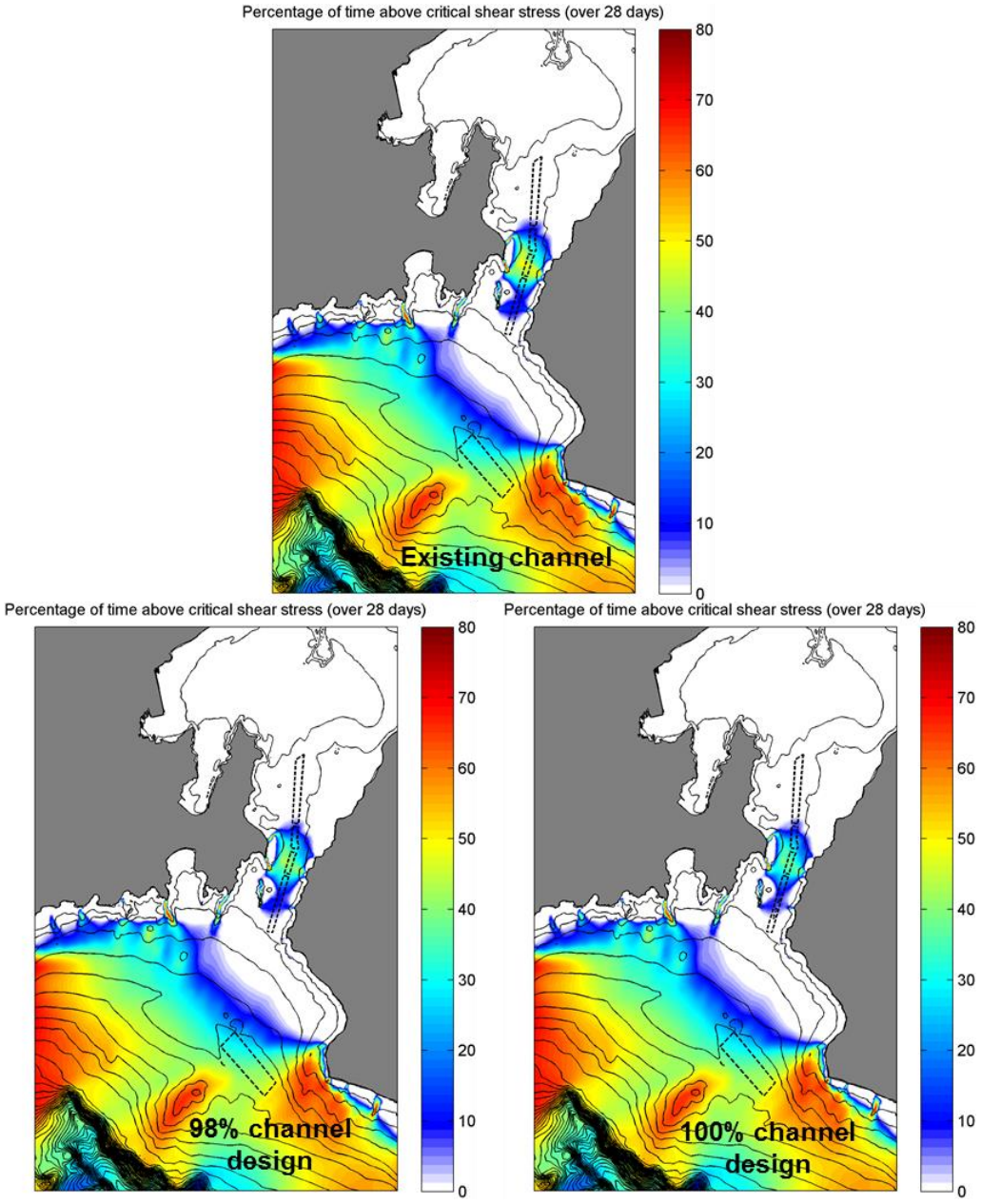

Figure 5.18 Percentage of time of bed shear stress exceedance calculated from a 28-day simulation of the existing channel, the 98% optimisation design and the 100% optimisation design, based on the critical bed shear stress threshold.

Draft for public consultation

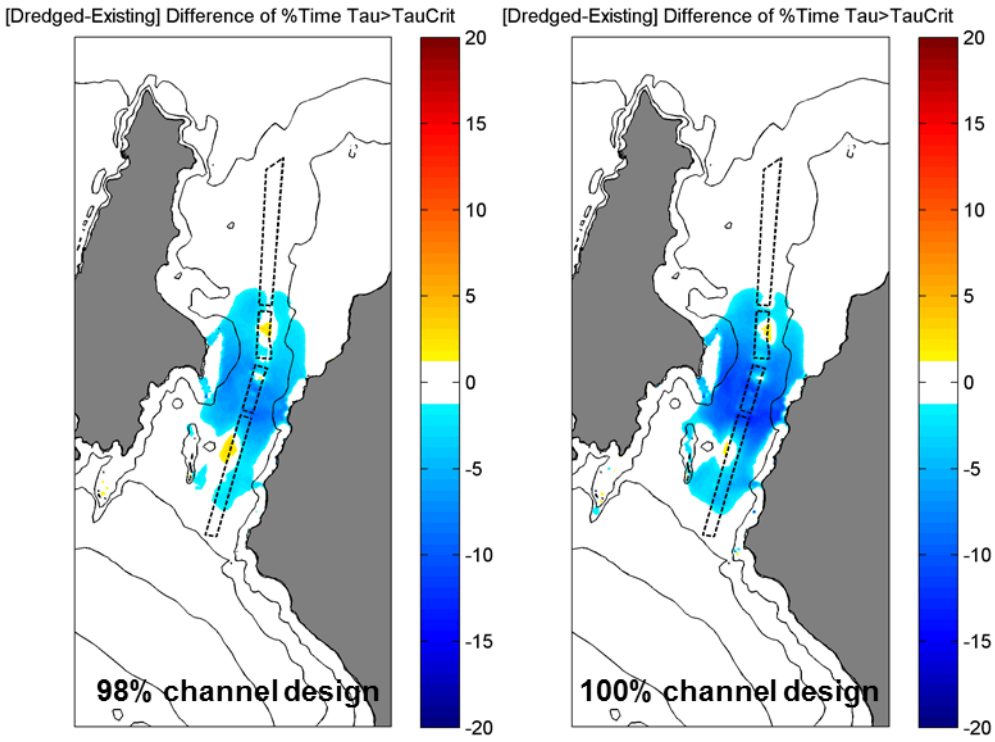

Figure 5.19 Differences of bed shear stress exceedance period calculated from a 28-day simulation for the existing channel, the 98% optimisation design (left) and the 100% optimisation design (right), based on the critical shear stress threshold.

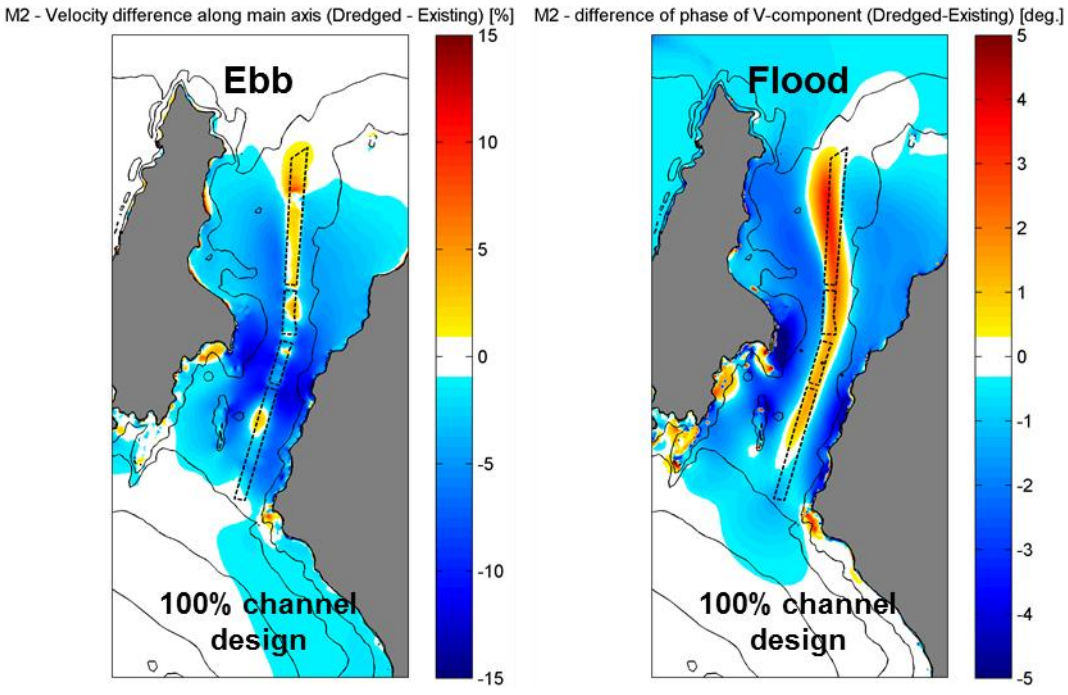

Figure 5.20 M2 velocity and phase differences post-dredging. A negative velocity difference indicates a smaller velocity on the post-dredging bathymetry (100% optimisation channel configurations). A positive phase difference indicates flow in advance over the post-dredging bathymetry relative to existing and vice versa.

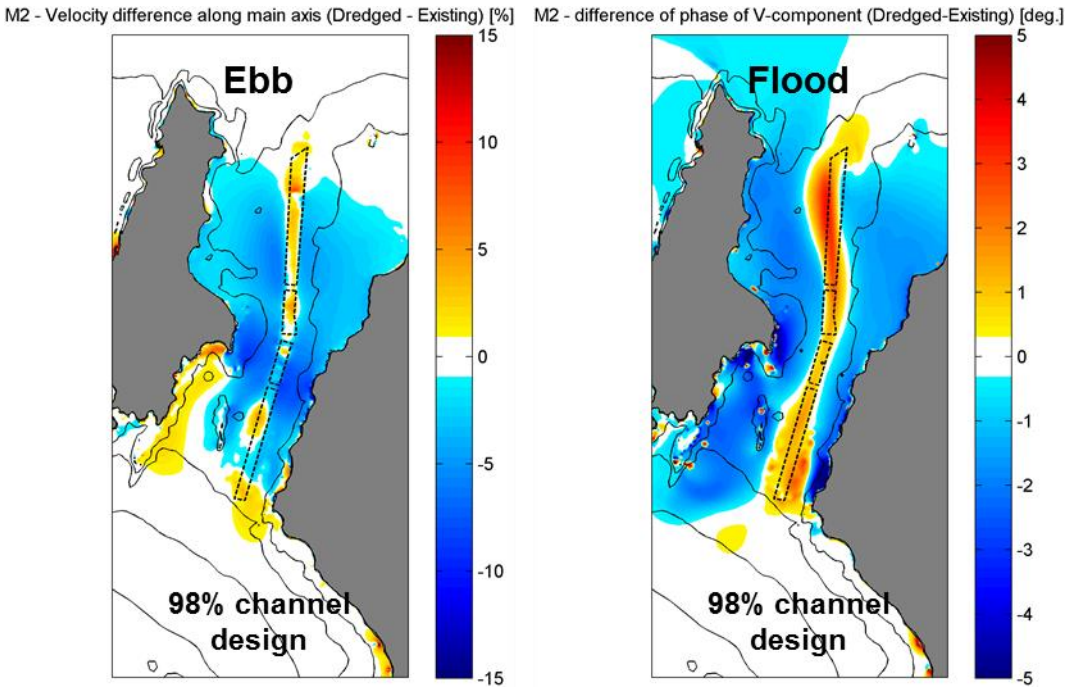

Figure 5.21 M2 velocity and phase differences post-dredging. A negative velocity difference indicates a smaller velocity on the post-dredging bathymetry (98% optimisation channel design). A positive phase difference indicates flow in advance over the post-dredging bathymetry relative to existing and vice versa.

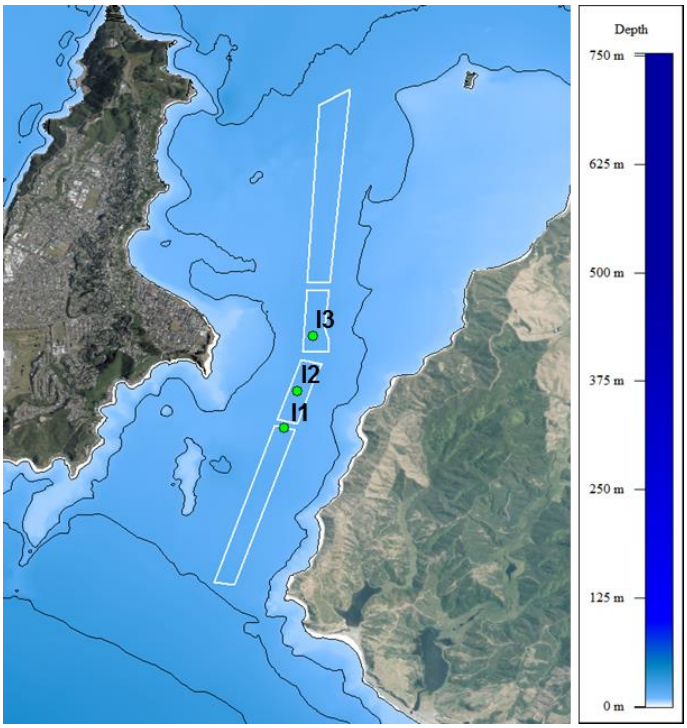

Figure 5.22 Positions I1, I2 and I3 used to extract modelled tidal velocities from constituents and estimate tidal asymmetry changes induced by the dredged channel designs.

Draft for public consultation

Table 5.4 Statistics of tidal asymmetry at spring tide calculated from modelled tidal constituents at the positions I1, I2 and I3 (Figure 5.22) for the existing channel, the 98% optimisation channel and the 100% optimisation channel configurations.

Positions	Spring tide				
	Mean ratio			Relative change (%)	
	Existing case	98% channel	100% channel	98% channel	100% channel
I1	1.105	1.025	1.065	-7%	-4%
I2	1.102	1.104	1.105	0%	0%
I3	1.103	1.145	1.146	4%	4%

Positions	Spring tide				
	p50 ratio			Relative change	
	Existing case	98% channel	100% channel	98% channel	100% channel
I1	1.091	1.033	1.042	-5%	-4%
I2	1.084	1.085	1.097	0%	1%
I3	1.043	1.097	1.093	5%	5%

Positions	Spring tide				
	p90 ratio			Relative change	
	Existing case	98% channel	100% channel	98% channel	100% channel
I1	1.102	1.097	1.101	0%	0%
I2	1.108	1.109	1.114	0%	1%
I3	1.113	1.124	1.127	1%	1%

Positions	Spring tide				
	Peak ratio			Relative change	
	Existing case	98% channel	100% channel	98% channel	100% channel
I1	1.105	1.100	1.103	0%	0%
I2	1.110	1.112	1.115	0%	0%
I3	1.122	1.130	1.133	1%	1%

Draft for public consultation

Table 5.5 Statistics of tidal asymmetry at neap tide calculated from modelled tidal constituents at the positions I1, I2 and I3 (Figure 5.22) for the existing channel, the 98% optimisation channel and the 100% optimisation channel configurations.

Positions	Neap tide				
	Mean ratio			Relative change	
	Existing case	98% channel	100% channel	98% channel	100% channel
I1	1.139	1.059	1.100	-7%	-3%
I2	1.228	1.138	1.140	-7%	-7%
I3	1.136	1.139	1.141	0%	0%

Positions	Neap tide				
	p50 ratio			Relative change	
	Existing case	98% channel	100% channel	98% channel	100% channel
I1	1.151	1.061	1.124	-8%	-2%
I2	1.201	1.125	1.134	-6%	-6%
I3	1.131	1.094	1.103	-3%	-2%

Positions	Neap tide				
	p90 ratio			Relative change	
	Existing case	98% channel	100% channel	98% channel	100% channel
I1	1.153	1.145	1.153	-1%	0%
I2	1.162	1.164	1.170	0%	1%
I3	1.187	1.193	1.201	1%	1%

Positions	Neap tide				
	Peak ratio			Relative change	
	Existing case	98% channel	100% channel	98% channel	100% channel
I1	1.152	1.145	1.149	-1%	0%
I2	1.161	1.165	1.171	0%	1%
I3	1.189	1.200	1.207	1%	2%

5.2.2. Effects on the swell wave climate

A total of 12 wave events (see Table 3.6) have been modelled with DELFT3D – WAVE to examine the effect of a disposal mound on the swell wave climate. The results for a mound of 4.5 m in height are shown in Figure 5.23 to Figure 5.25. The difference in wave climate induced by a mound of this height in this water depth is very small. For the modelled cases (with incoming waves of 2 to 4 m height), changes in height of the order 10 cm are predicted in the offshore regions adjacent to the mound, reducing to around 1 cm along the shoreline.

Regarding the dredged channel, the high-resolution SWAN model coupled to the tidal flow results was run with and without the deepened channel options

Draft for public consultation

to assess the effects of the new channel morphology on wave propagation and transformation. Both channel design have been considered, and the modelling technique has included wave generation within Wellington Harbour as well as the incoming swell energy from the open ocean.

Data spanning a 1-year period has been extracted and summary statistics for sites P1-P10 (Figure 5.26) are presented in Table 5.7. The spatial distribution in the mean and maximum significant wave height are given in Figure 5.27 and Figure 5.28 respectively, while the spatial distribution in the absolute changes are presented in Figure 5.29. Time-series and Quantile-Quantile plots comparing pre and post dredging channel configurations at both the 98% and 100% optimisation channel configuration for sites P1 though P10 are given in Figure 5.30 to Figure 5.40.

The model results show that because the entrance channel is nearly co-linear with the incoming swell waves, any deepening of the entrance will have an effect on the wave transformations. Enhanced refraction occurs along the steep sides of the dredged channel, directing energy predominantly to the western side of the entrance because of the slight orientation bias near the Pencarrow Head. This process occurs all along the channel length because wave diffraction also allows the progressive refraction and redirection of wave energy to persist over a relatively long distance. The net result is less wave energy reaching the eastern side of the harbour and an increase in energy along parts of the western side. On average, the 98% optimisation design is predicted to locally increase wave heights by 15% - 30% along the western side of the entrance, and cause a general decrease of 15% - 30% on the east side. Specifically:

- The amount of wave energy entering the harbour is unchanged. The effect of dredging is the redistribution of that energy.

- On the western side, the wave height increases show spatially variability. Along Seatoun Beach the average wave height increase is 11%, but only 5% during storm events. At Steeple Reef, the increase is up to around 50% during southerly storms. At Falcon Shoal, the wave heights increase 11% on average and up to 15% during the most energetic conditions.

- Within the shipping channel itself, the wave energy is consistently lower with the post-dredged bathymetry.

- Deepening the channel is not predicted to have any measurable effect on wave height at Lyall Bay and Breaker Bay.

Along the east side of the harbour, the systematic reduction in wave height has the potential to reduce surfing amenity. eCoast (2015) make note of a number of valued surf breaks in this area, and here Camp Bay has been selected as a representative site for quantitative analysis. The surf break at Camp Bay (Pipes) is classified as having a minimum required surfable height of 0.5 m. This is equivalent to a significant swell wave height of around 0.3 m, as the significant height is close to the average of the highest third of the waves.

Draft for public consultation

Considering this swell wave height criteria, the 98% optimisation design will reduce the percentage of potential surfable time from 29% to 6% (e.g. Figure 5.40). Accordingly, while the wave height will reduce around 25% at this site, the effect will be also be a five-fold reduction in the number of surfing opportunities, based on the minimum surfable height.

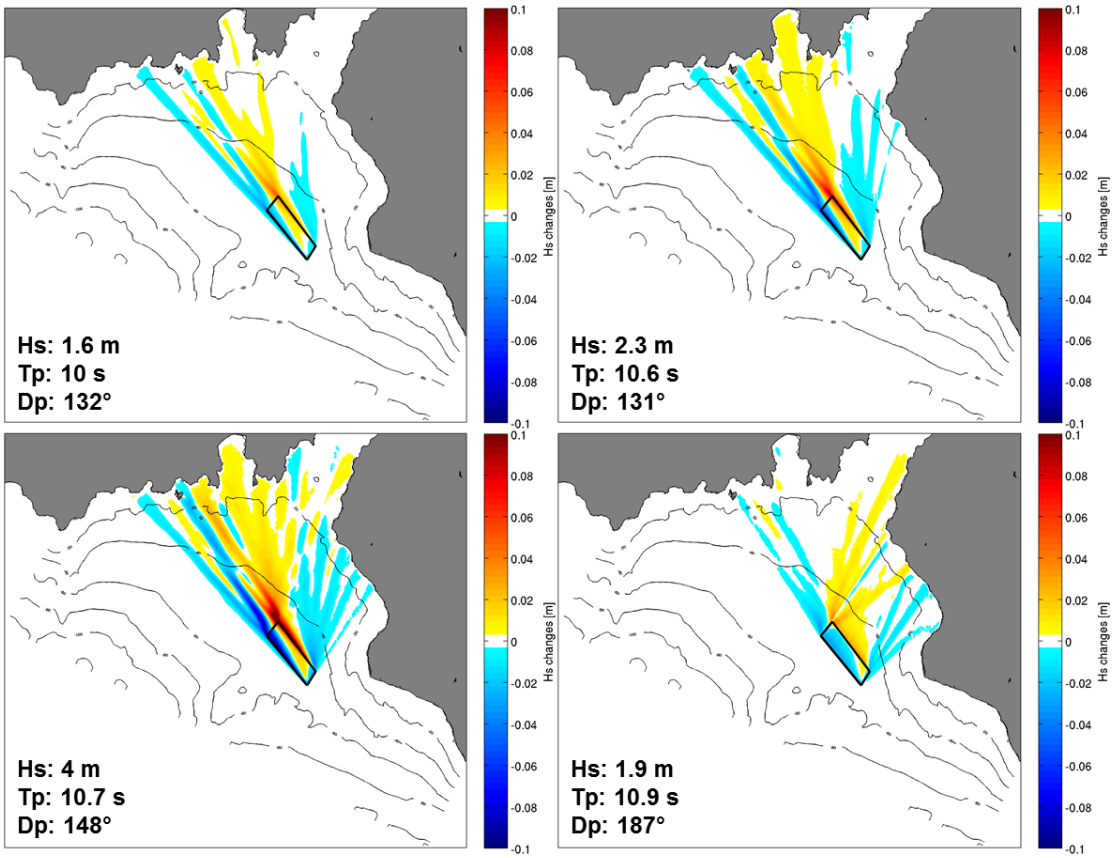

Figure 5.23 Absolute difference in significant wave height field between pre- and post-disposal ground configurations (4.5 m height) modelled Delft3D – WAVE for Runs 1 to 4 detailed in Table 3.6 without tidal and local wind forcing. Wave conditions prescribed at the boundaries of the coarser Delft3D domain are shown in the bottom left corner.

Draft for public consultation

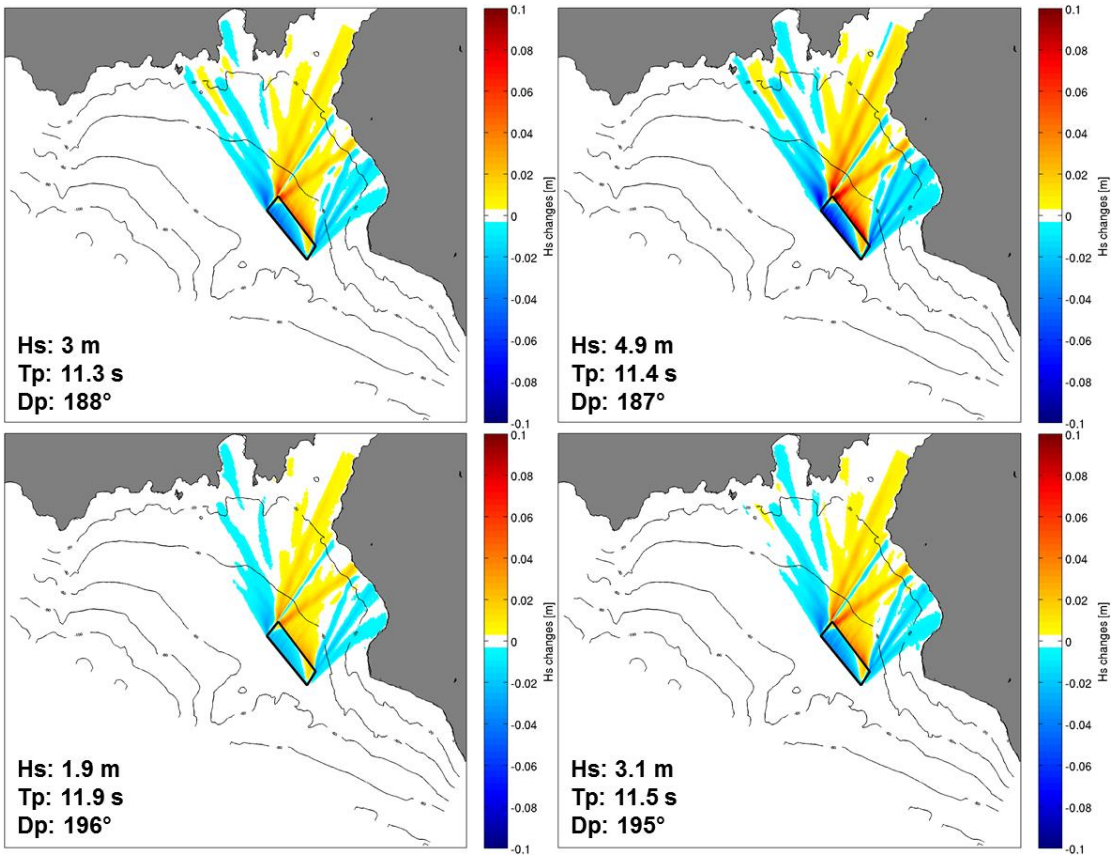

Figure 5.24 Absolute difference in significant wave height field between pre- and post-disposal ground configurations (4.5 m height) modelled Delft3D – WAVE for Runs 5 to 8 detailed in Table 3.6 without tidal and local wind forcing. Wave conditions prescribed at the boundaries of the coarser Delft3D domain are shown in the bottom left corner.

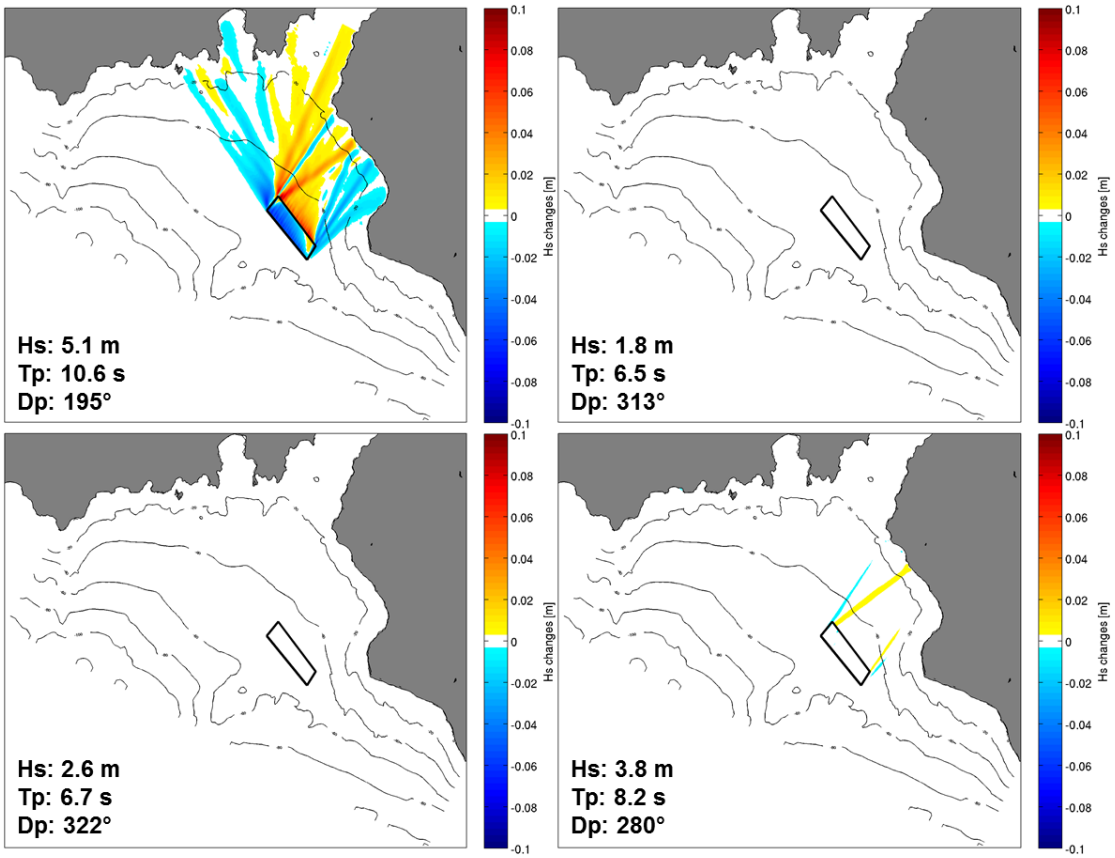

Figure 5.25 Absolute difference in significant wave height field between pre- and post-disposal ground configurations (4.5 m height) modelled Delft3D – WAVE for Runs 9 to 12 detailed in Table 3.6 without tidal and local wind forcing. Wave conditions prescribed at the boundaries of the coarser Delft3D domain are shown in the bottom left corner.

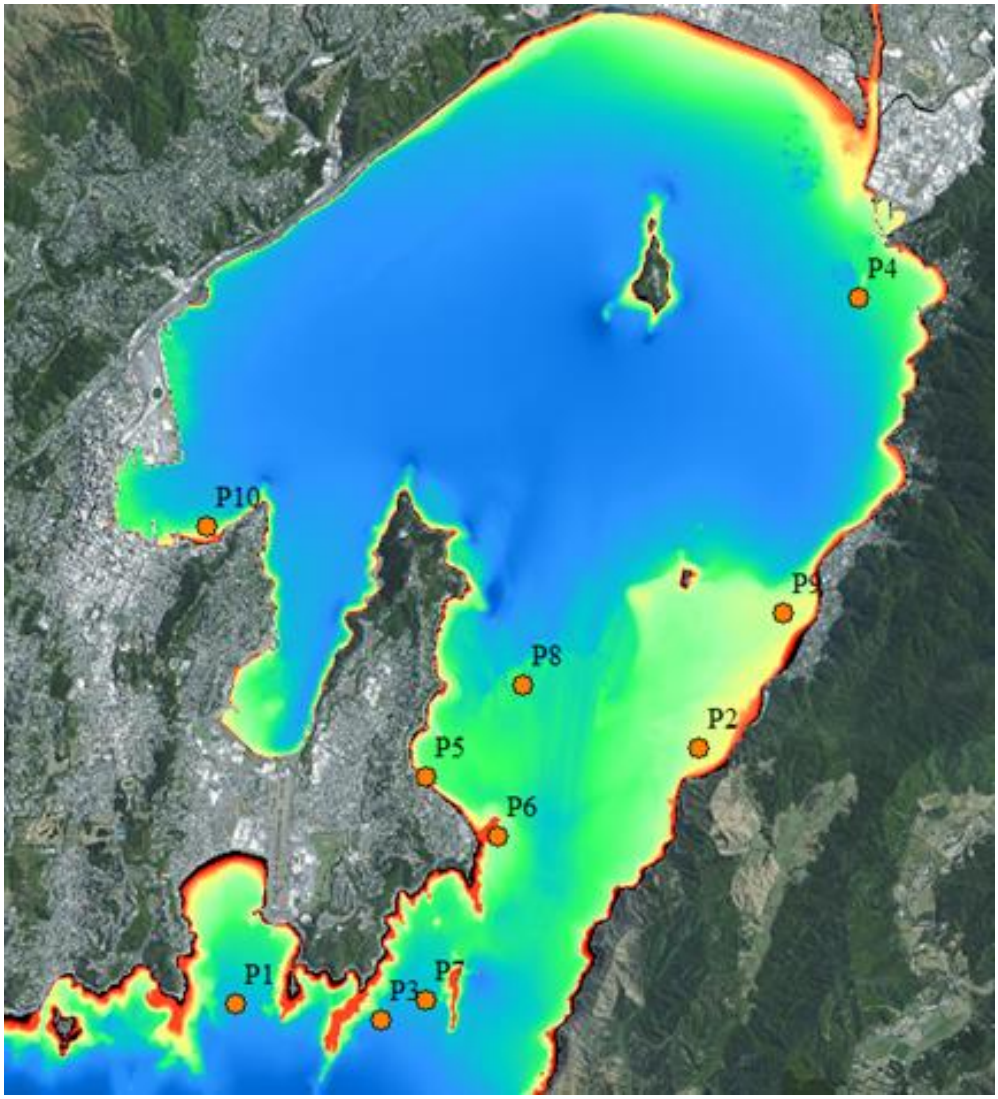

Figure 5.26 Locations of the 10 positions used to compare the wave climate at Wellington Harbour between the pre- and post-dredging configurations. Geographic coordinates of the positions are detailed in Table 3.3

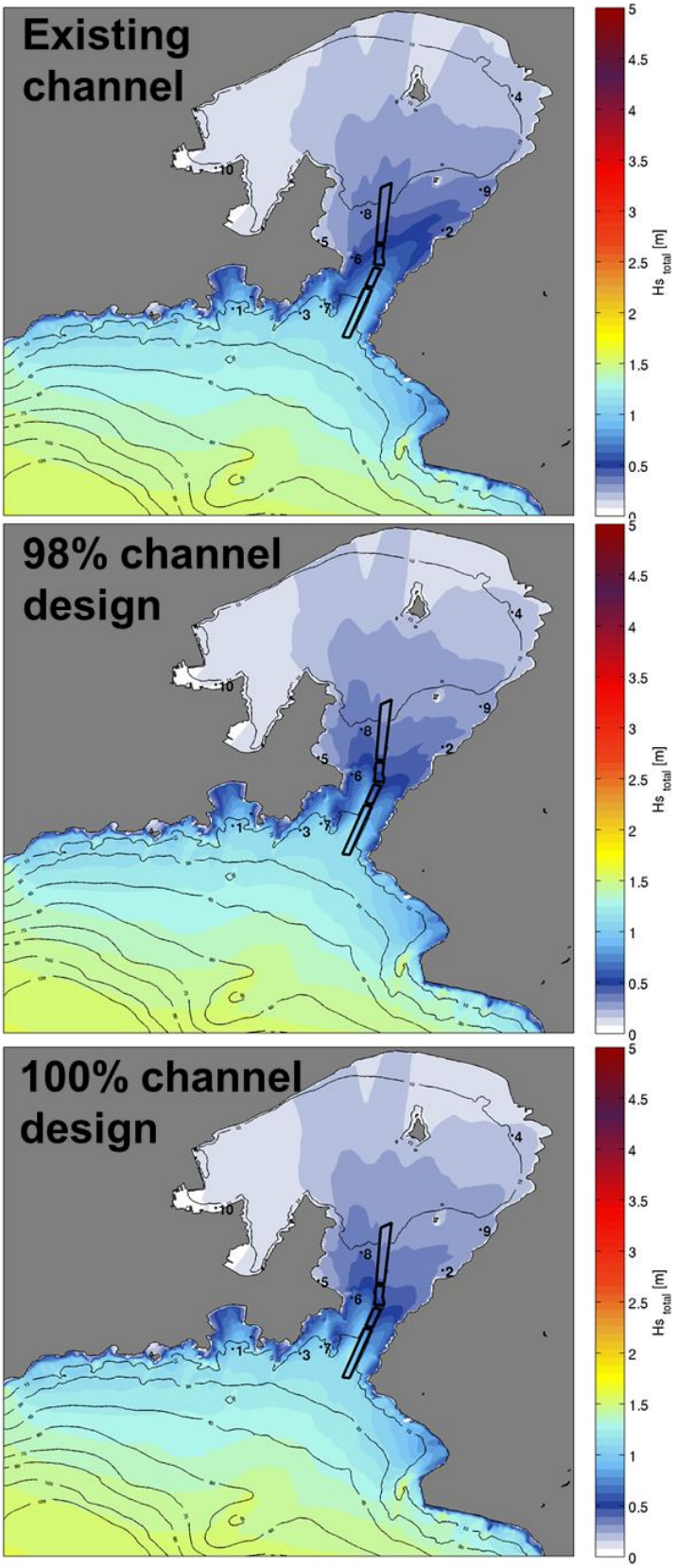

Figure 5.27 Mean significant wave height for pre- and post-dredge (98% and 100% optimisation channel designs) configurations calculated from the annual (2012) modelled wave conditions. The positions P1 to P10 have been used to compare the wave climate between configurations.

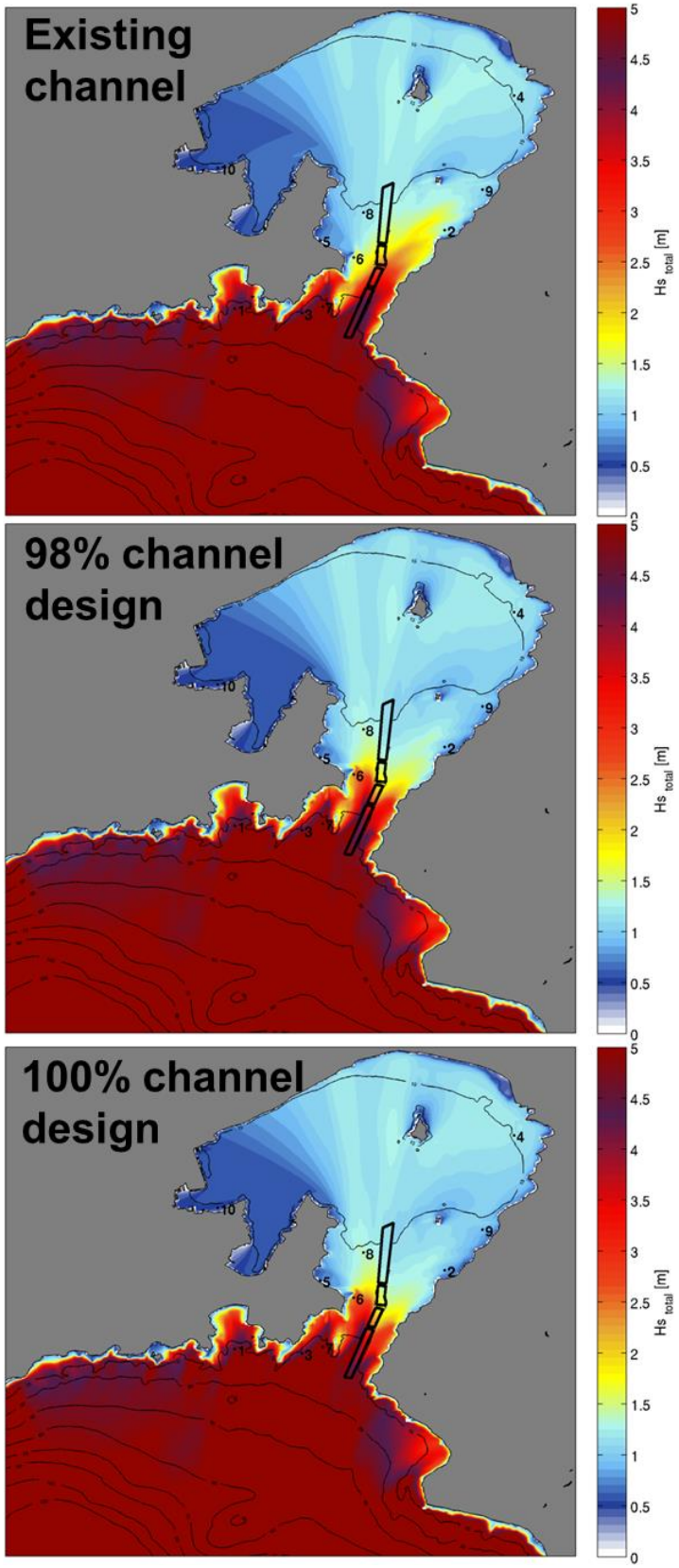

Figure 5.28 Maximum significant wave height for pre- and post-dredging (98% and 100% optimisation channel designs) configurations calculated from 1 year (2012) modelled wave conditions. The positions P1 to P10 have been used to compare the wave climate between configurations.

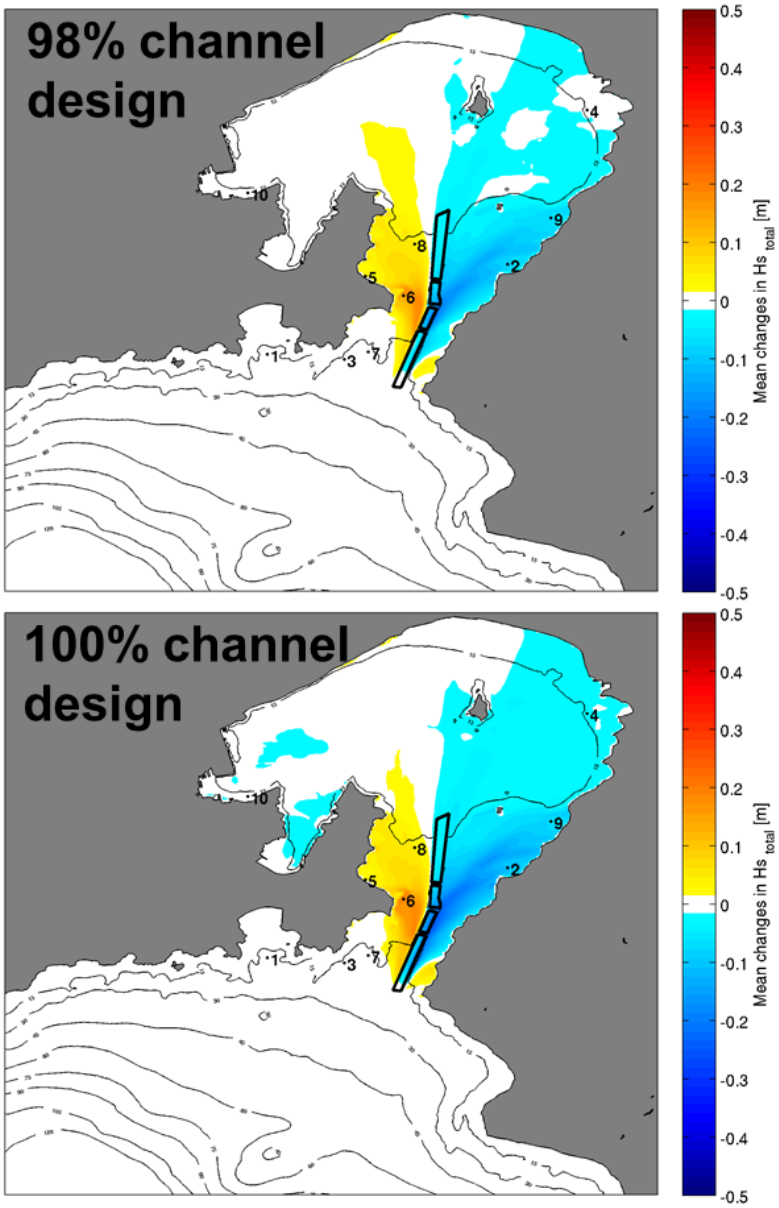

Figure 5.29 Absolute mean changes (m) in significant wave height calculated from the modelled wave conditions for the pre- and post-dredging conditions (98% and 100% optimisation channel designs). Positive magnitudes indicate an increase of the wave height induced by the dredging. The positions P1 to P10 have been used to compare the wave climate between configurations.

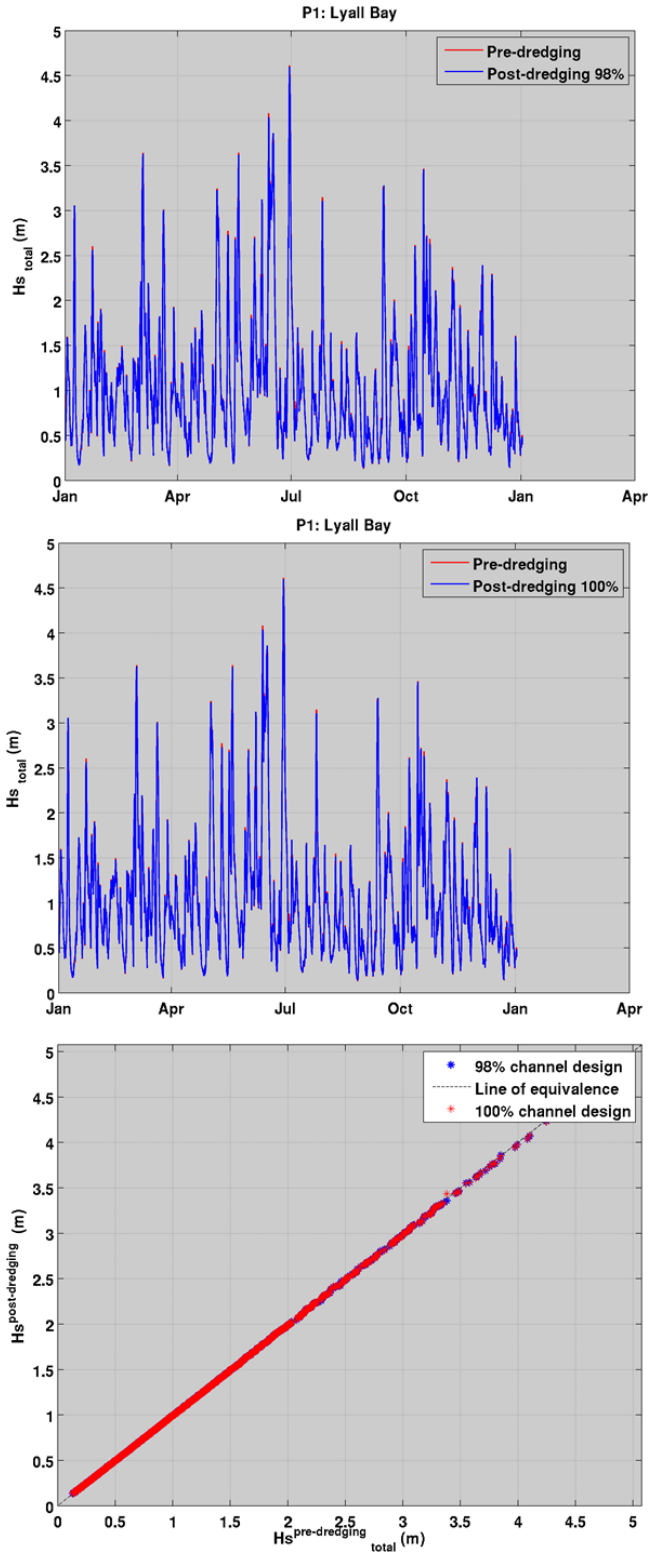

Figure 5.30 Time series and quantile-quantile plots of total significant wave height at Lyall Bay (Site P1, Fig 5.26) calculated from 1 year (2012) of modelled wave conditions for the existing channel, the 98% optimisation channel and the 100% optimisation channel configurations.

Draft for public consultation

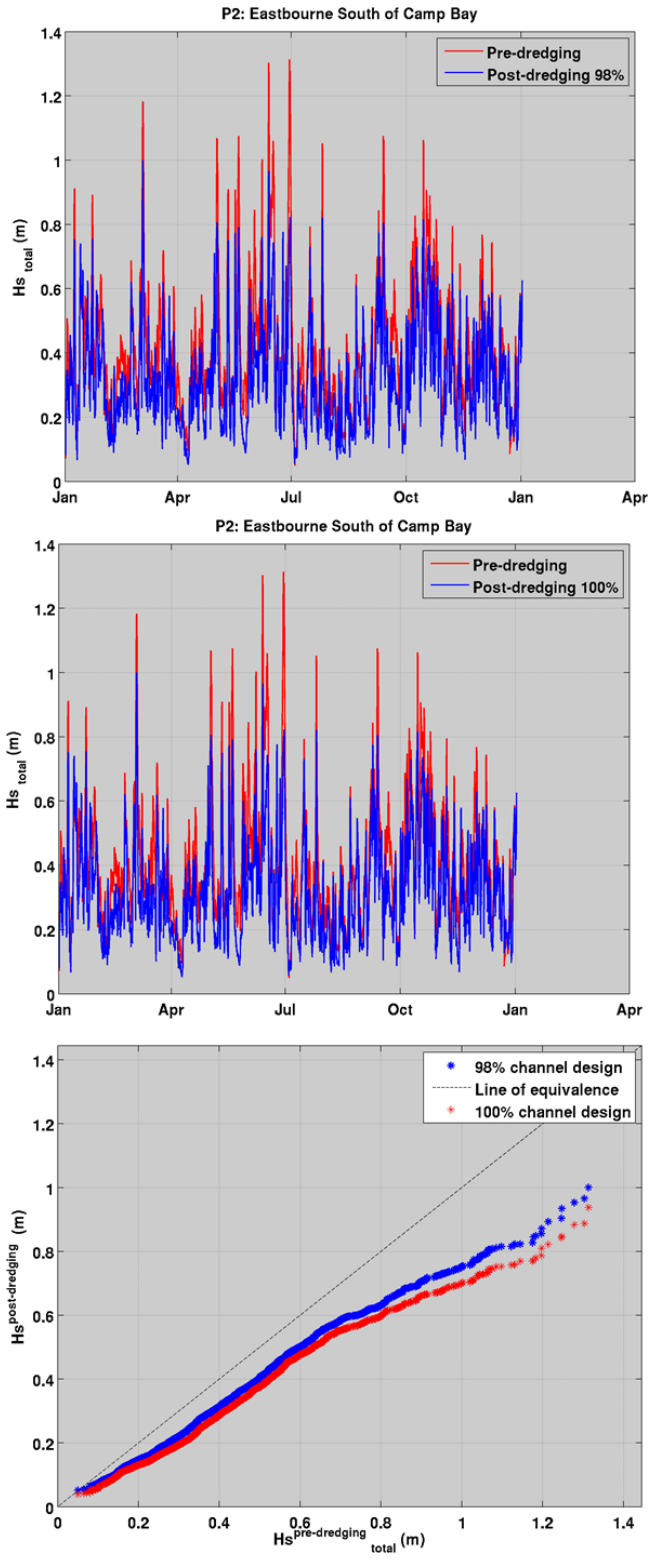

Figure 5.31 Time series and quantile-quantile plots of total significant wave height at Eastbourne South of Camp Bay (Site P2, Fig 5.26) calculated from 1 year (2012) of modelled wave conditions for the existing channel, the 98% optimisation channel and the 100% optimisation channel configurations.

Draft for public consultation

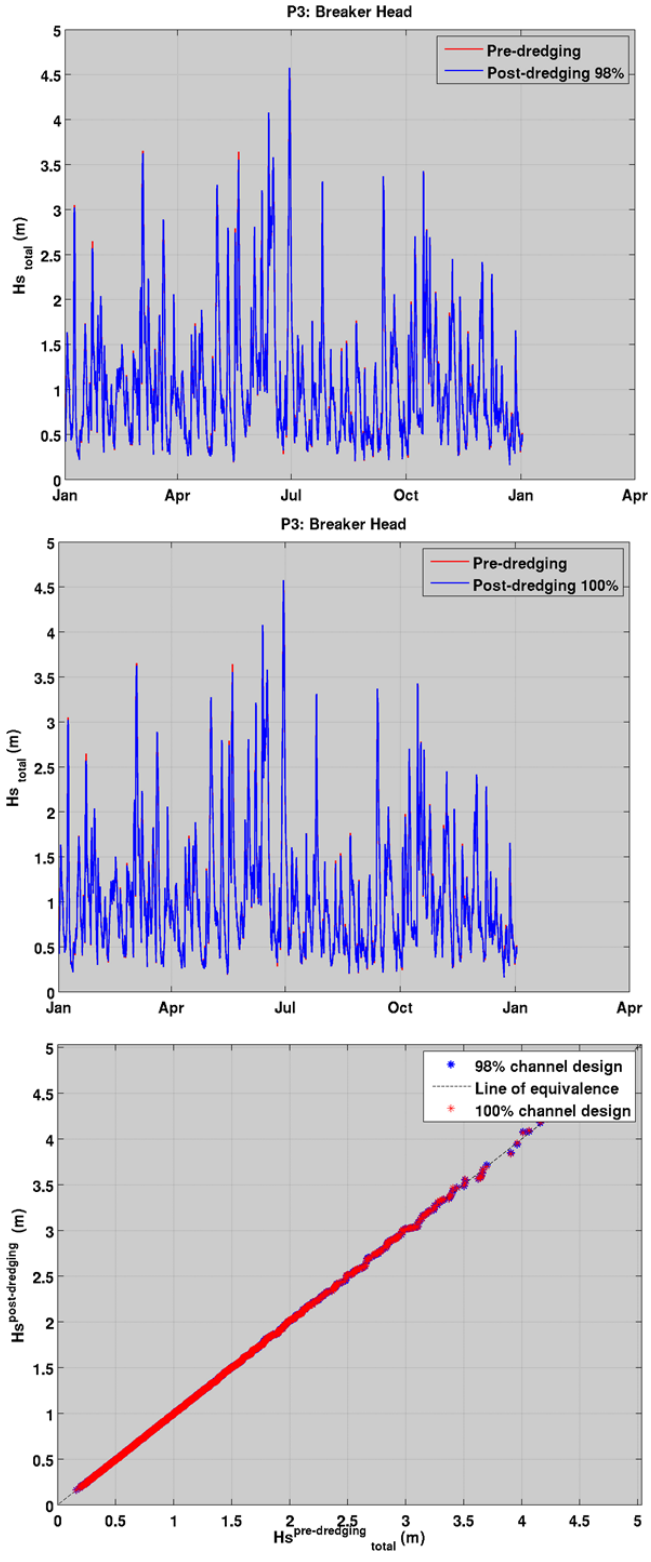

Figure 5.32 Time series and quantile-quantile plots of total significant wave height at Breaker Head (Site P3, Fig 5.26) calculated from 1 year (2012) of modelled wave conditions for the existing channel, the 98% optimisation channel and the 100% optimisation channel configurations.

Draft for public consultation

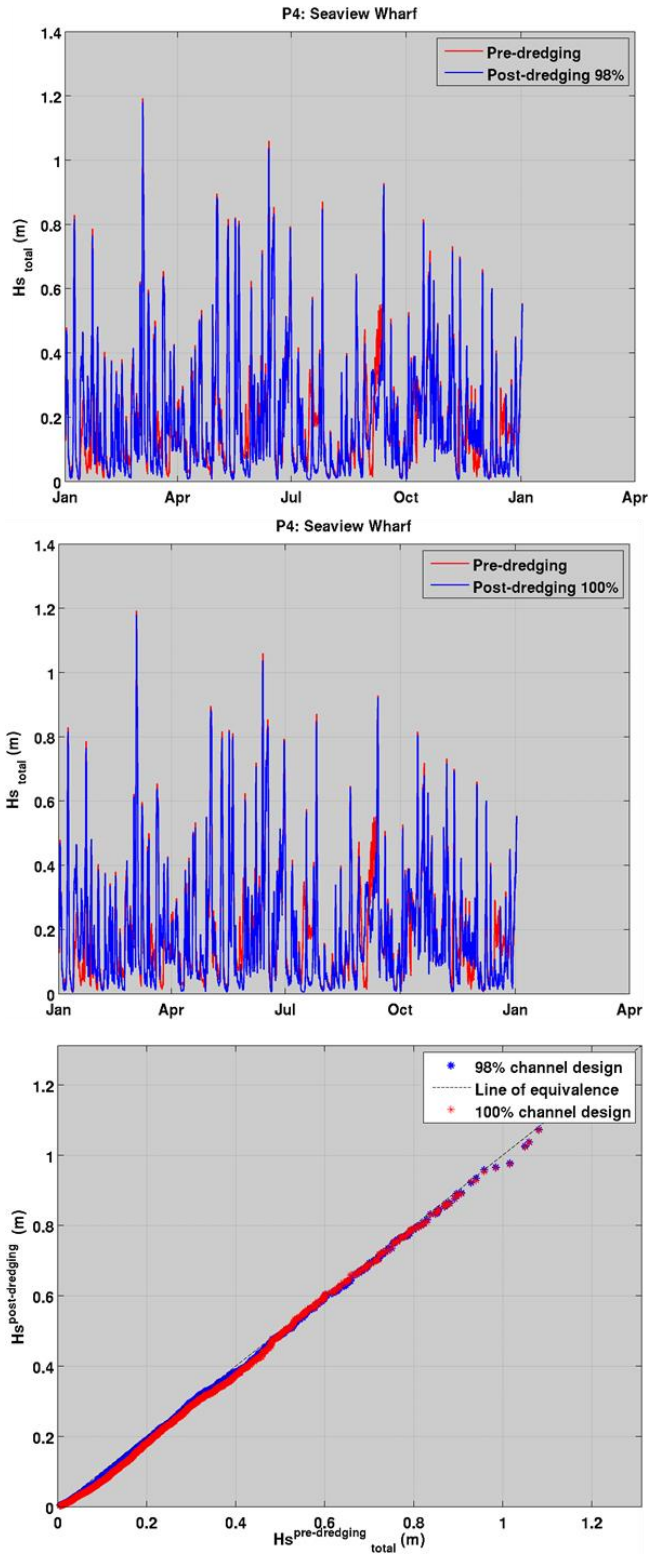

Figure 5.33 Time series and quantile-quantile plots of total significant wave height at Seaview Wharf (Site P4, Fig 5.26) calculated from 1 year (2012) of modelled wave conditions for the existing channel, the 98% optimisation channel and the 100% optimisation channel configurations.

Draft for public consultation

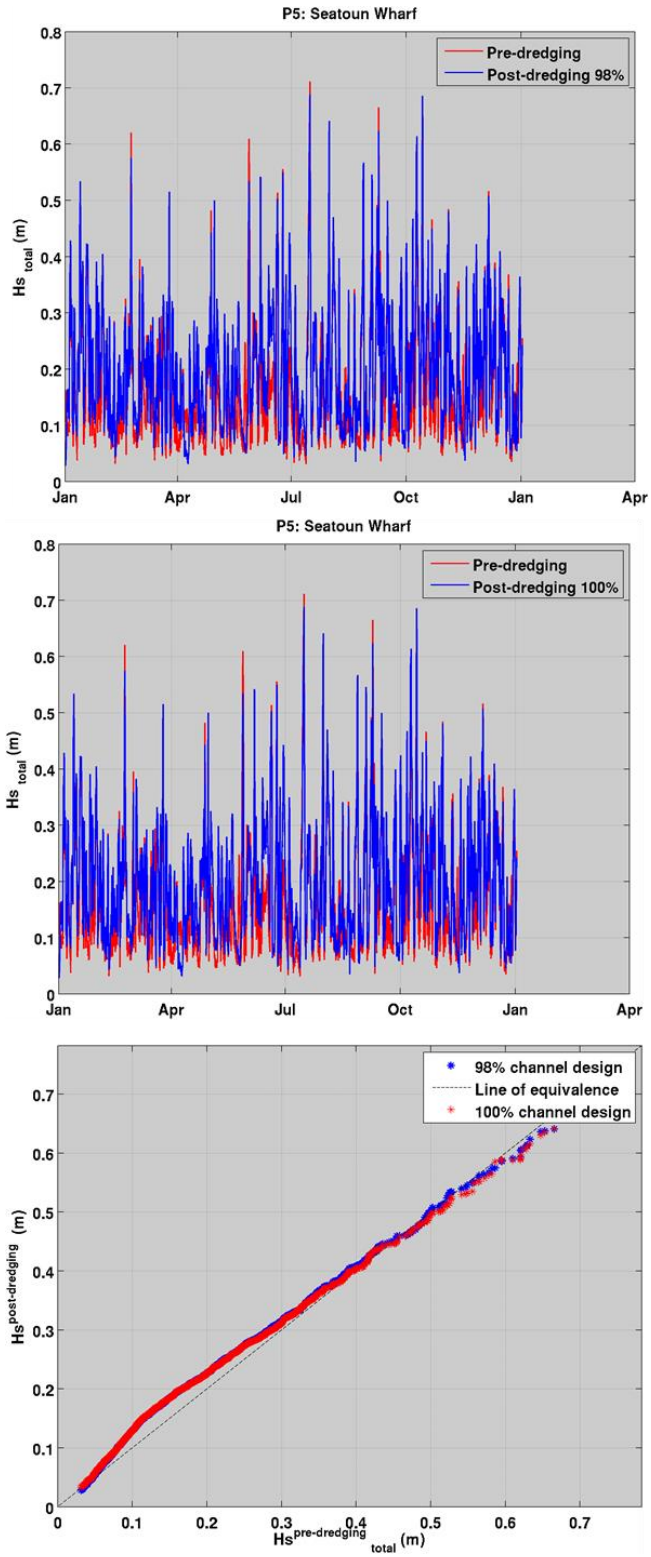

Figure 5.34 Time series and quantile-quantile plots of total significant wave height at Seatoun wharf (Site P5, Fig 5.26) calculated from 1 year (2012) of modelled wave conditions for the existing channel, the 98% optimisation channel and the 100% optimisation channel configurations.

Draft for public consultation

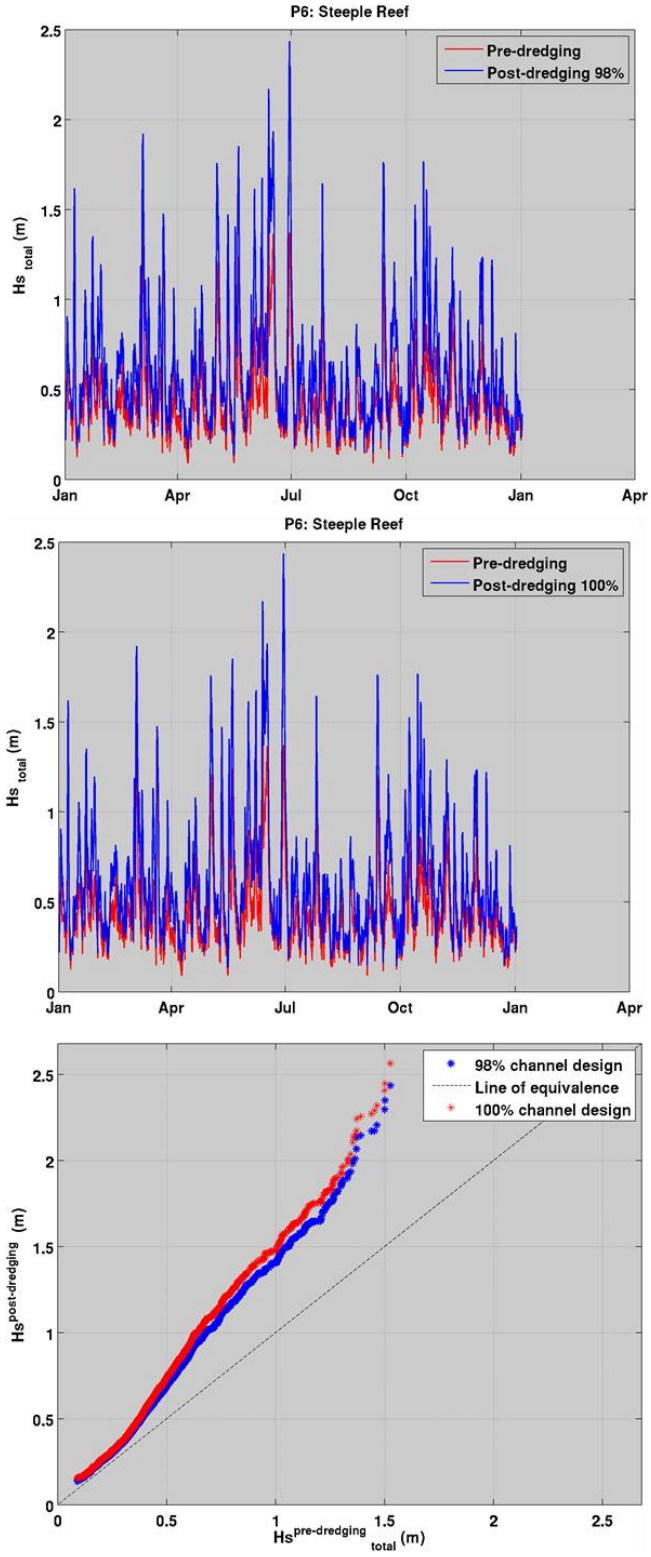

Figure 5.35 Time series and quantile-quantile plots of total significant wave height at Steeple Reef (Site P6, Fig 5.26) calculated from 1 year (2012) of modelled wave conditions for the existing channel, the 98% optimisation channel and the 100% optimisation channel configurations.

Draft for public consultation

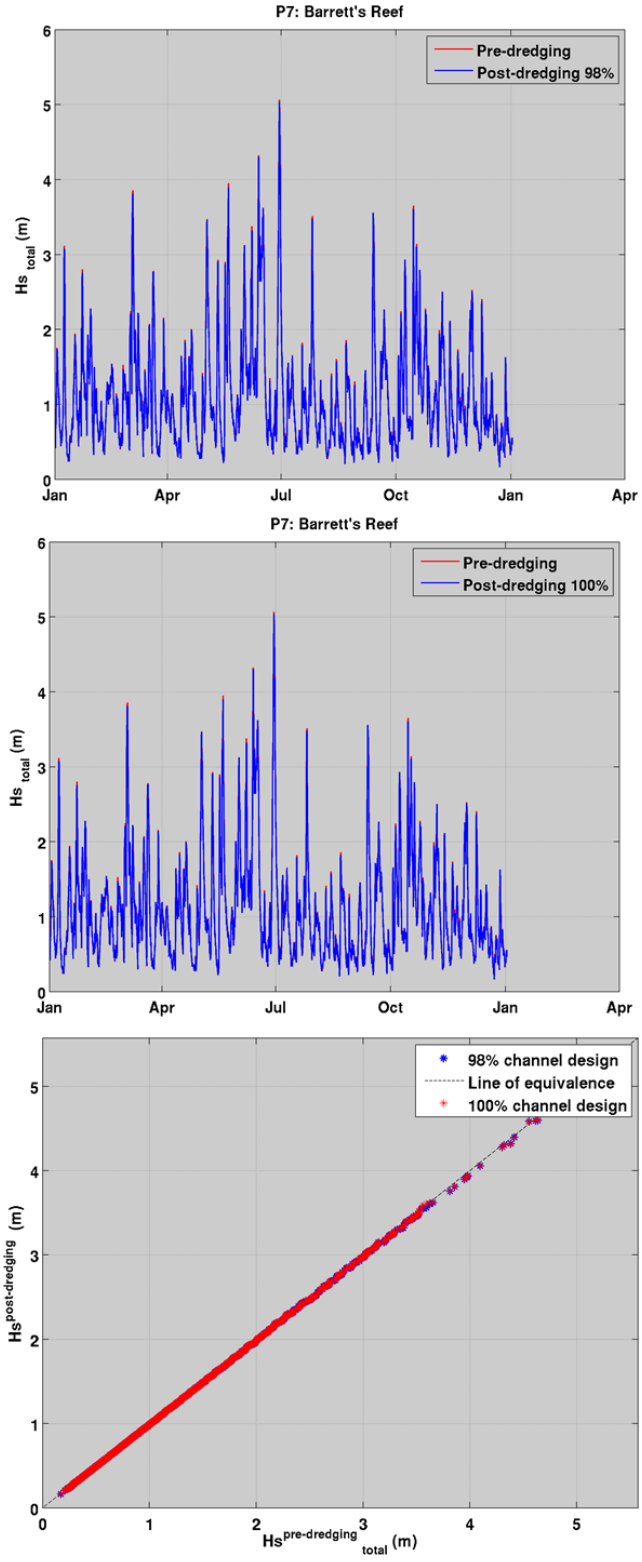

Figure 5.36 Time series and quantile-quantile plots of total significant wave height at Barrett's Reef (Site P7, Fig 5.26) calculated from 1 year (2012) of modelled wave conditions for the existing channel, the 98% optimisation channel and the 100% optimisation channel configurations.

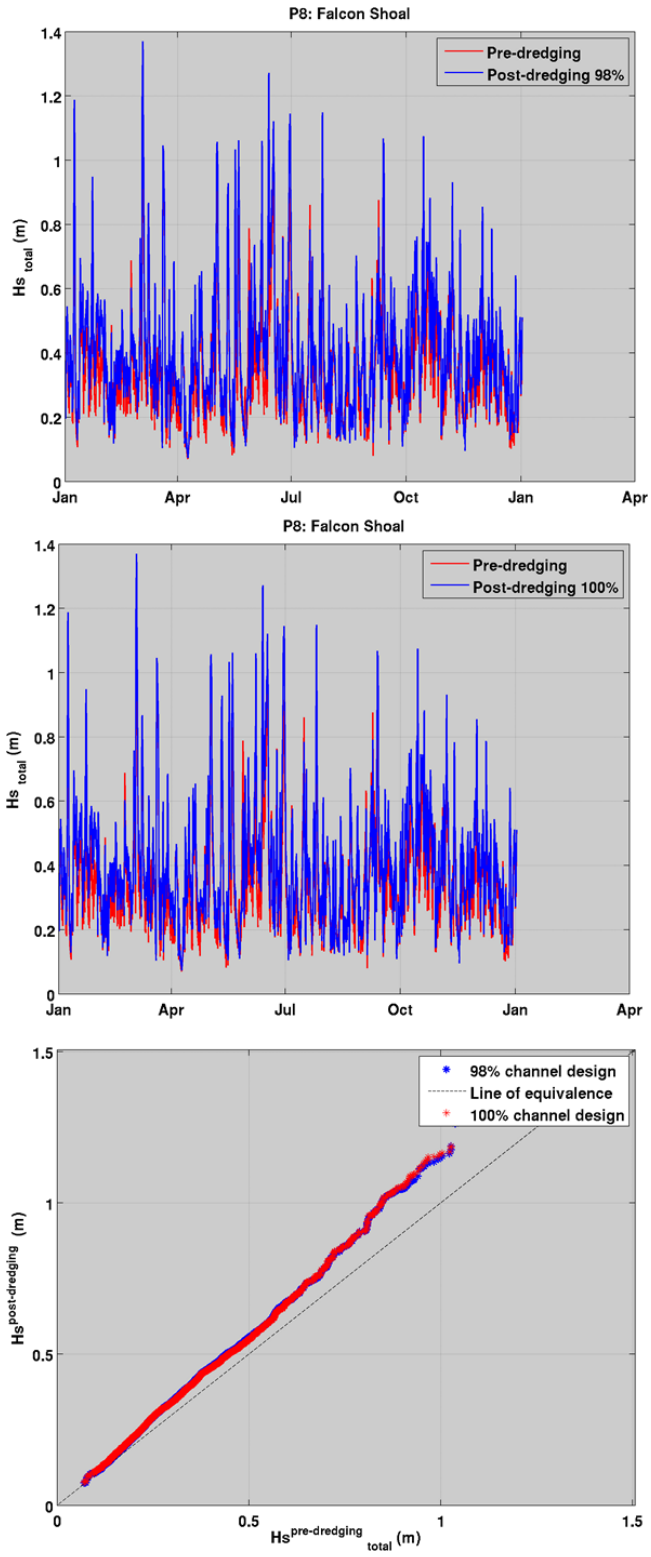

Figure 5.37 Time series and quantile-quantile plots of total significant wave height at Falcon Shoal (Site P8, Fig 5.26) calculated from 1 year (2012) of modelled wave conditions for the existing channel, the 98% optimisation channel and the 100% optimisation channel configurations.

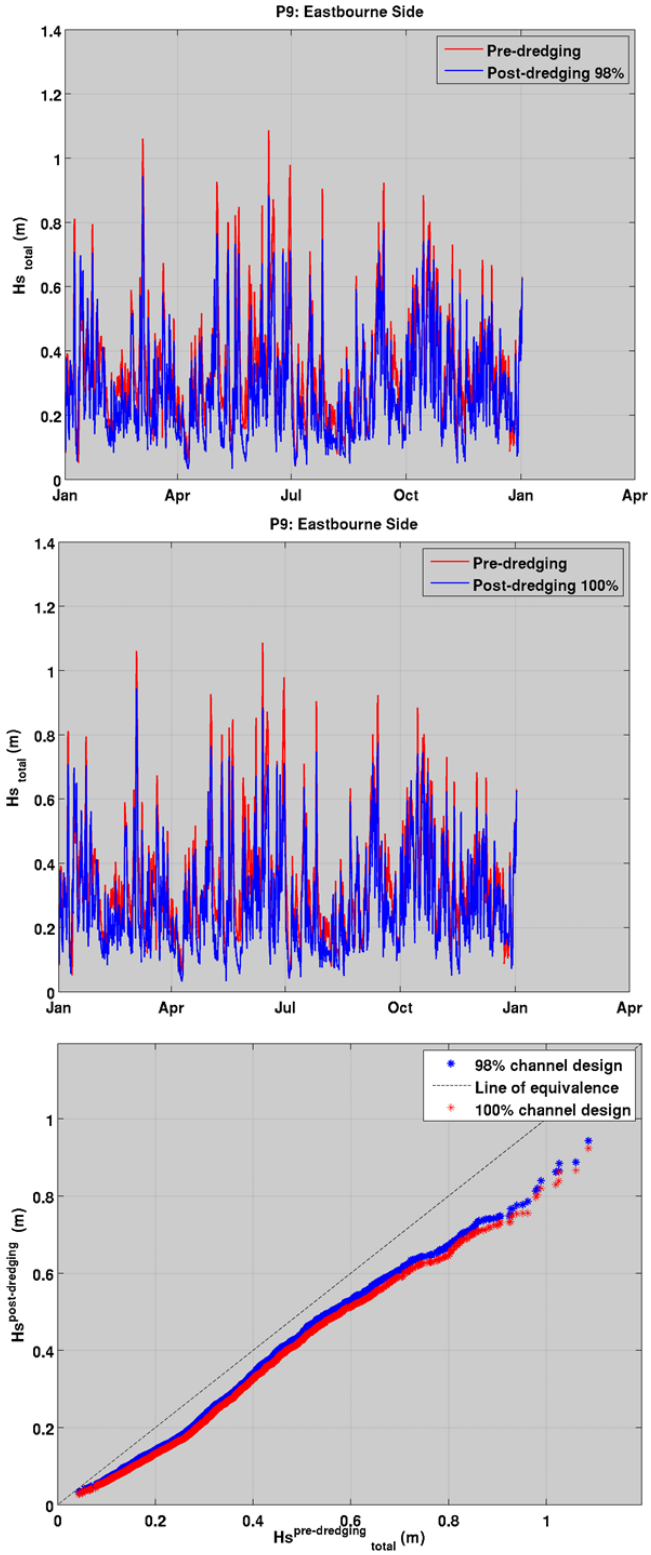

Figure 5.38 Time series and quantile-quantile plots of total significant wave height at Eastbourne Side (Site P9, Fig 5.26) calculated from 1 year (2012) of modelled wave conditions for the existing channel, the 98% optimisation channel and the 100% optimisation channel configurations.

Draft for public consultation

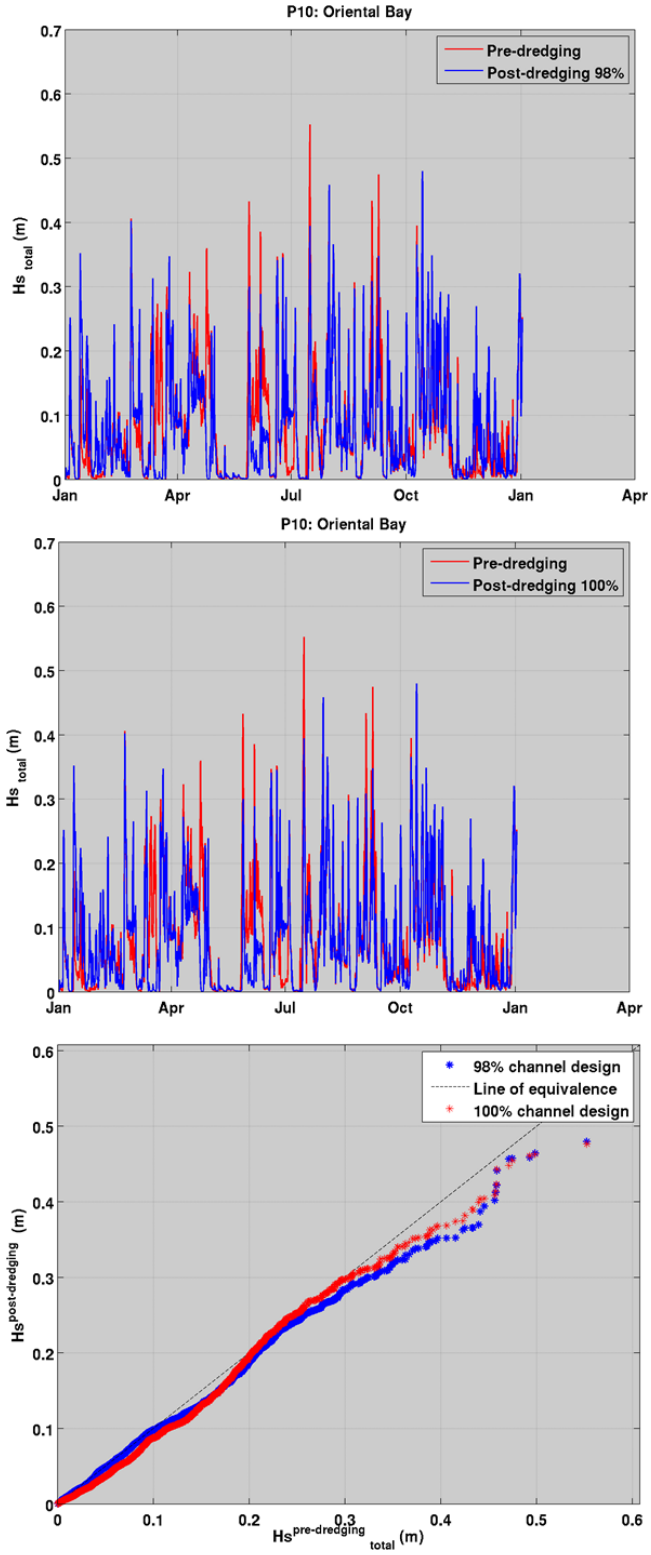

Figure 5.39 Time series and quantile-quantile plots of total significant wave height at Oriental Bay (Site P10, Fig 5.26) calculated from 1 year (2012) of modelled wave conditions for the existing channel, the 98% optimisation channel and the 100% optimisation channel configurations.

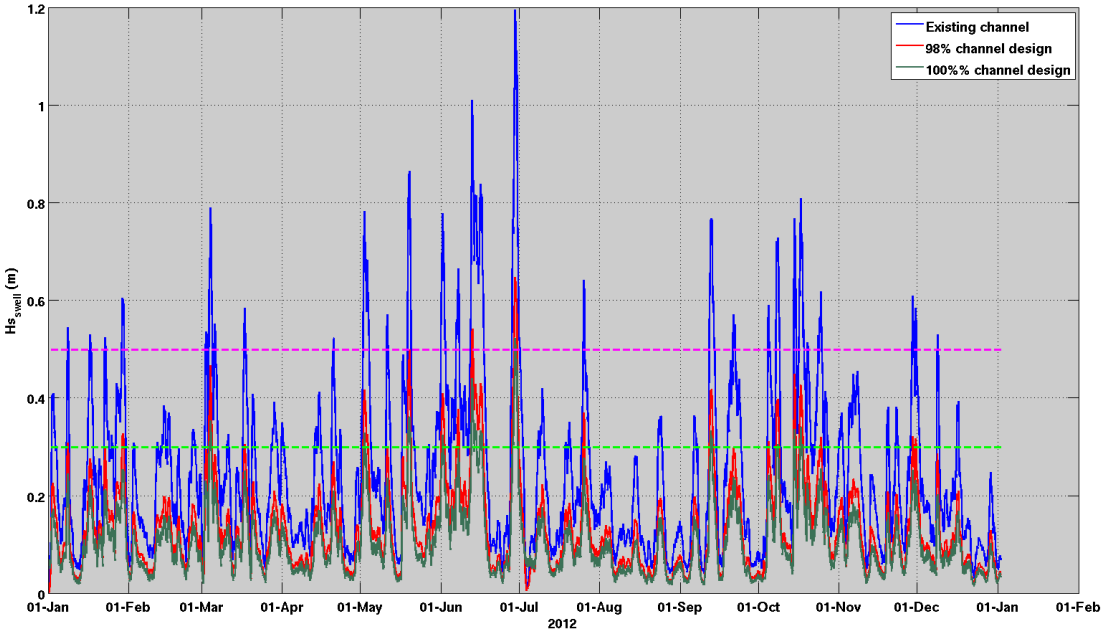

Figure 5.40 Time series total significant wave height at Camp Bay calculated from 1 year (2012) of modelled wave conditions for the existing channel, the 98% optimisation channel and the 100% optimisation channel configurations. Dashed green and magenta lines indicate the 0.3 m and 0.5 m wave height thresholds.

Table 5.6 Location of the sites to examine wave effects from channel deepening.

Positions		Site S1			
		Geographic (deg.)		NZTM (m)	
		Longitude	Latitude	X	Y
P1	Lyall Bay	174.800455	-41.346472	1750628	5421216
P2	South Camp Bay	174.874095	-41.314434	1756866	5424642
P3	Breaker Head	174.823981	-41.348218	1752592	5420981
P4	Seaview Wharf	174.898406	-41.259609	1759034	5430685
P5	Seatoun Wharf	174.830469	-41.318643	1753204	5424253
P6	Steeple Reef	174.842117	-41.325598	1754163	5423460
P7	Barrett's Reef	174.831306	-41.345624	1753211	5421256
P8	Falcon Shoal	174.845555	-41.307215	1754494	5425495
P9	Eastbourne Side	174.887352	-41.297912	1758016	5426453
P10	Oriental Bay	174.794386	-41.289021	1750253	5427605

Draft for public consultation

Table 5.7 Statistics calculated from the annual (2012) modelled Hs time series at 10 locations in the Wellington Harbour with the existing channel, the 98% optimisation channel and the 100% optimisation channel configurations. See Table 3.3 for coordinates. Hs max and Hs mean indicates the mean and the maximum values of significant wave height, respectively. Hs (95) and Hs (95) corresponds to the 95th and 99th percentile of the significant wave height distribution.

Position		Configuration	Hs max (m)	Hs mean (m)	Hs (95) (m)	Hs (99) (m)
P1	Lyall Bay	Existing	4.61	1.03	2.50	3.36
		98% optimisation	4.60	1.02	2.48	3.34
		100% optimisation	4.60	1.02	2.48	3.35
P2	South Camp Bay	Existing	1.31	0.40	0.79	1.04
		98% optimisation	1.00	0.32	0.62	0.78
		100% optimisation	0.94	0.29	0.59	0.73
P3	Breaker Head	Existing	4.57	1.02	2.43	3.32
		98% optimisation	4.58	1.02	2.42	3.33
		100% optimisation	4.59	1.02	2.42	3.33
P4	Seaview Wharf	Existing	1.19	0.19	0.56	0.82
		98% optimisation	1.18	0.18	0.55	0.81
		100% optimisation	1.18	0.17	0.56	0.80
P5	Seatoun Wharf	Existing	0.71	0.17	0.38	0.53
		98% optimisation	0.69	0.19	0.39	0.53
		100% optimisation	0.69	0.19	0.39	0.52
P6	Steeple Reef	Existing	1.53	0.44	0.92	1.26
		98% optimisation	2.44	0.60	1.34	1.77
		100% optimisation	2.56	0.63	1.41	1.86
P7	Barrett's Reef	Existing	5.07	1.09	2.59	3.51
		98% optimisation	5.04	1.08	2.57	3.47
		100% optimisation	5.02	1.08	2.57	3.47
P8	Falcon Shoal	Existing	1.17	0.35	0.70	0.91
		98% optimisation	1.37	0.39	0.78	1.06
		100% optimisation	1.37	0.39	0.78	1.06
P9	Eastbourne Side	Existing	1.09	0.34	0.66	0.85
		98% optimisation	0.94	0.27	0.58	0.72
		100% optimisation	.92	0.26	0.56	0.71
P10	Oriental Bay	Existing	0.55	0.08	0.26	0.37
		98% optimisation	0.48	0.08	0.25	0.33
		100% optimisation	0.48	0.07	0.26	0.35

Table 5.8 Annual and monthly swell wave height exceedance statistics at Camp Bay.

% exceedance	Hs_{swell} > 0.3 m	
	Existing channel	98% channel design
Jan	32%	3%
Feb	14%	0%
March	34%	4%
April	15%	0%
May	40%	9%
June	64%	30%
July	23%	2%
August	6%	0%
September	30%	5%
October	49%	13%
November	32%	1%
December	9%	0%
Total	**29%**	**6%**
Days/year	**106**	**22**

Draft for public consultation

5.3. Morphodynamic effects

A range of annual morphological simulations were undertaken to first characterize the existing sediment dynamics of the Wellington Harbour region and then identify key changes resulting from the proposed dredging and offshore disposal activities.

5.3.1. Offshore disposal ground morphology

An overview of the existing circulation, wave and bed shear stress fields for the region beyond the harbour entrance are presented in Figure 5.41 to Figure 5.43 for the three different wave events of the reduced annual wave climate (i.e. Events 1, 3 and 9 from Table 3.6). Total morphological changes predicted after 1 year for a generic disposal ground with 4.5 m elevation are presented in Figure 5.44 for three discrete grain sizes (100, 200 and 300 µm). These annual morphological changes show a general north-westward migration of the disposed sediments; consistent with the tidal ellipse and residual currents in Fitzroy Bay. The model does not predict significant sediment transport directly towards the coastal areas or the shipping channel. The decadal morphological simulation (Figure 5.45) of the design disposal ground with 6.0 M m^3 produces similar patterns of morphological change, with a slow north-westward migration of the disposed sediments.

As described in Section 3.4 (see Table 3.7), historical extreme events were run to test the input reduction approach by applying a realistic time-varying forcing scenario. Wave, current and bed shear stress fields associated with these events are presented in Figure 5.46 – 5.51. Notably, the magnitude of sediment transport induced by these discrete extreme events is relatively minor compared to the annual changes, especially for the 200 and 300 µm grain sizes. General erosion and sedimentation patterns obtained with a 100 µm grain size are consistent with the previous results obtained for the input reduction. The southern part of the disposal ground is subject to erosion while sediments are slightly transported in the northwest direction, mostly following the tidal flow forcing. These results suggest that although strong wind-driven current or energetic wave events may significantly affect the instantaneous sediment transport forcing over the ground at times, the long term behaviour of the disposal mound will rather be governed by the continuous tidal forcing superimposed with net residuals, rather than by the succession of discrete energetic events.

The ambient wave energy field does not appear to be significantly affected by the offshore disposal mound (i.e. no obvious focusing effect) which is due to the scale of depth change expected from the disposal activity. Note the presence of a reef located southwest of the proposed disposal ground acts to slightly reduce the wave energy through bottom friction during some events (i.e. Event 3 and 9). The water depth at the proposed offshore disposal ground means there is a limited effect from waves on local bed shear stresses. For example, the very energetic wave Event 9 produces shear stress magnitudes similar to these predicted for the wave Event 1 which was much less energetic, indicating the bed shear stress variability is mainly driven by the strong tidal flows rather than episodic events with high near-bed wave orbital velocities.

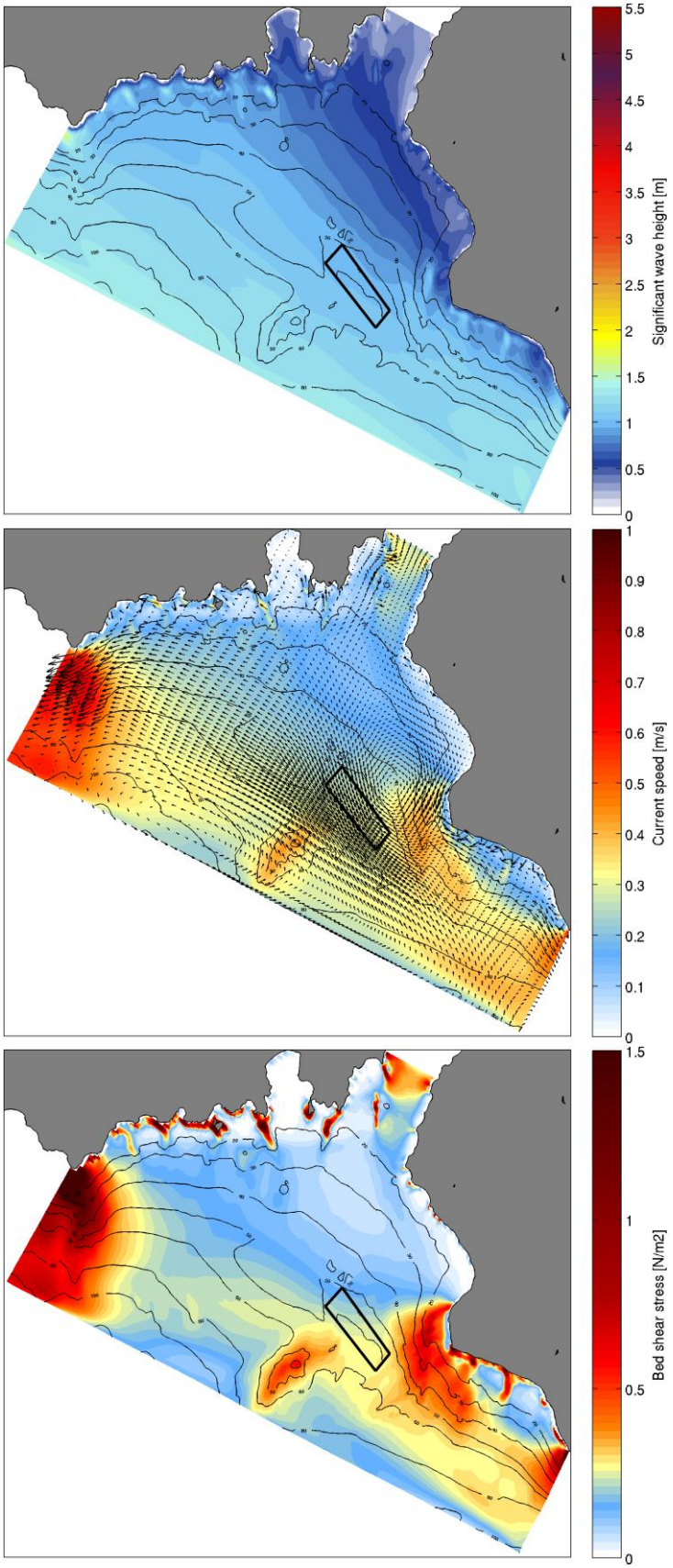

Figure 5.41 Wave, circulation and bed shear stress fields averaged over the representative tide for Event 1 of Table 3.6.

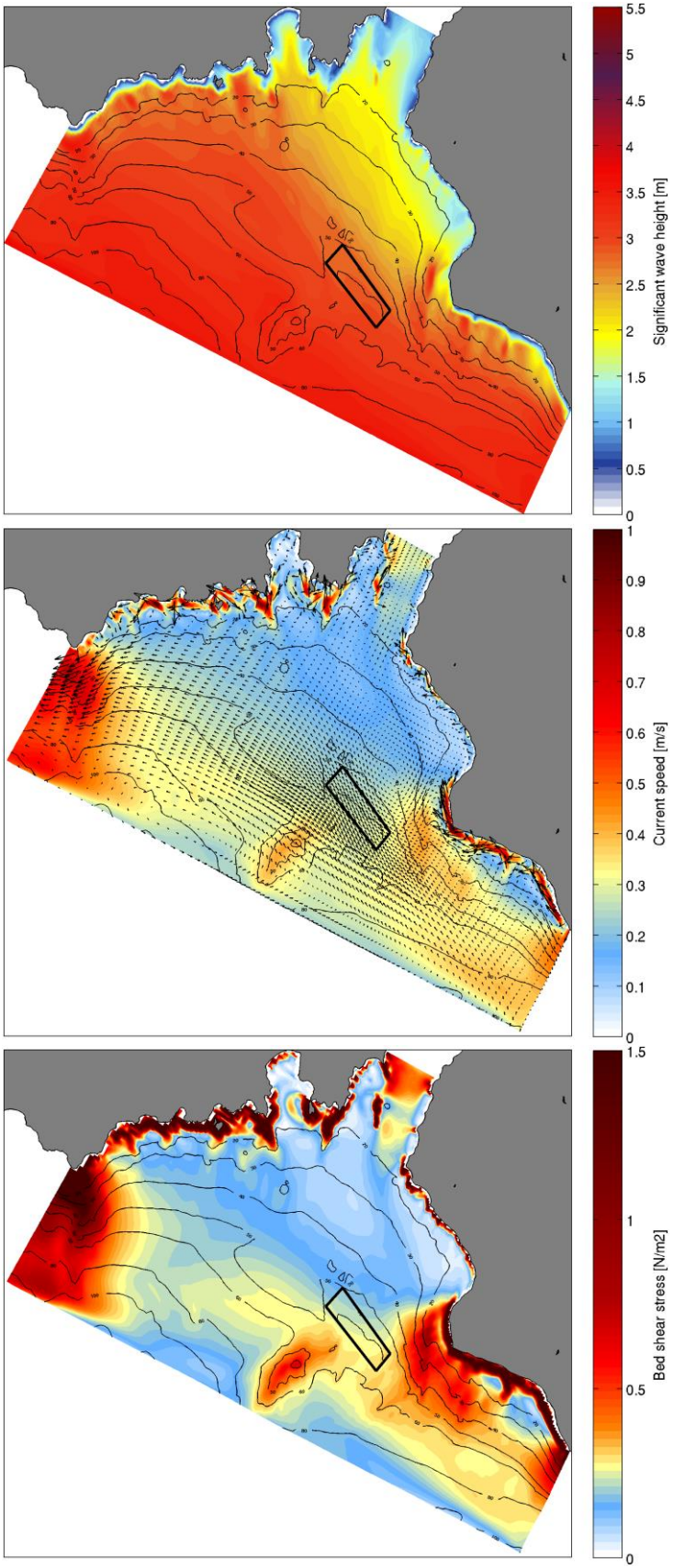

Figure 5.42 Wave, circulation and bed shear stress fields averaged over the representative tide for Event 3 of Table 3.6.

Draft for public consultation

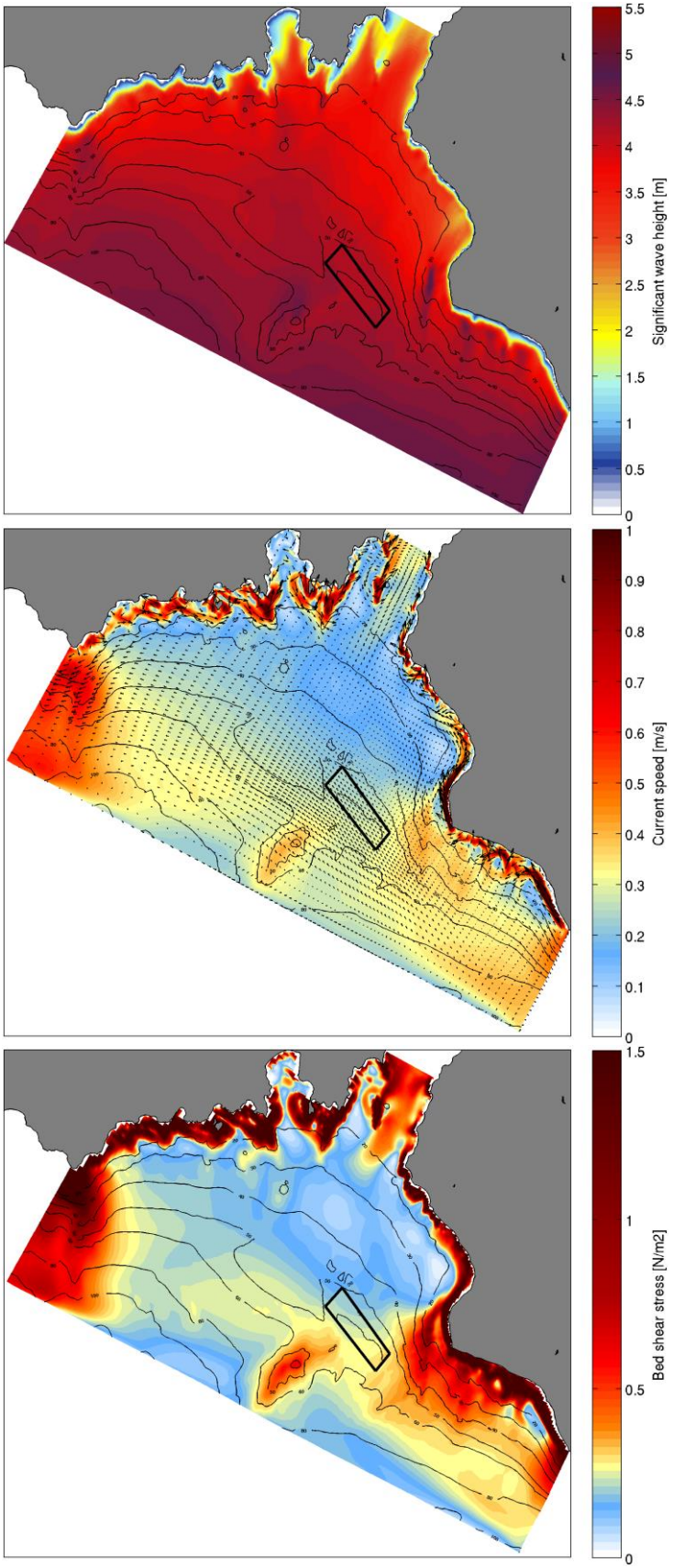

Figure 5.43 Wave, circulation and bed shear stress fields averaged over the representative tide for Event 9 of Table 3.6.

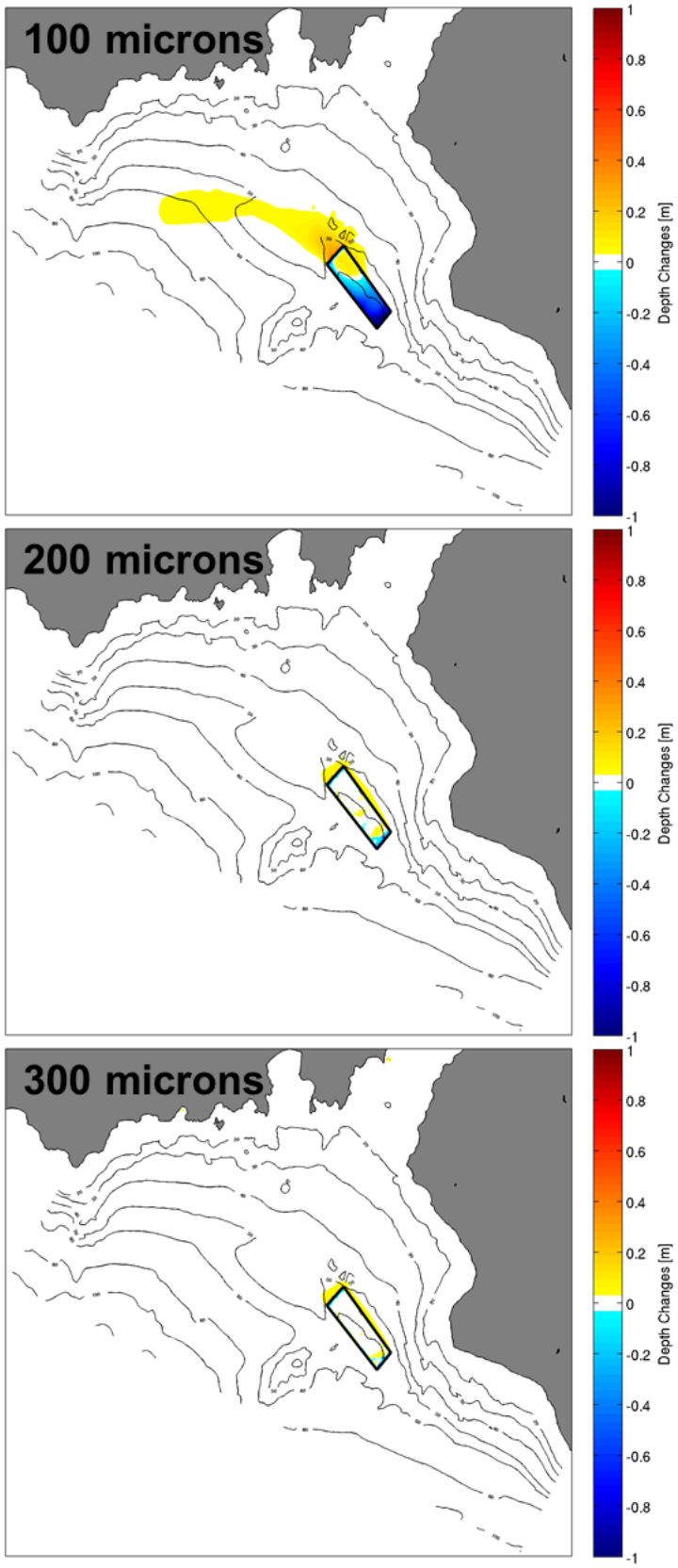

Figure 5.44 Morphological changes predicted after 1 year for D50 grain size values of 100 µm (top), 200 µm (middle) and 300 µm post disposal (bottom). Sedimentation and erosion are indicated by positive and negative magnitudes, respectively. Sediment transport modelled for a generic disposal ground of 4.5 m elevation.

Draft for public consultation

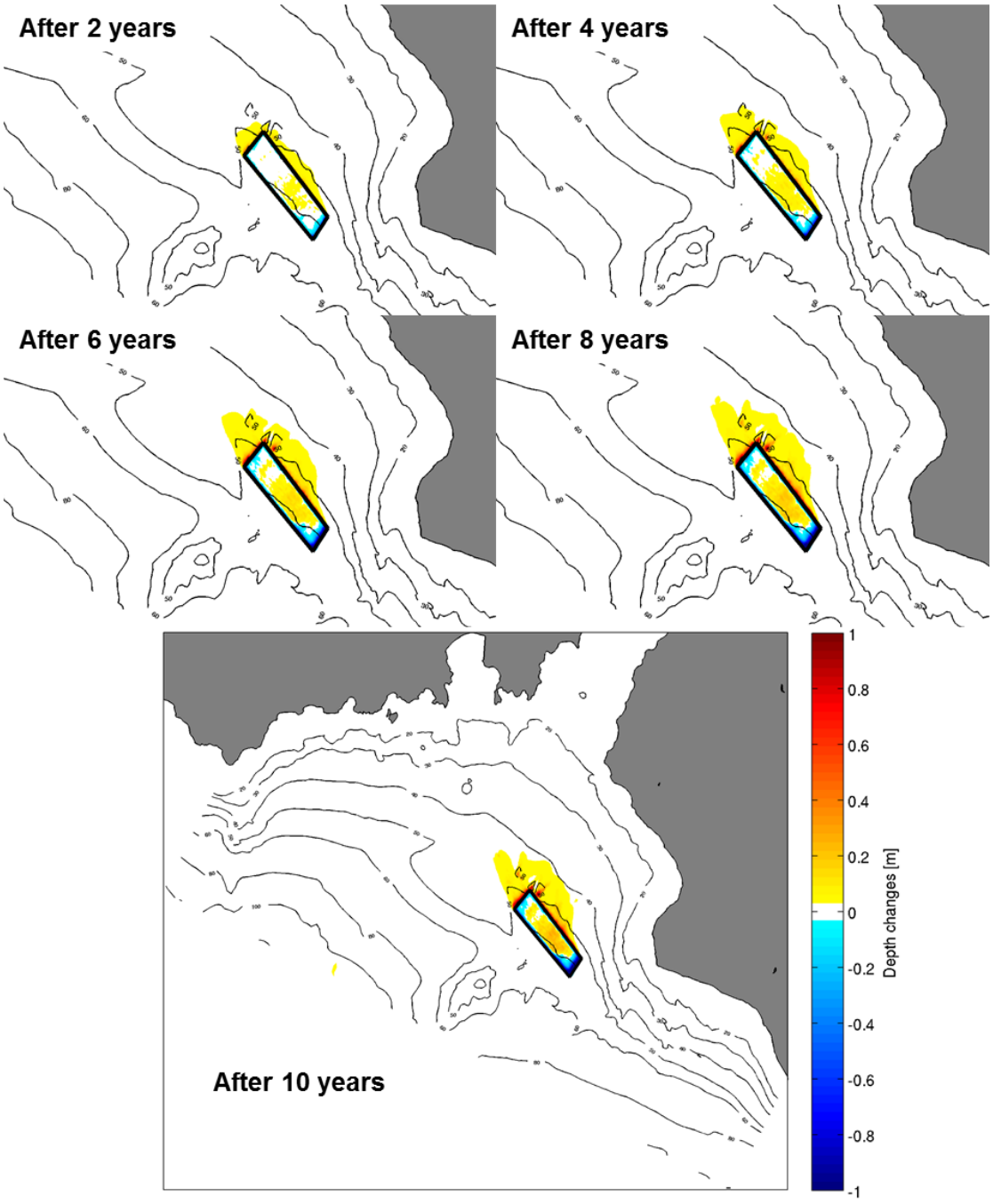

Figure 5.45 Morphological changes predicted after 2, 4, 6, 8, and 10 years for the disposal ground, assuming a D50 of 200 µm. A positive magnitude indicates sedimentation while a negative magnitude indicates erosion. Sediment transport modelled for a 6.0 M m^3 disposal ground.

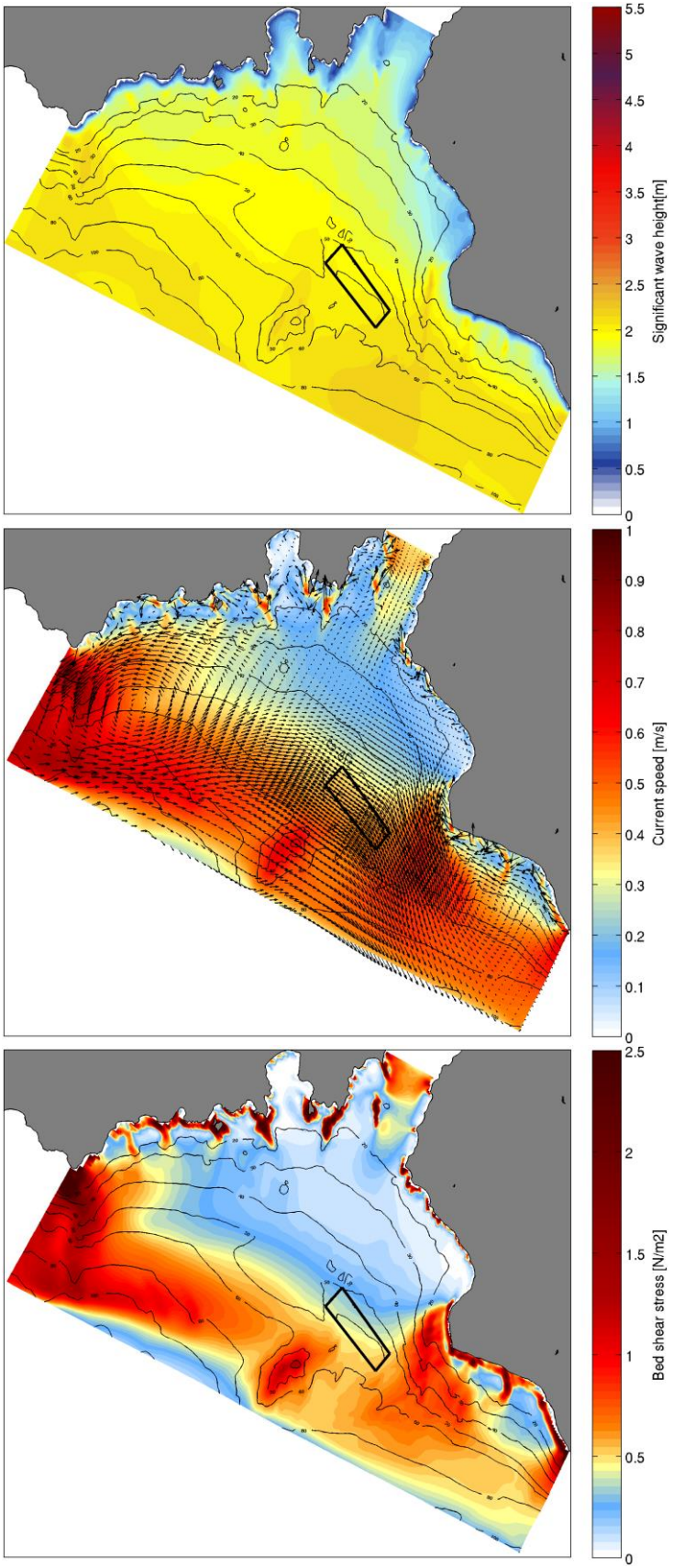

Figure 5.46 Wave, circulation and bed shear stress fields averaged during Event 1 with Hs = 1.41 m, Dp = 175 deg and Tp = 9.7 s (offshore and at peak wave height).

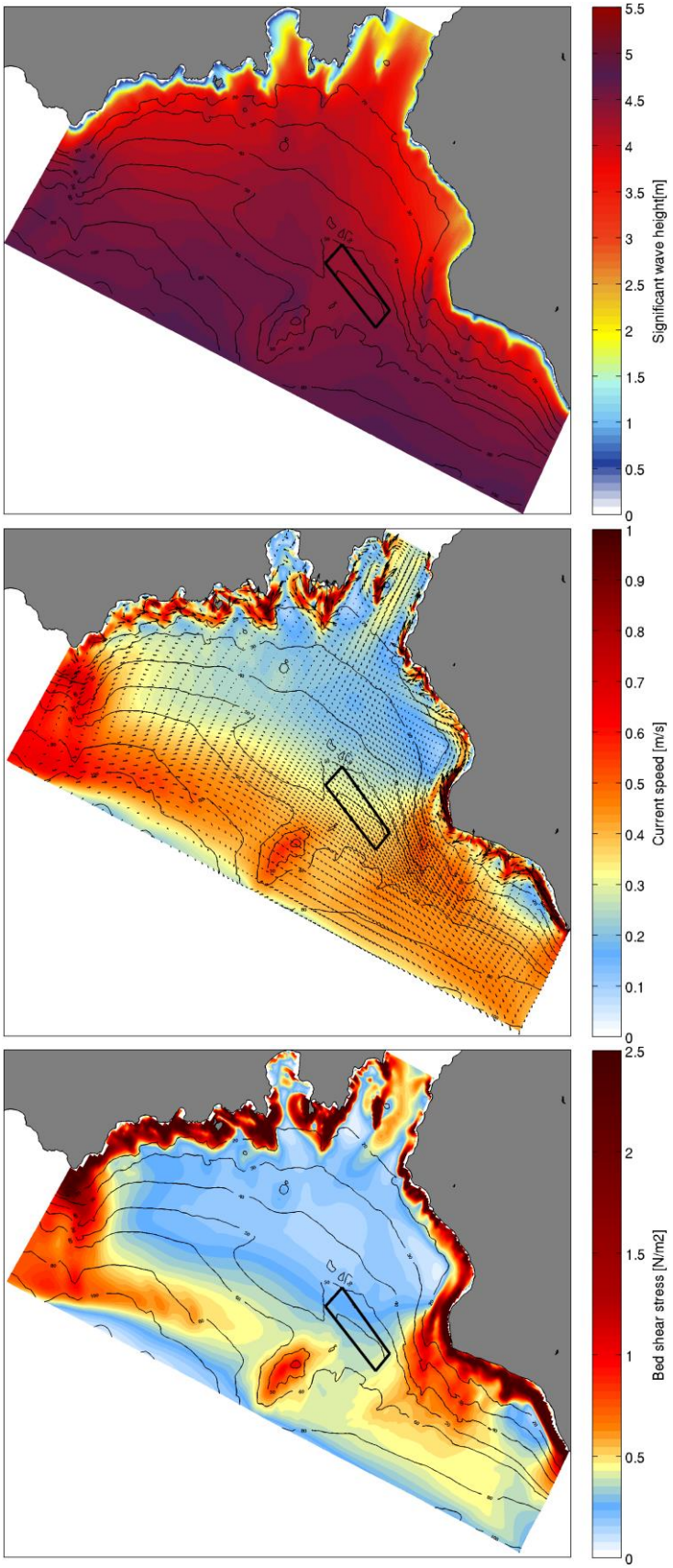

Figure 5.47 Wave, circulation and bed shear stress fields averaged during Event 2 with Hs = 8.41 m, Dp = 176 deg and Tp = 11.6 s (offshore and at peak wave height).

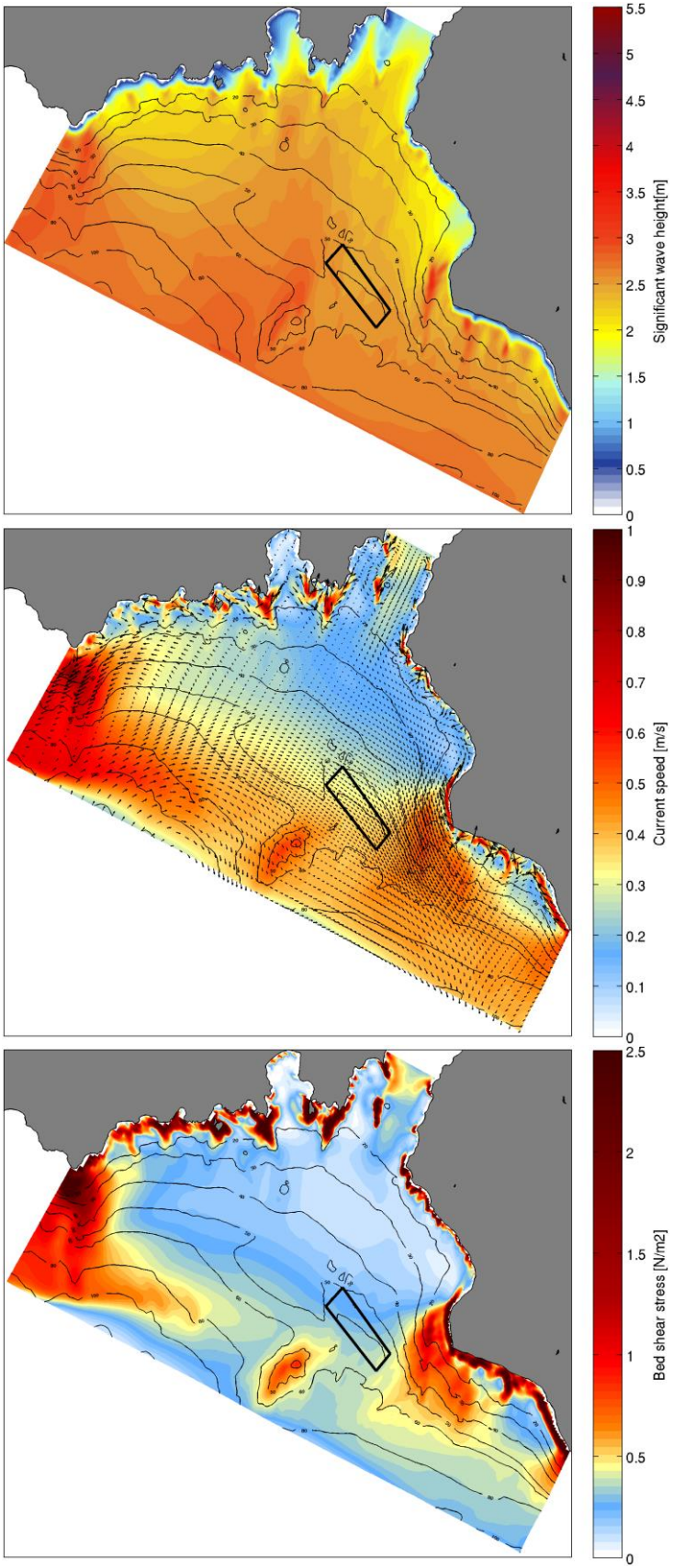

Figure 5.48 Wave, circulation and bed shear stress fields averaged during Event 3 with Hs = 5.21 m, Dp = 332 deg.and Tp = 9.1 s (offshore and at peak wave height).

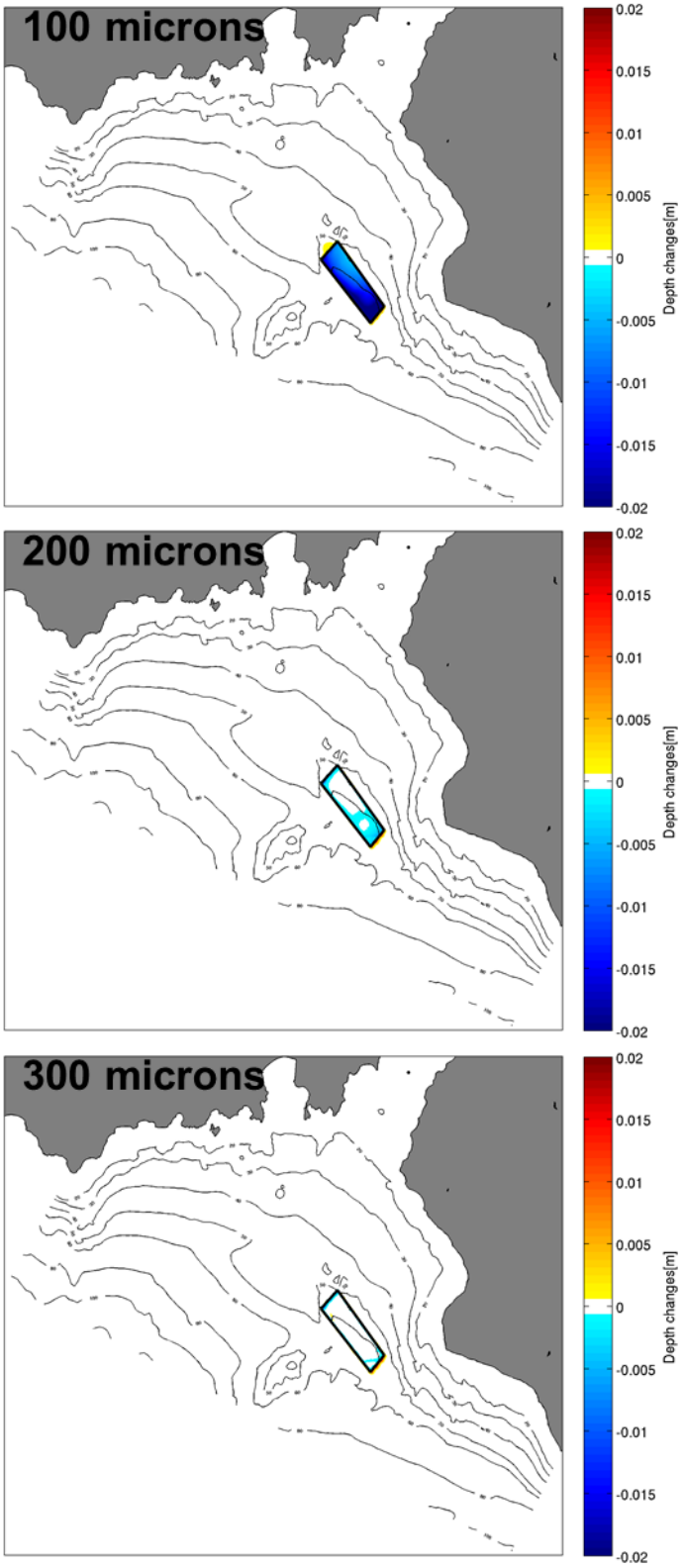

Figure 5.49 Morphological changes predicted at the end of Event 1 for D50 grain size values of 100 µm (top), 200 µm (middle) and 300 µm post disposal (bottom). Sedimentation and erosion are indicated by positive and negative magnitudes, respectively. Sediment transport modelled for a generic disposal ground of 4.5 m elevation.

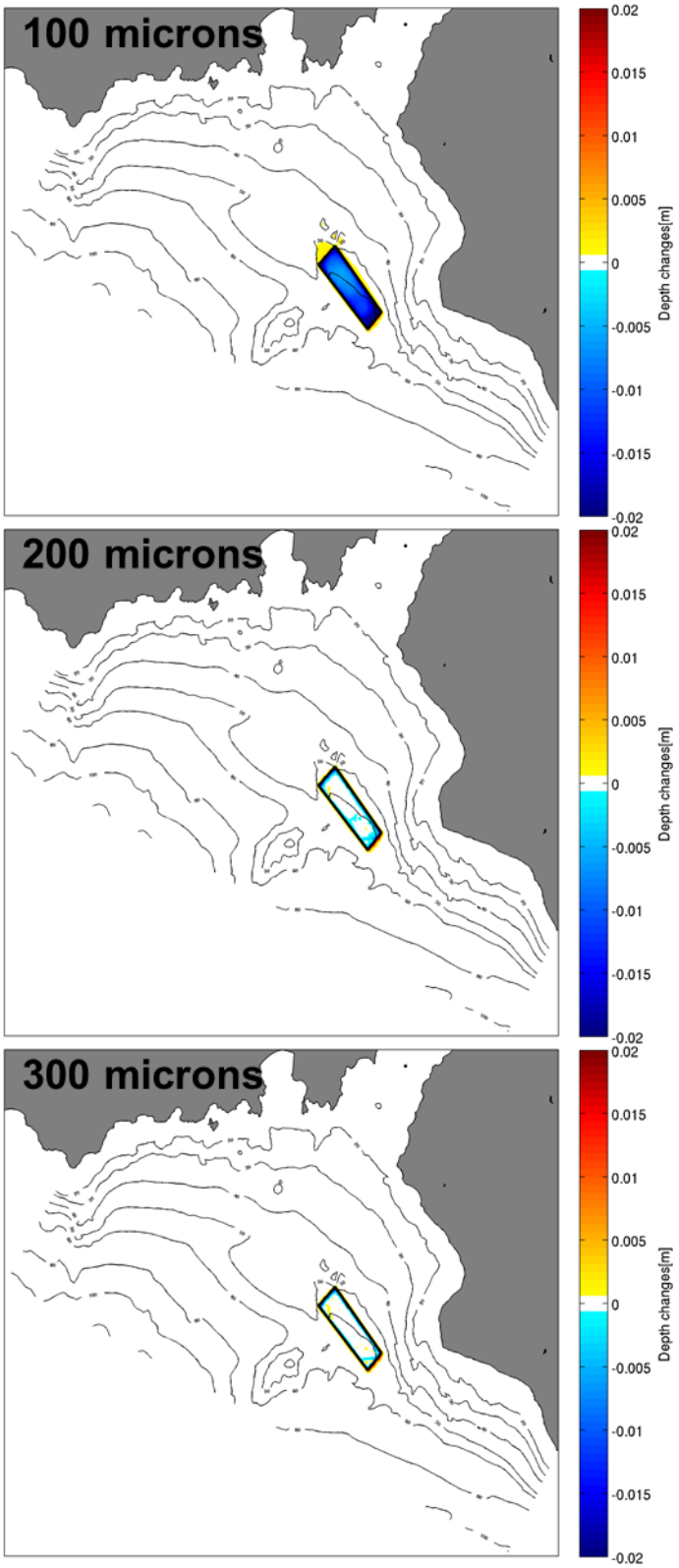

Figure 5.50 Morphological changes predicted at the end of Event 2 for D50 grain size values of 100 µm (top), 200 µm (middle) and 300 µm post disposal (bottom). Sedimentation and erosion are indicated by positive and negative magnitudes, respectively. Sediment transport modelled for a generic disposal ground of 4.5 m elevation.

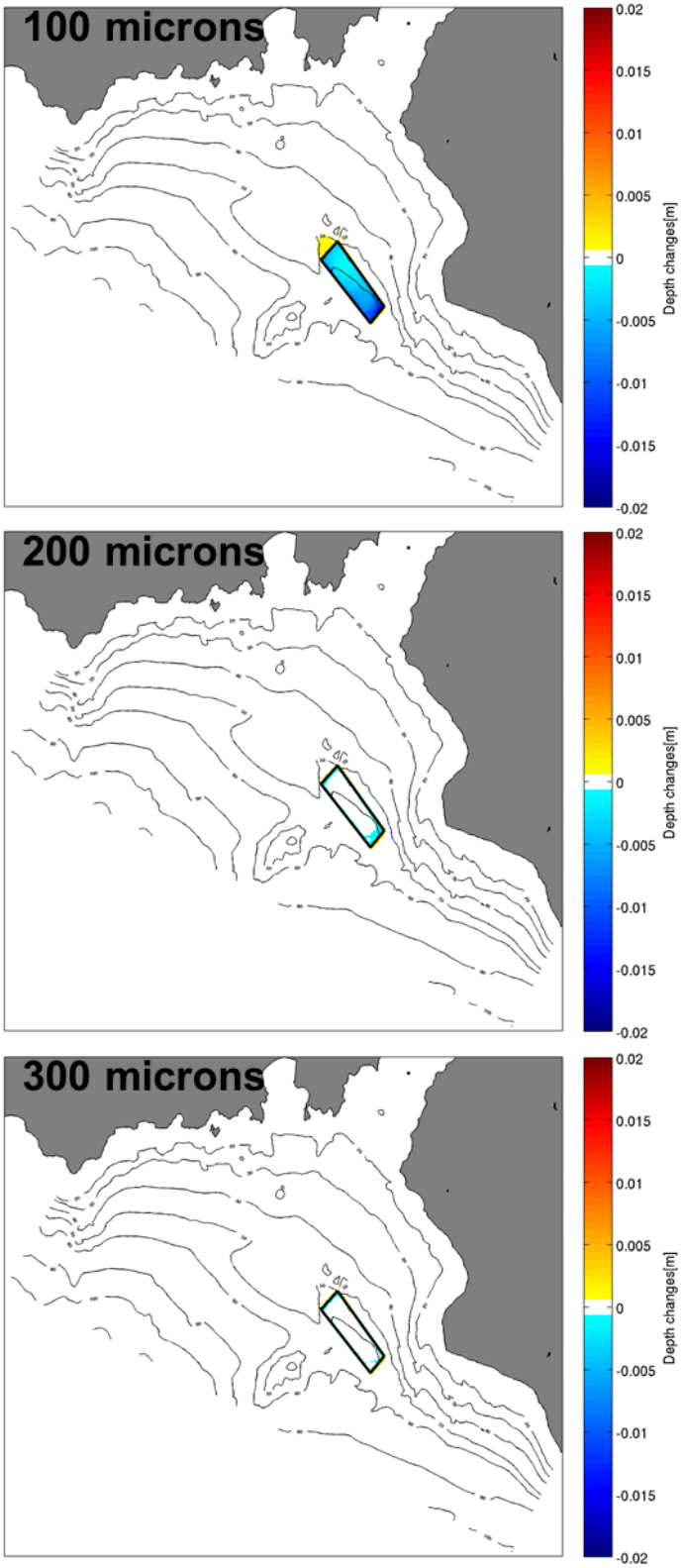

Figure 5.51 Morphological changes predicted at the end of Event 3 for D50 grain size values of 100 µm (top), 200 µm (middle) and 300 µm post disposal (bottom). Sedimentation and erosion are indicated by positive and negative magnitudes, respectively. Sediment transport modelled for a generic disposal ground of 4.5 m elevation.

Draft for public consultation

5.3.2. Channel morphology

The changes to the waves and currents due to deepening the entrance channel are presented for the real time Events 1 to 7 in Figure 5.52, Figure 5.53 and Figure 5.54. As shown in section 5.2.2, in the vicinity of the entrance channel, the wave height changes induced by dredging are quite significant and particularly evident during the energetic wave conditions (i.e. Events 5 and 6). Such changes tend to modify the sediment transport patterns, particularly in the western region of the channel. The modelled morphological changes are shown in Figure 5.55, Figure 5.56 and Figure 5.57.

The western side of the entrance, including Steeple Rock area, will be exposed to larger waves due to the channel deepening, and these may cause increased variability in the seabed morphology. Conversely, the eastern side of the channel is expected to receive less wave energy. However, the morphology model results for the seven historical events do not indicate any systematic erosion or deposition patterns adjacent to the dredged channel. Excepting storm conditions, a dredged channel does not appear to significantly affect the sediment dynamics in the harbour entrance. However, during energetic events when the seabed becomes highly mobile due to wave stirring, there is relatively more movement of the bed sediments on the western side, which may lead to gradual erosion of the mobile material over year to decadal scales.

The modelled and measured currents do not suggest strong alongshore directed currents with the potential to cause rapid infilling of a dredged channel. The tidal currents remain essentially co-linear with the axis of the channel, and the regional coastal flows (tidal and non-tidal) do not directly impinge on the dredged channel due to sheltering from the adjacent Pencarrow Headland.

A degree of accretion is expected to occur in the dredged channel, particularly along the southern third of its length, and predominantly during storm events. The model results for the energetic real time cases (i.e. Events 5 and 6) predict infilling of the order of centimetres from a single storm over a few days. However, this cannot be extrapolated to an annual maintenance volume as the strong tidal flows will act to further redistribute these sediments. Also, the constrained flow regime in this region means that the source of sediment for infilling is likely to be from a diffusive process from the adjacent sides of the channel, which is a source with a finite volume. Differences observed in the bed shear stress fields in section 5.2.1 for the 98% optimisation channel designs are translated into differences in the sediment transport patterns in the middle of the dredged channel. This is particularly visible in Figure 5.58 and Figure 5.59 for 7 days simulations including only tidal flows.

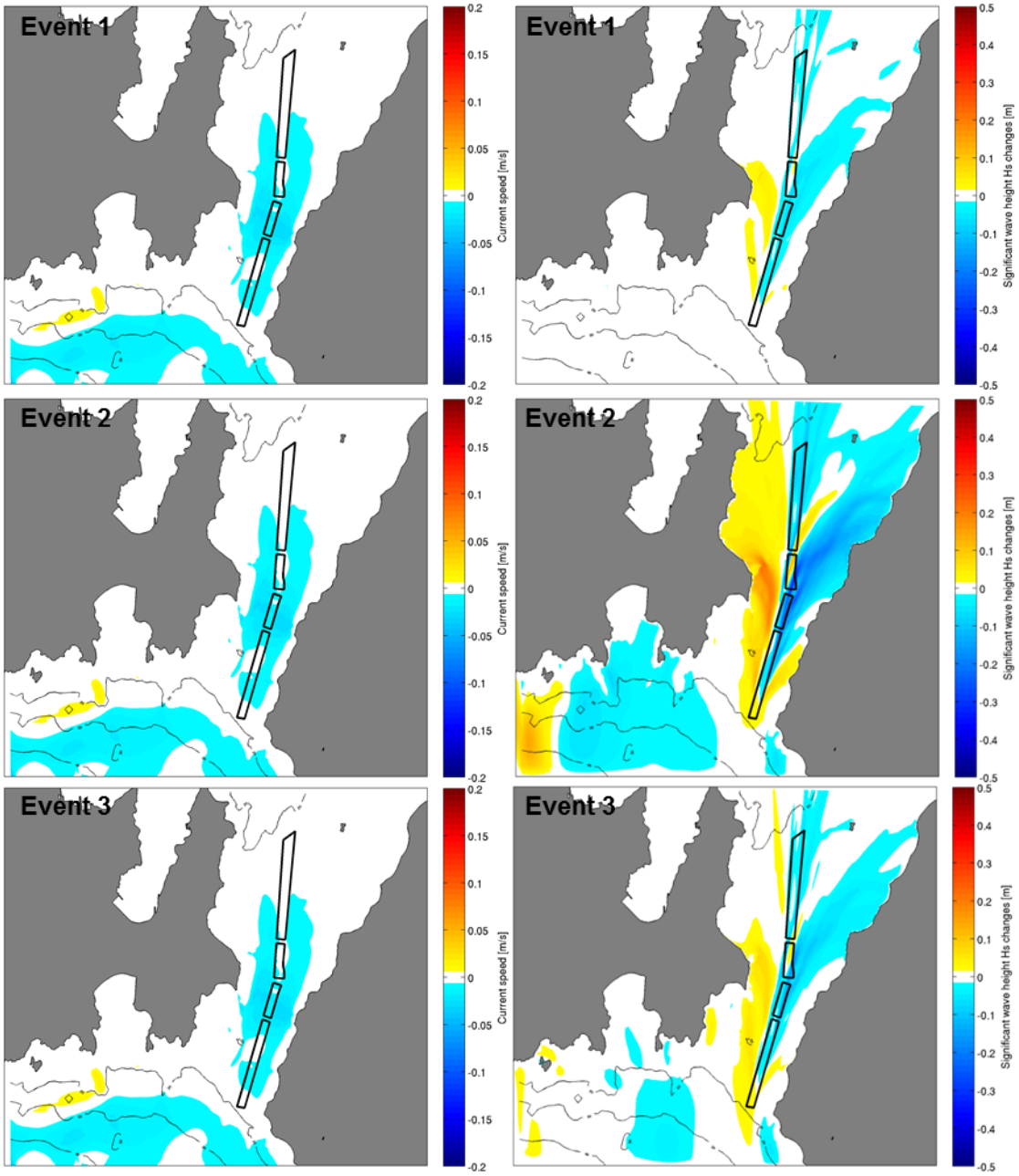

Figure 5.52 Current speed changes (left) and significant wave height changes (right) predicted at the end of the 48h real simulations for Events 1 to 3 considering the existing channel and the 98% optimisation channel. A positive magnitude indicates an increase of the current speed or of the wave height due to deepening.

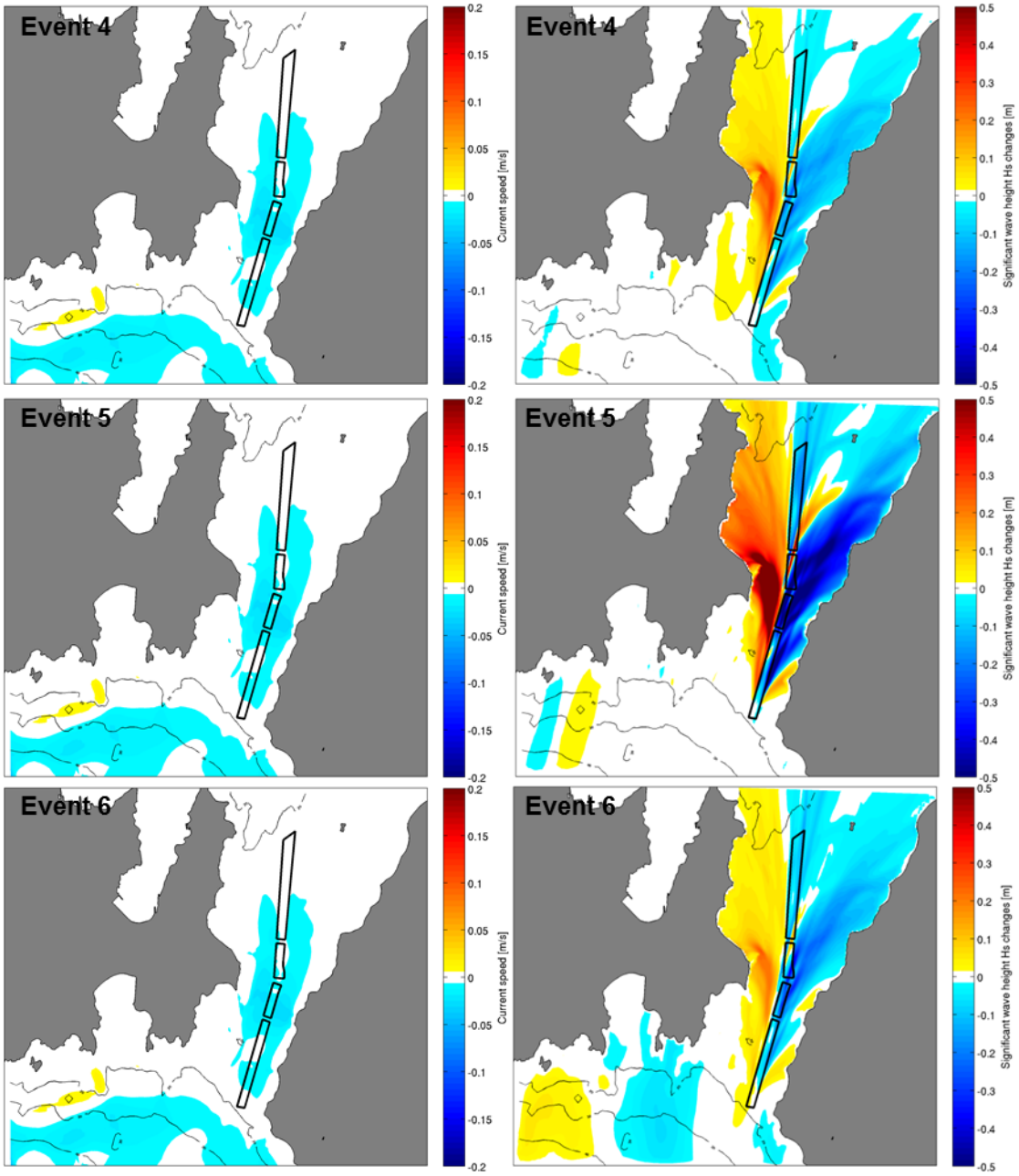

Figure 5.53 Current speed changes (left) and significant wave height changes (right) predicted at the end of the 48h real simulations for Events 4 to 6 considering the existing channel and the 98% optimisation channel. A positive magnitude indicates an increase of the current speed or of the wave height due to deepening.

Draft for public consultation

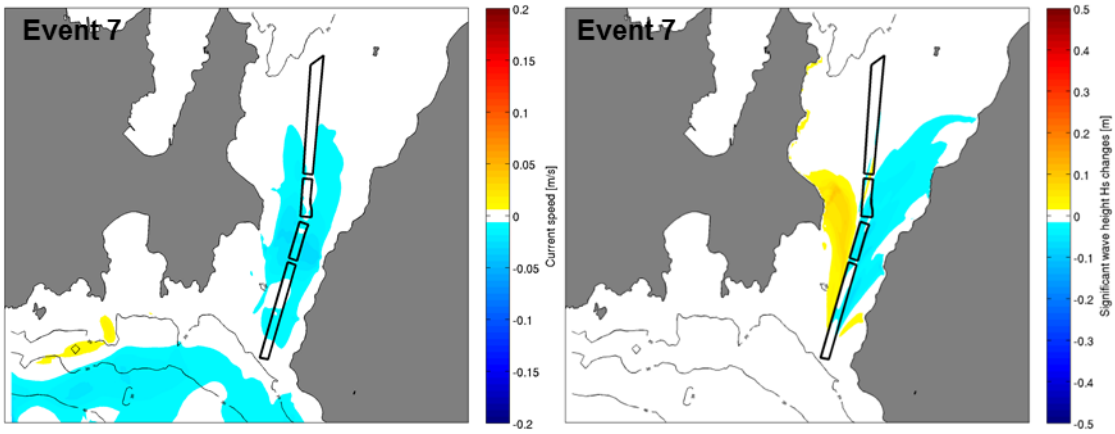

Figure 5.54 Current speed changes (left) and significant wave height changes (right) predicted at the end of the 48h real simulations for Event 7 considering the existing channel and the 98% optimisation channel. A positive magnitude indicates an increase of the current speed or of the wave height due to deepening.

.

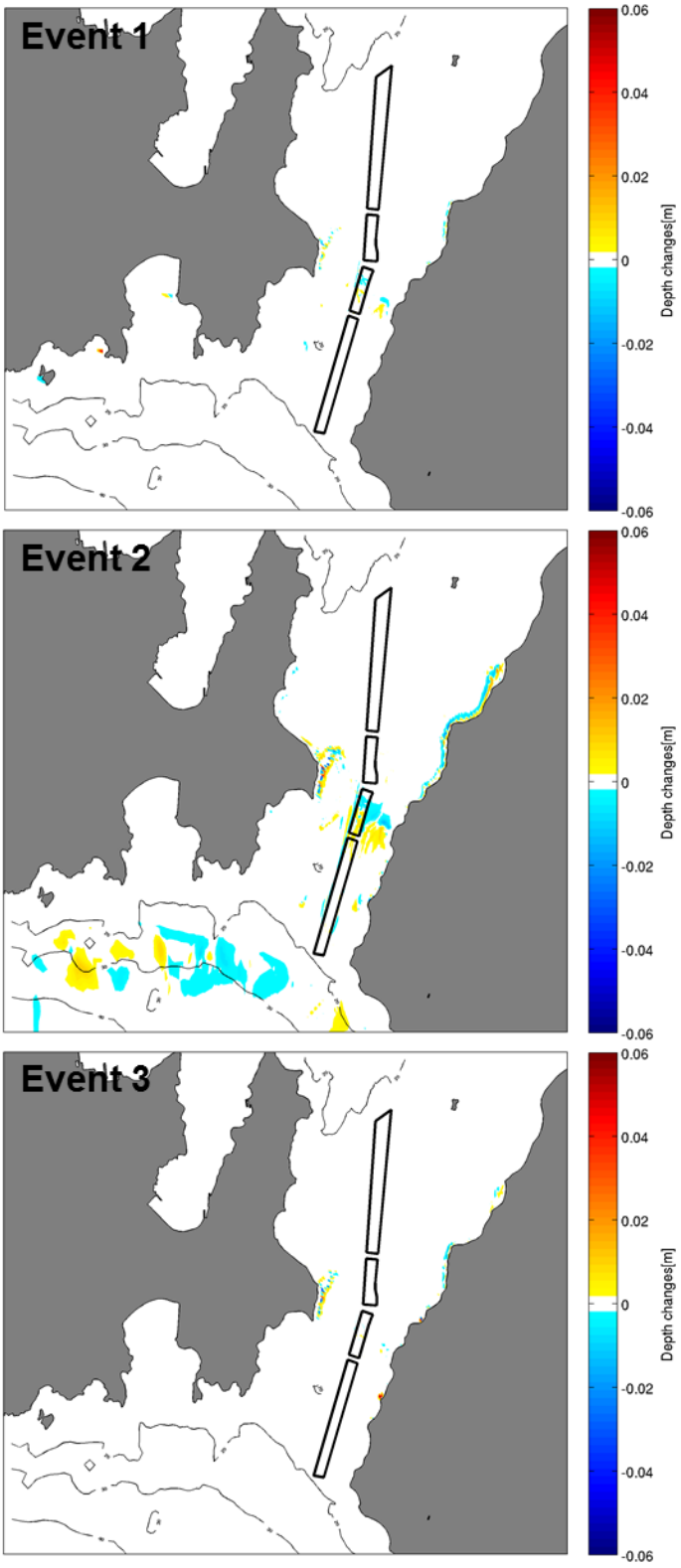

Figure 5.55 Morphological changes predicted at the end of the 48h realistic simulation for Events 1 to 3 considering the existing channel and the 98% optimisation channel. A positive magnitude indicates sedimentation as a result of deepening.

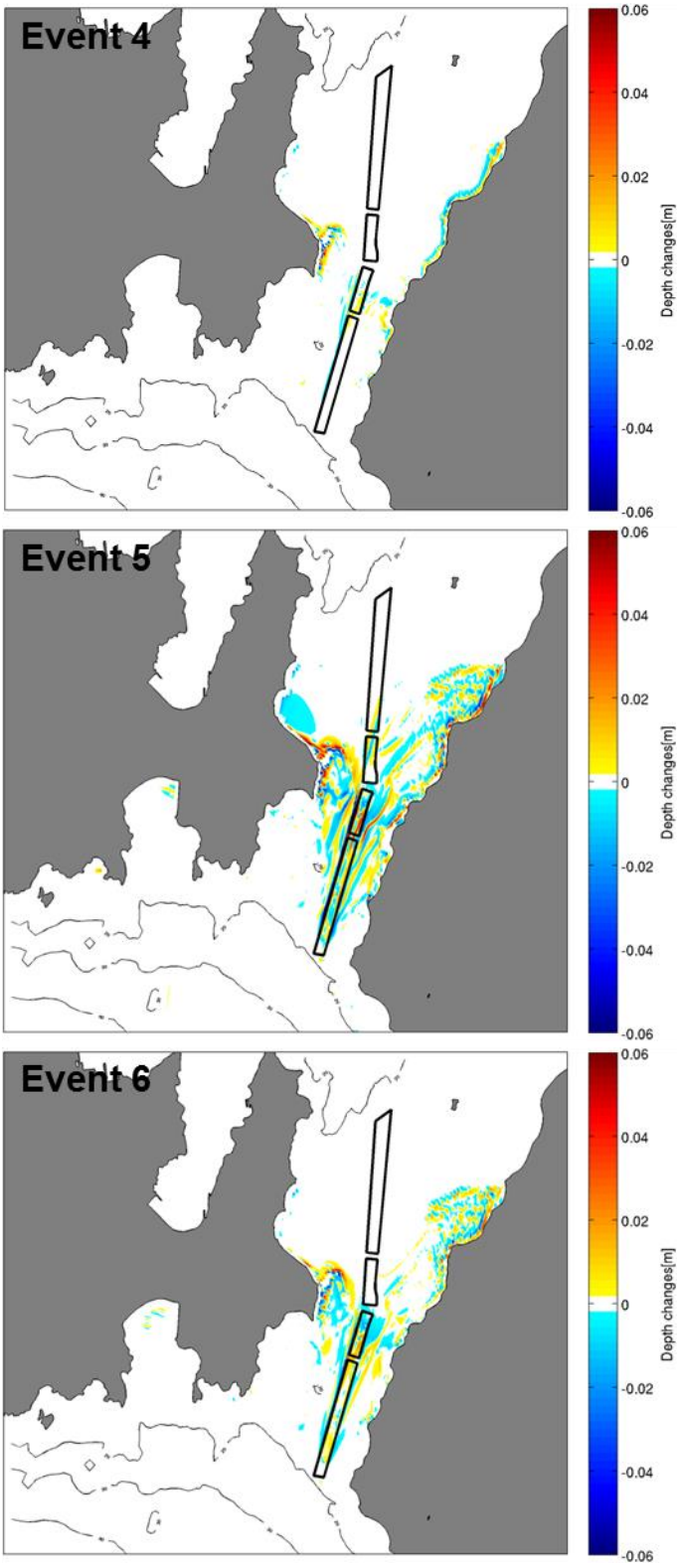

Figure 5.56 Morphological changes predicted at the end of the 48h realistic simulation for Events 4 to 6 considering the existing channel and the 98% optimisation channel. A positive magnitude indicates sedimentation as a result of deepening.

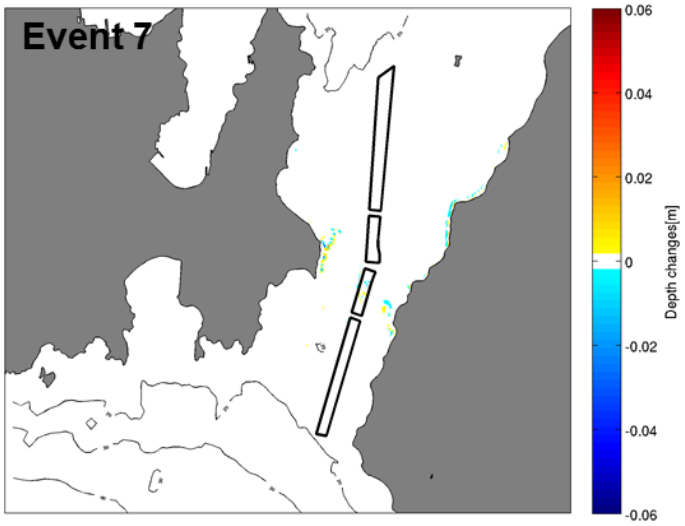

Figure 5.57 Morphological changes predicted at the end of the 48h realistic simulation for Event 7 considering the existing channel and the 98% optimisation channel. A positive magnitude indicates sedimentation as a result of deepening.

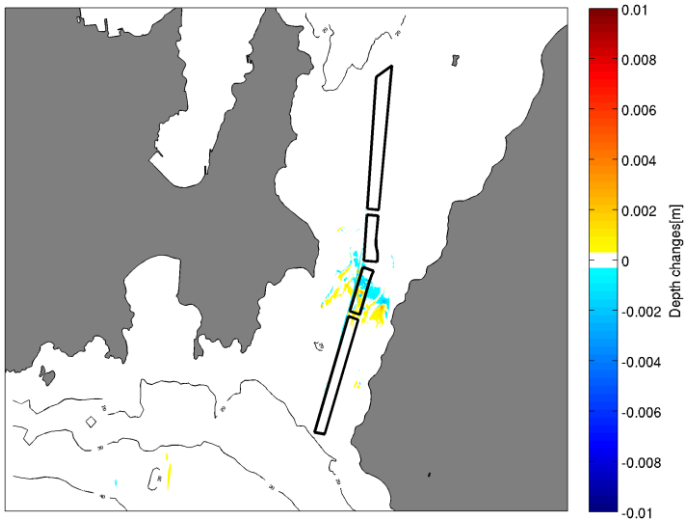

Figure 5.58 Difference of morphological changes predicted at the end of the 7-day simulation including only tidal forcing between the existing channel and the 98% optimisation channel. A positive magnitude indicates sedimentation as a result of deepening.

Draft for public consultation

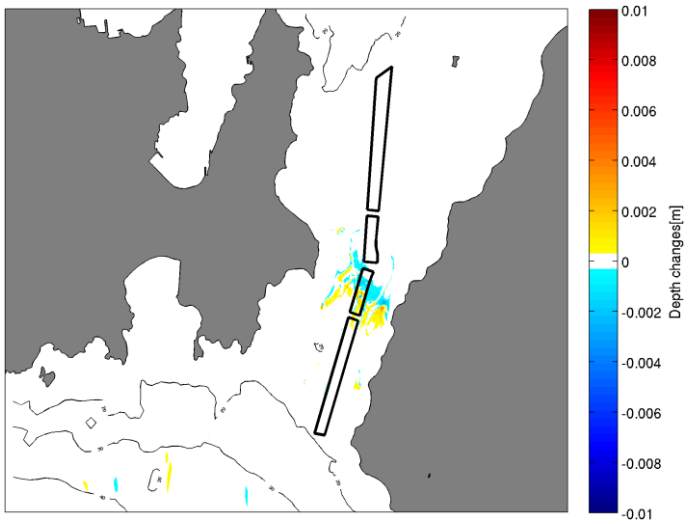

Figure 5.59 Difference of morphological changes predicted at the end of the 7-day simulation including only tidal forcing between the existing channel and the 98% optimisation channel. A positive magnitude indicates sedimentation as a result of deepening.

5.4. Dredging and disposal plumes

For consideration of the sediment plumes associated with dredging and offshore disposal, the results presented in this section are the normalized concentrations. They were obtained by finding the overall maximum concentration within the 3 levels considered (bottom, mid water and surface) and dividing all computed concentration fields by that value. A normalized Suspended Sediment Concentration (SSC) of 0.01 indicates a magnitude that is 1% of the maximum plume concentration found in the water column - which will be directly at the release point.

5.4.1. Effects of channel dredging

Results of the particle tracking simulations of the dredging activities in the channel are presented in Figure 5.60 to Figure 5.64. Here, for conservatism the sediment is assumed to be fine sand with a diameter of 100 µm, and the release sites are shown in Figure 4.2.

Given the relatively coarse sediment size expected in the channel (representative d=100 µm, w_s =6.67e-03 m/s), and relatively shallow depth within the channel (~15 m), the extents of the predicted SSC plumes resulting from the channel dredging activities are very limited. The overall SSC plumes shapes are generally consistent with the tidal roses (see Figure 5.65) and follow the channel main axis. Levels of SSC are generally insignificant at the surface and progressively increase in the mid and bottom layers. This slight downward widening of the plume is due to the increasing time during which the particles are subject to advection and diffusion as they settle.

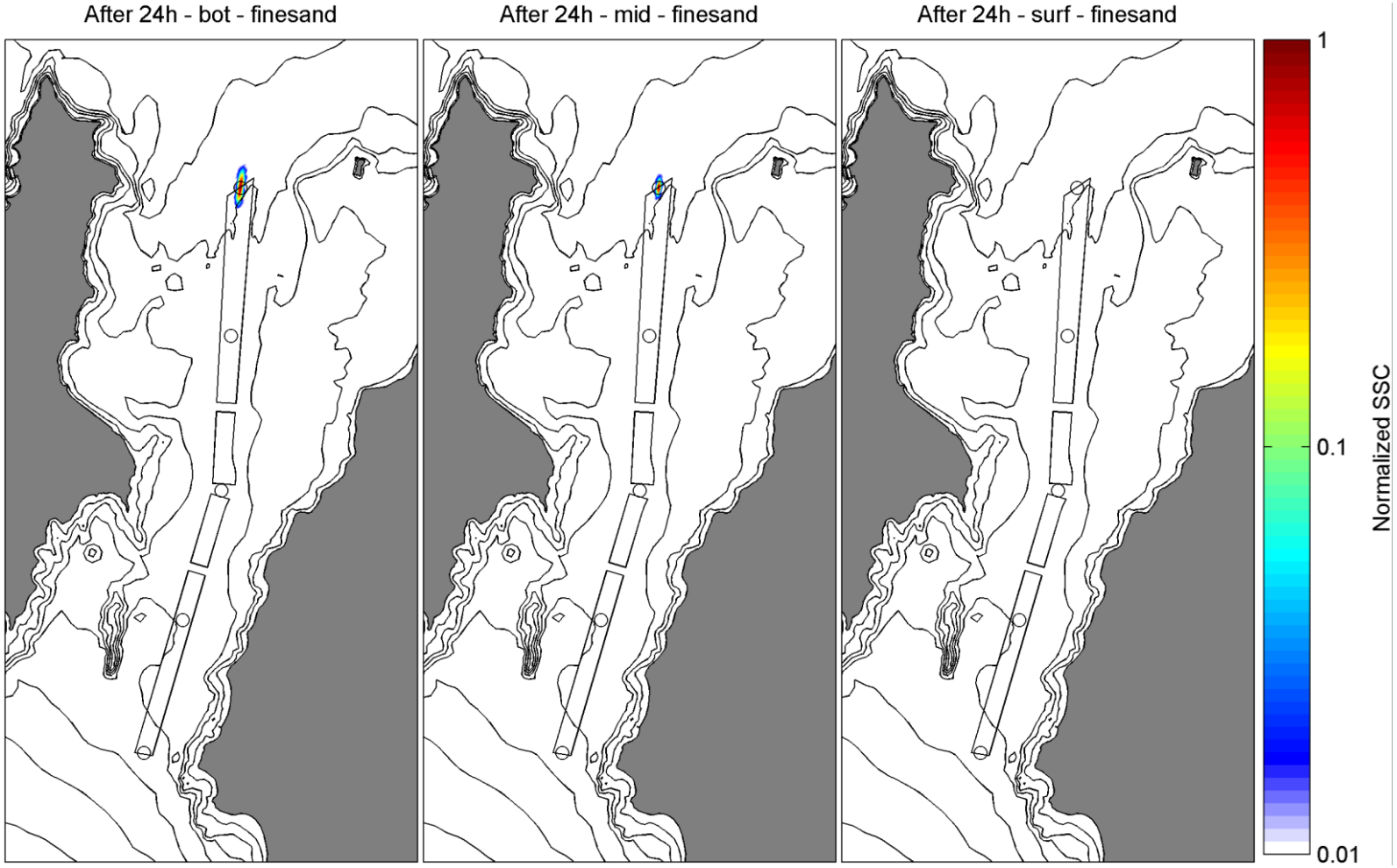

Figure 5.60 Normalized suspended sediment concentrations (SSC) at bottom, mid water and surface levels for a release of fine sand (d=100 µm) at site C1 (see Figure 4.2) after 24 h of continuous dredging.

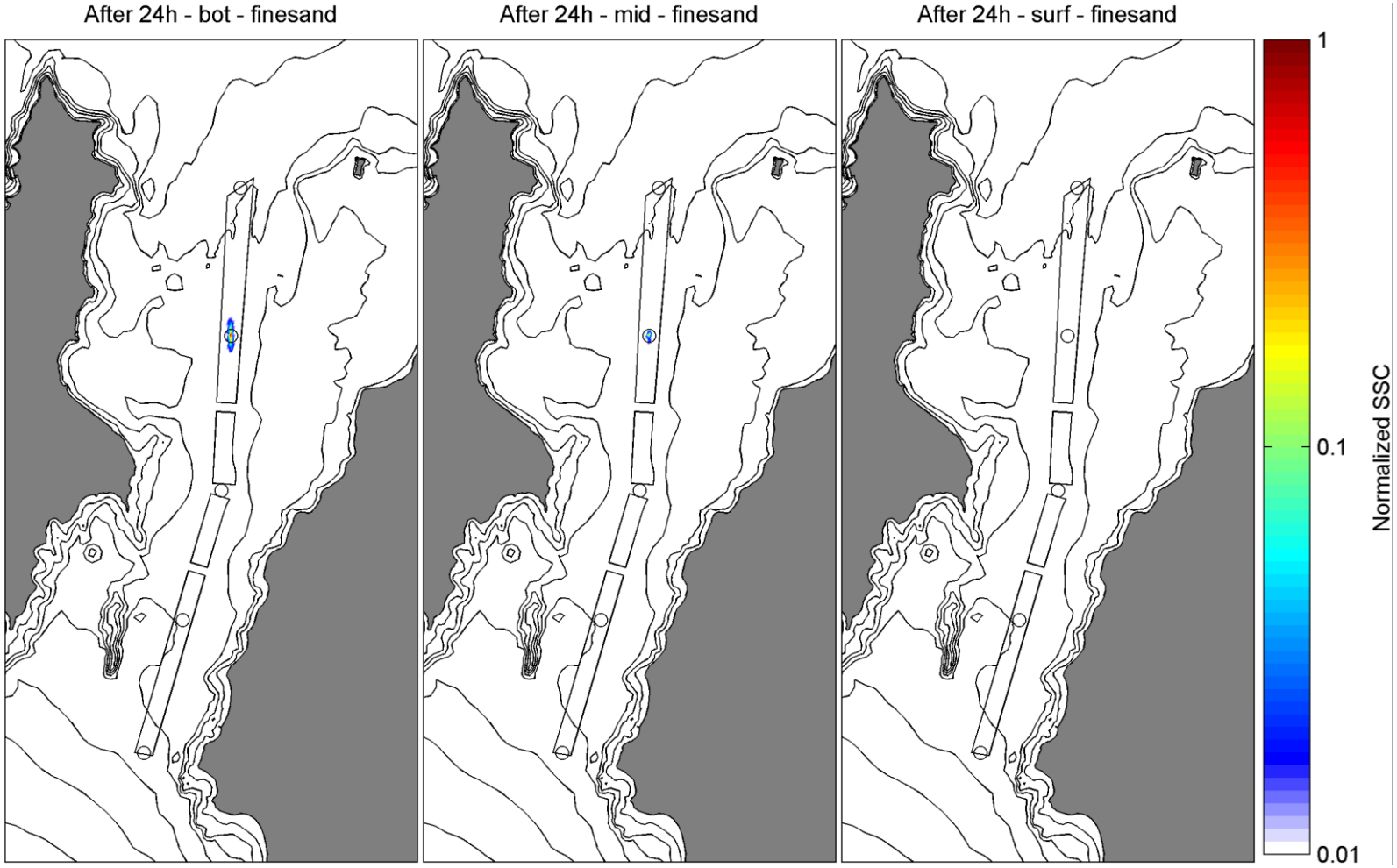

Figure 5.61 Normalized suspended sediment concentrations (SSC) at bottom, mid water and surface levels for a release of fine sand (d=100 µm) at site C2 (see Figure 4.2) after 24 h of continuous dredging.

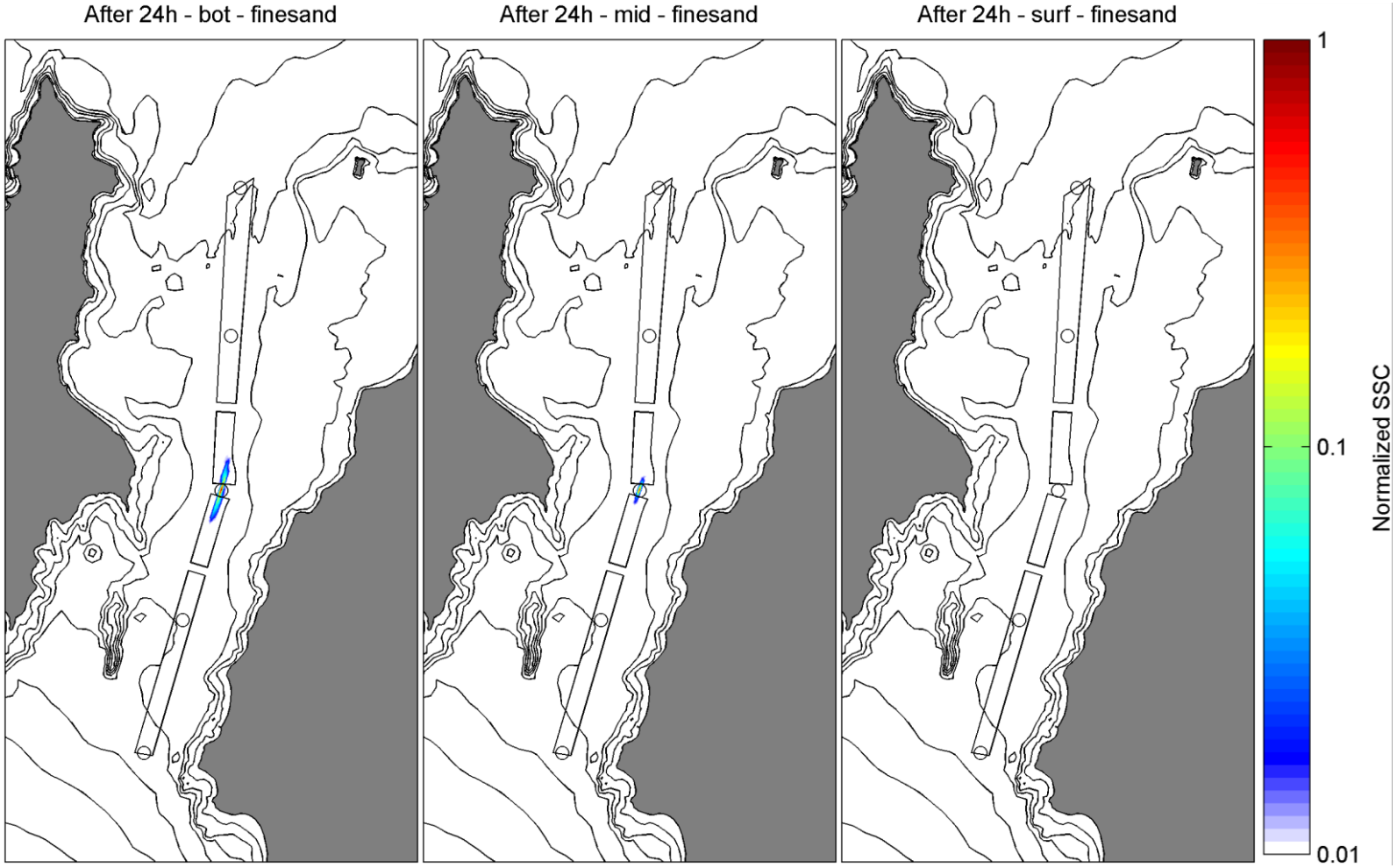

Figure 5.62 Normalized suspended sediment concentrations (SSC) at bottom, mid water and surface levels for a release of fine sand (d=100 µm) at site C3 (see Figure 4.2) after 24 h of continuous dredging.

Draft for public consultation

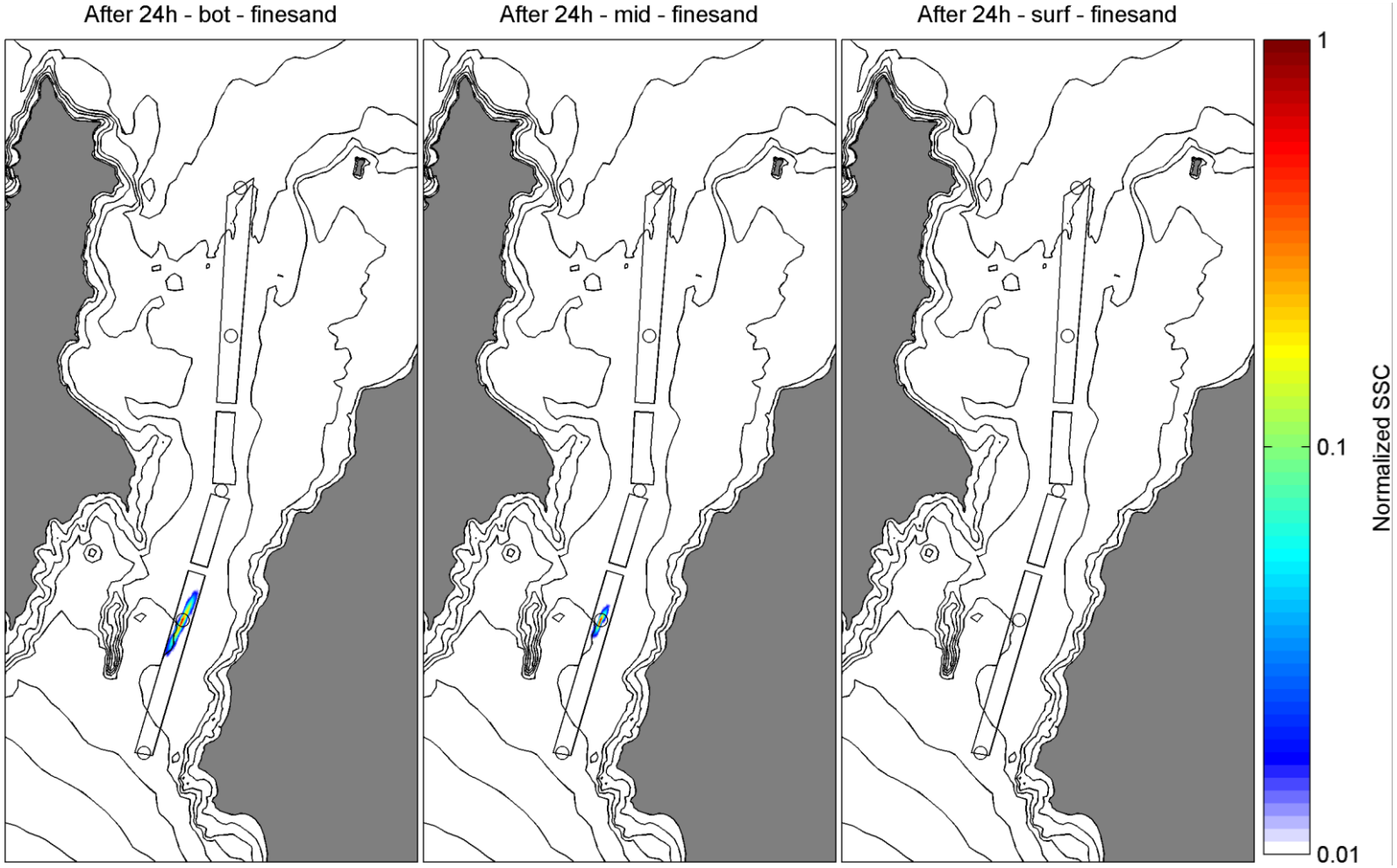

Figure 5.63 Normalized suspended sediment concentrations (SSC) at bottom, mid water and surface levels for a release of fine sand (d=100 µm) at site C4 (see Figure 4.2) after 24 h of continuous dredging.

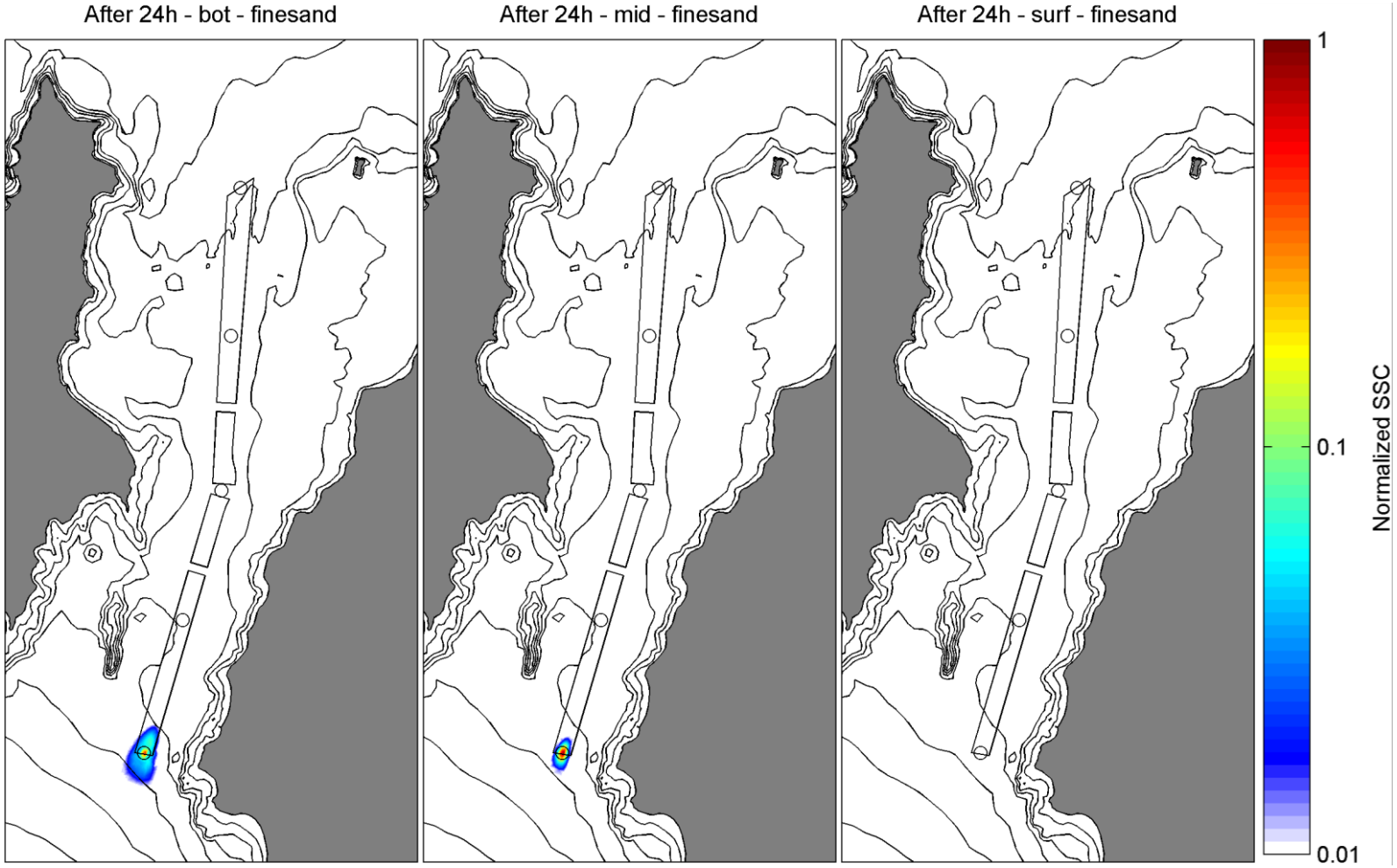

Figure 5.64 Normalized suspended sediment concentrations (SSC) at bottom, mid water and surface levels for a release of fine sand (d=100 µm) at site C5 (see Figure 4.2) after 24 h of continuous dredging.

Draft for public consultation

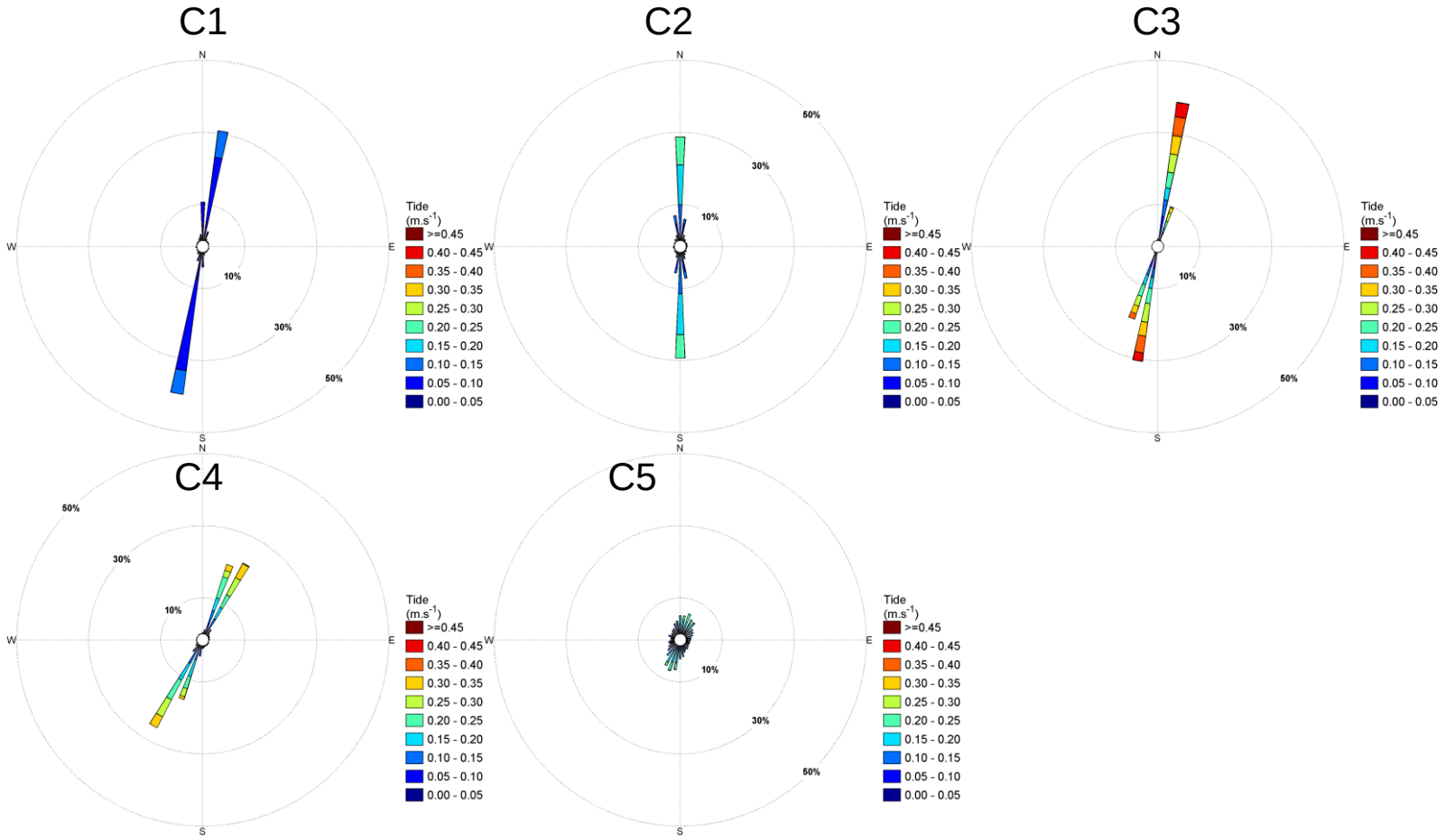

Figure 5.65 Tidal roses at plume study locations in the entrance channel.

Draft for public consultation

5.4.2. Effects of offshore disposal

Results of the particle tracking simulations of the disposal activities at the proposed offshore ground are presented in Figure 5.66. The sediment was assumed to be fine sand with a diameter of 100 µm. The mean SSC after 24h of continuous disposal were determined from a 1-year simulation (2004) using both tides and large-scale residual currents as particle movers.

The predicted SSC plume clearly follows a northwest-southeast axis, which was expected given the general tidal and residual current climate at the disposal ground (see Figure 5.66). Although the fine sand modelled has a relatively high settling velocity (d=100 µm, w_s =6.67e-03 m/s) the depth at the site provides some time for the sediment discharged in the water column (release at 8 m below surface) to be advected and diffused away from the release point. Surface SSC are essentially insignificant and plume extents progressively increase moving deeper in the water column. The present simulations suggest that the mid water sediment plume may extend about 3-4 km away from the release, to the 1% of maximum concentration value. However, most of the SSC are retained within a radius of 1.5 km from the release site. Notably, the largest SSC levels in the lower water column are consistently predicted to the northwest of the disposal ground; consistent with the flow asymmetry.

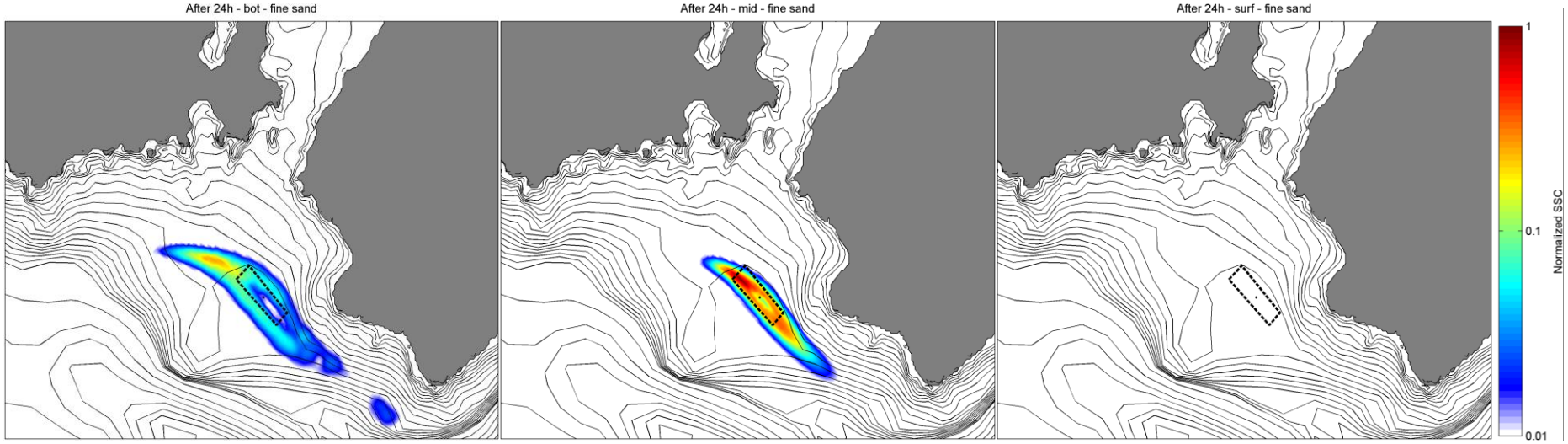

Figure 5.66 Normalized suspended sediment concentrations (SSC) at bottom, mid water and surface levels for a release of fine sand (d=100 µm) at site D1 (see Figure 4.2) after 24 h of continuous disposal.

Draft for public consultation

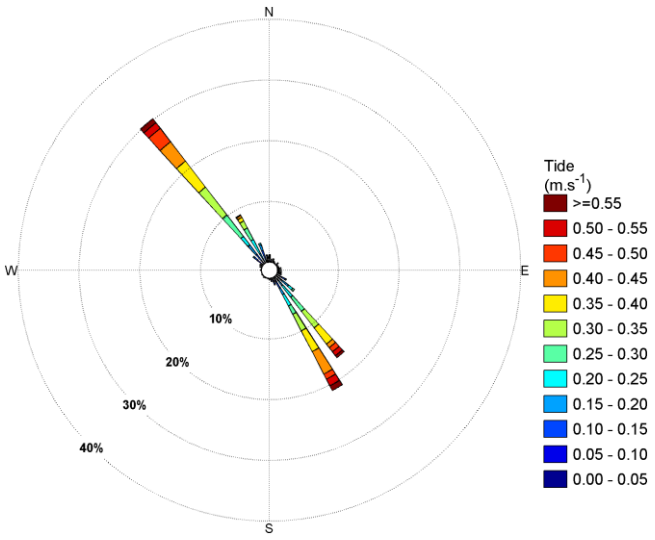

Figure 5.67 Tidal rose at the proposed offshore disposal ground.

Draft for public consultation

6. SUMMARY

A numerical study of the wave, hydrodynamic and sediment dynamics in the Wellington Harbour and the adjacent environment has been undertaken. Industry-standard numerical models have been established and validated using historical and contemporary measurements. It has been demonstrated that the models can replicate the dominant physical processes in the area, and may be reliably used to examine the potential physical effects arising from the CentrePort Channel Deepening Project.

- A 35-year wind hindcast at 4 km resolution was used to prescribe the spatially-varying wind conditions in the harbour and in the Cook Strait region. These data have been used as the boundary conditions to hydrodynamic and wave simulations.

- The 2- and 3-dimensional hydrodynamics have been modelled at various spatial scales with regular, curvilinear and finite-element numerical domains. A 10-year regional hindcast of the tidal and non-tidal flows was utilised, along with a nested tidal domain for the Wellington Harbour. These data were used to describe the existing flow regime in the entrance channel as well as in the vicinity of the proposed offshore disposal ground.

- Wave conditions were considered with a high-resolution model that includes the tidal hydrodynamics as well as local wind-wave generation inside the harbour. A 10-year hindcast was produced for the Wellington Harbour, which was nested inside a 35-year national wave hindcast.

- The sediment dynamics were simulated with a fully-coupled wave, current and sediment transport model. Climatic conditions were modelled to consider potential transport and morphology evolution over decadal time scales, as well as the discrete outcomes from a series of energetic historical events.

This suite of models was used to make an assessment of the likely effects of deepening the entrance channel, and disposing of capital volumes in an offshore ground in Fitzroy Bay. This was achieved by undertaking identical simulations with, and without, the dredging / disposal activity. Two potential channel designs were tested in this manner, along with the respective disposal volumes. An evaluation of the impact of plumes associated with dredging and disposing has also been made.

A summary of the physical effects and a detailed interpretation of the findings is presented the companion report (MSL Report P0214-03).

7. REFERENCES

Arron, E.S.; Lewis, K. B. 1993: Wellington south coast substrates New Zealand Oceanographic Institute Miscellaneous chart series 1:15000.

Bell, R.G.; Oldman, J.W.; Beamsley, B.; Green, M.O.; Pritchard, M.; Johnson, D.; McComb, P.; Hancock, N.; Grant, D.; Zyngfogel, R. (2009). Port of Otago dredging project: Harbour and offshore modelling. NIWA Client Report HAM2008-179 prepared for the Port Otago Ltd, 340 p

Brown, J.M., Davies A.G., 2009. Methods for Medium-term Prediction of the Net Sediment Transport by Waves and Currents in Complex Coastal Regions. Cont. Shelf Res. 29, 1502–1514.

Collins, J., 1972. Prediction of Shallow Water Spectra. J. Geophys. Res. 77, 2693–2707.

Dastgheib, A., 2012. Long-term Process-based Morphological Modeling of Large Tidal Basins (Ph. D.). UNESCO-IHE.

Deltares, 2013a. User Manual Delft3D-WAVE. version: 3.05.27794.

Deltares, 2013b. User Manual Delft3D-FLOW. version: 3.15.2789. Deltares.

De Vriend, H.J., Capobianco, M., Chesher, T., de Swart, H.J., Latteux, B., Stive, M.J.F., 1993. Approaches to long-term modelling of coastal morphology: a review. Coast. Eng. 21, 225–226.

eCoast 2015 Regionally significant surf breaks in the Greater Wellington Region. Report prepared for the Greater Wellington Regional Council, May 2015.

Egbert, G.D., Erofeeva, S.Y., 2002. Efficient inverse modeling of barotropic ocean tides. J. Atmospheric Ocean. Technol. 19, 183–204.

Engelund, F., Hansen, E., 1967. A Monography on Sediment Transport in Alluvial Streams. Danish Technical ITeknisk Forlag).

Fredsøe, J., 1984. Turbulent Boundary Layer in Wave-current interaction. J. Hydraul. Eng. ASCE 110, 1103–1120.

Grunnet, N. M., Walstra, D.J.R., Ruessink, B.G., 2004. Process-Based Modelling of a Shoreface Nourishment. Coast. Eng. 7, 581–607.

Haidvogel, D.B., Arango, H.G., Hedstrom, K., Beckmann, A., Malanotte-Rizzoli, P., Shchepetkin, A.F., 2000. Model Evaluation Experiments in the North Atlantic Basin: Simulations in Non-linear Terrain-Following Coordinates. Dyn. Atmosphere Oceans 32, 239–281.

Holthuijsen, L.H., 2007. Waves in oceanic and coastal waters. Cambridge University Press.

Latteux, B., 1995. Techniques for Long-term Morphological Simulation Under Tidal Action. Mar. Geol.

Lesser, G.R., 2009. An approach to medium-term coastal morphological modelling (Ph. D.). UNESCO-IHE & Delft Technical University.

Lesser, G.R., Stelling, G.S.,, Roelvink J.A., 2004. Development and Validation of a Three-Dimensional Morphological Model. Coast. Eng. 51, 883–915.

MetOcean Solutions Ltd., 2014. Lyttelton Harbour Dredging Project, Numerical modelling of sediment dynamics for proposed offshore disposal grounds. Technical report prepared for Lyttelton - Port of Christchurch.

Draft for public consultation

MetOcean Solutions Ltd., 2016. CentrePort Harbour Deepening Project – Summary of physical effects. Client Report P0283-03.

MetOcean Solutions Ltd., 2016. CentrePort Harbour Deepening Project – Numerical model studies on deepening the Thorndon Container Wharf and disposal of the dredged material. Client Report P0283-02.

NIWA., 2014. Wellington Harbour Entrance Channel – Bathymetric and geophysical surveys. Technical report prepared for Tonkin and Taylor 120 p.

Okubo, A., 1971. Oceanic diffusion diagrams. Deep-Sea Research 18, 789-802.

Pallentin, A., Verdier, A.-L, Mitchell, J., 2009. Beneath the Waves: Wellington harbour. NIWA chart, Miscellaneous Series 87. Wellington, New Zealand: National Institute of Water & Atmospheric Research (NIWA) Ltd.

Reniers, A.J.H.., Roelvink, J.A., Thornton, E.B., 2004. Morphodynamic Modeling of an Embayed Beach Under Wave Group Forcing. J. Geophys. Res. 109, 148–227.

Roelvink J.A., 2006. Coastal morphodynamic evolution techniques. Coast. Eng. 277–287.

Saha, S., Moorthi, S., Pan, H.-L., Wu, X., Wang, J., Nadiga, S., Tripp, P., Kistler, R., Woollen, J., Behringer, D., Liu, H., Stokes, D., Grumbine, R., Gayno, G., Wang, J., Hou, Y.-T., Chuang, H.-Y., Juang, H.-M.H., Sela, J., Iredell, M., Treadon, R., Kleist, D., Van Delst, P., Keyser, D., Derber, J., Ek, M., Meng, J., Wei, H., Yang, R., Lord, S., Van Den Dool, H., Kumar, A., Wang, W., Long, C., Chelliah, M., Xue, Y., Huang, B., Schemm, J.-K., Ebisuzaki, W., Lin, R., Xie, P., Chen, M., Zhou, S., Higgins, W., Zou, C.-Z., Liu, Q., Chen, Y., Han, Y., Cucurull, L., Reynolds, R.W., Rutledge, G., Goldberg, M., 2010. The NCEP Climate Forecast System Reanalysis. Bull. Am. Meteorol. Soc. 91, 1015–1057. doi:10.1175/2010BAMS3001.1

Smith, S.J., and Friedrichs, C.T., 2011. Size and settling velocities of cohesive flocs and suspended sediment aggregates in a trailing suction hopper dredge plume. Continental Shelf Research, 10 (Issue 10, Supplement 1): S50-S63

Sneddon, R., 2009. Assessment of Impacts to Benthic Ecology and Marine Ecological Resources from Proposed Capital Dredging and Spoil Disposal Offshore from Lyttelton Harbour (Technical report prepared for Lyttelton Port of Christchurch). Cawthron.

Tolman, H.L., 1991. A Third-Generation Model for Wind Waves on Slowly Varying, Un-steady and Inhomogeneous Depths and Currents. J. Phys. Oceanogr. 21, 782–797.

Van der Wegan, M., Roelvink, J.A., 2008. Long-term Morphodynamic Evolution of a Tidal Embayment using a Two-Dimensional, Process-based Model. J. Geophys. Res. 114.

Van Rijn, L.C., 1993. Principles of Sediment Transport in Rivers, Estuaries and Coastal Seas. Aqua Publications, 386 pp.

Van Rijn, L.C., 2007. A unified view of sediment transport by current and waves, Part II: Suspended transport, Journal of Hydraulic Engineering, ASCE.

Vitali, L., Monforti, F., Bellasio, R., Bianconi, R., Sachero, V., Mosca, S., Zanini, G., 2006. Validation of a Lagrangian dispersion model implementing different kernel methods for density reconstruction. Atmos. Environ. 40, 8020–8033.

Walstra, D.J.R., Hoekstra, R., Tonnon, P.K., Ruessink, B.G., 2013. Input reduction for long-term morphodynamic simulations in wave-dominated coastal settings. Coast. Eng. 77, 57 – 70. doi: http://dx.doi.org/10.1016/j.coastaleng.2013.02.001

Zhang, Y. L. and Baptista, A.M. (2008). SELFE: A semi-implicit Eulerian-Lagrangian finite-element model for cross-scale ocean circulation. Ocean Modelling, 21 (3-4), 71-96.